INFORMATION TO USERS

This manuscript has been reproduced from the microfilm master. UMI films the text directly from the original or copy submitted. Thus, some thesis and dissertation copies are in typewriter face, while others may be from any type of computer printer.

The quality of this reproduction is dependent upon the quality of the copy submitted. Broken or indistinct print, colored or poor quality illustrations and photographs, print bleedthrough, substandard margins, and improper alignment can adversely affect reproduction.

In the unlikely event that the author did not send UMI a complete manuscript and there are missing pages, these will be noted. Also, if unauthorized copyright material had to be removed, a note will indicate the deletion.

Oversize materials (e.g., maps, drawings, charts) are reproduced by sectioning the original, beginning at the upper left-hand corner and continuing from left to right in equal sections with small overlaps.

Photographs included in the original manuscript have been reproduced xerographically in this copy. Higher quality 6" x 9" black and white photographic prints are available for any photographs or illustrations appearing in this copy for an additional charge. Contact UMI directly to order.

Bell & Howell Information and Learning
300 North Zeeb Road, Ann Arbor, MI 48106-1346 USA

UMI®
800-521-0600

A Model of the Electric Arc Attachment on Non-Refractory (Cold) Cathodes

Sylvain Coulombe

Plasma Technology Research Centre (CRTP)
Department of Chemical Engineering
McGill University

Dr. Jean-Luc Meunier, Supervisor

A Thesis Submitted to the Faculty of Graduate Studies
and Research in Partial Fulfilment of the Requirements
for the Degree of Doctor of Philosophy

McGill University
Montréal, Canada

à Marie-Claude

"N'écoutez pas les prophètes de la mémorisation qui attachent peu d'importance à la compréhension. Cette compréhension doit être la première vertue en importance dans la hiérarchie de l'intelligence humaine. La Nature est d'une beauté telle qu'elle mérite d'être *comprise* et non d'être *apprise* par l'Homme pour être appréciée à sa juste valeur."

A MODEL OF THE ELECTRIC ARC ATTACHMENT ON NON-REFRACTORY (COLD) CATHODES

ABSTRACT

In this work, a physical model describing the electric arc attachment on electron emitting non-refractory (cold) cathodes is developed and applied to Cu, Fe and Ti cathodes. The model considers the possibility of a pressure build up in the cathode region due to the strong vaporization of the cathode, the formation of a cathode sheath according to the Bohm's model, and the ion-enhanced thermo-field emission of electrons by the cathode surface. The self-sustaining operating conditions of the discharge are defined by two simple criteria based on particle and energy balance considerations. Results clearly show the necessity of having high local metallic vapor pressures in the cathode region of non-refractory cathodes in order to have a self-sustaining arc attachment. A minimum pressure of at least 19 atm is needed for a Cu cathode. This minimum pressure is shown to decrease as the cathode material boiling temperature increases according to an exponential decay law. Current densities of the order of 10^{10} A m^{-2} are maintained at the surface of a Cu cathode mainly by the emitted electrons. A comparison of the three different models for the electron emission current found in the literature allowed to define the limits of validity of each model for two typical arc-cathode interaction systems, and to evaluate the underestimation made on the emission current density when a less appropriate model is used. This underestimation is shown to cause an overestimation of important parameters such as the cathode surface temperature and metallic vapor pressure in the cathode region. An analysis of the mechanisms of heat transfer to the cathode surface allowed to show that the confinement of the cathode spot plasma forming the arc attachment could favor the production of vapors to the detriment of liquids. Such a phenomenon is of importance in Arc Ion Plating for instance. Heat losses by conduction in the cathode bulk larger than 10^{10}

W m^{-2} are shown to favor the formation of liquid volumes in a μs time scale. This liquid volume formation is shown to increase with the initial cathode temperature and current carried at the arc attachment point.

UN MODÈLE DE L'ATTACHEMENT DES ARCS ÉLECTRIQUES SUR LES CATHODES NON-RÉFRACTAIRES (CATHODES FROIDES)

RÉSUMÉ

Un modèle physique décrivant l'attachement d'un arc électrique sur une cathode non réfractaire et émettrice d'électrons est développé et appliqué à des cathodes en cuivre (Cu), fer (Fe) et titane (Ti). Le modèle considère la possibilité d'une pression importante de vapeurs métalliques dans la zone cathodique due à la forte vaporization de la cathode, la formation d'une gaine électrique selon le modèle de Bohm, et l'émission thermo-champ d'électrons de la cathode accentuée par la présence d'ions dans la zone cathodique. Le régime auto-entretenu de la décharge électrique est défini par la validation de deux critères simples basés sur des balances particulaires et énergétiques. Les résultats montrent clairement la nécessité d'avoir de fortes pressions de vapeurs métalliques dans la zone cathodique pour l'obtention d'un régime d'attachement auto-entretenu. Une pression minimum d'environ 19 atm a été évaluée dans le cas du Cu. Cette pression minimum s'est montrée décroître exponentiellement avec l'augmentation de la température de vaporization du matériau de la cathode. Des densités de courant de l'ordre de 10^{10} A m^{-2} sont maintenues à la surface de la cathode et ce, principalement par les électrons émis de cette dernière. Une comparison des différents modèles utilisés pour le calcul de la densité de courant d'électrons emis a permis de définir les limites de validité de chaque modèle pour deux situations particulières d'intéractions arc-cathode, et aussi d'évaluer les sous-estimations de ce paramètre induites par l'utilisation d'un modèle moins approprié. Ces sous-estimations induisent une sur-estimation des paramètres importants comme la température de surface de la cathode et la pression des vapeurs métalliques présentes dans la zone cathodique. Une analyse des transferts de chaleur à la surface de la cathode a permis de constater que le confinement du plasma métallique formant la tache cathodique

pourrait favoriser la production de vapeurs au détriment de la production de liquides, ceci ayant une importance pratique dans le cas de la déposition par pulvérisation cathodique par exemple. Des pertes par conduction thermique dans la cathode supérieures à 10^{10} W m^{-2} causent la formation de volumes liquides à la surface de la cathode dans des temps de l'ordre de la microseconde. Cette formation de volumes liquides s'est montrée dépendre de la temperature initiale de la cathode et du courant transporté dans la zone d'attachement.

REMERCIEMENTS

Mes premiers remerciements seront pour mon superviseur, le professeur Jean-Luc Meunier, qui part son intérêt envers le projet a sû me guider tout au long de ces trois années. Je le remercie sincèrement de m'avoir laissé exprimer mes idées, bien souvent farfelues, d'avoir toujours laissé sa porte ouverte et d'avoir sû me motiver dans les périodes difficiles. Merci beaucoup!

Je tiens à remercier le professeur Richard J. Munz, co-directeur du CRTP et directeur du département de génie chimique de l'Université McGill. Ces commentaires et suggestions fûrent précieux. Je le remercie aussi d'avoir facilité les contacts avec les autres membres du groupe de recherche et de m'avoir fait entière confiance.

Merci au Dr. Serge Vacquié du Centre de Physique Atomique de l'Université Paul Sabatier de Toulouse pour son aide apportée au tout début du projet et de m'avoir si chaleureusement acceuillis lors d'un court échange.

Mes remerciements aux étudiants(es) gradués(es) et stagiaires du CRTP/McGill. Je pense à Tony Addona, Theodora Alexakis, Jörg Oberste Berghaus, Antonio Carlos da Cruz, Julie Filion, Munther Kandah, Georges Kim, Hong Sun Seon, Karen Sum et Teh Hau Chua. Je tiens à remercier tout spécialement Tony Addona qui est devenu un ami cher et qui fût un excellent conseiller tant en matière de langue anglaise qu'en matière de génie chimique!

Un gros merci aux professeurs(es) qui m'ont enseigné. Merci à Marie-Claude Heuzey ma compagne de cours.

Merci à Alain Gagnon, Lou Cusmish, Walter Greenland, Charles Dolan, Jean Dumont, Mike Harrigan et Helen Campbell qui par leur apport technique m'ont permis de mener à terme ce projet. Merci à mesdames Anne Prioda, Pat Fong et Joanne Terrassi du sécrétariat. Merci à tous d'avoir contribué au maintien d'une ambiance de travail agréable.

Je voudrais remercier le Fonds pour les Chercheurs et l'Aide à la Recherche du Ministère de l'Education du Québec (FCAR) et le département de génie chimique de l'Université McGill pour leur soutient financier.

Merci à mes parents et amis qui par leur nombreux encouragements et leur compréhension m'ont permis de toujours continuer.

Les derniers remerciements seront pour Marie-Claude qui m'est si chère. Merci d'être une source intarrisable d'encouragements et de supports. Merci d'avoir compris ce que ce doctorat représente pour moi. Merci d'être là tous les jours.

TABLE OF CONTENTS

ABSTRACT iii

RÉSUMÉ v

REMERCIEMENTS vii

TABLE OF CONTENTS ix

LIST OF FIGURES xiii

LIST OF TABLES xix

1. GENERAL INTRODUCTION 1

1.1. Overall Objective 2

1.2. Organization of the Thesis 3

PART 1: PROBLEM DEFINITION

2. BACKGROUND AND PRELIMINARY RESULTS ON ARC-CATHODE INTERACTIONS 6

2.1. Introductory Concepts 7

2.1.1. A Definition of the High Pressure Arc 7

2.1.2. Principal Characteristics of the Cathode Region 8

2.2. Electron Emission from the Cathode 12

2.2.1. Field-Enhanced Thermionic Emission 14

2.2.2. Murphy and Good Formalism for Thermo-Field Emission 15

2.2.3. Effects of Slowly Moving Ions 17

2.2.4. Effects of Protusions 18

2.2.5. Effects of Adsorbates and Thin Films 19

2.2.6. Nottingham Effect 21

2.3. Attachment of High Pressure Arcs on Non-Refractory Arc Cathodes ... 22

2.3.1. General Observations 22

2.3.2. Fundamental Distinctions between Refractory and Non-Refractory Arc Cathodes 24
2.3.3. Crater Formation: Time Scale and Current Density 26
2.3.4. Limitations of the Actual Models 30
2.3.5. The Concept of High Local Pressure 32
2.3.6. Similarities with Vacuum Arc Cathode Spots 33
2.3.7. Cathode Spot Ignition 34

3. SEM SURFACE ANALYSIS 38
3.1. Introduction 38
3.2. Preparation of the Cathodes 38
3.2.1. Equipment and Materials 38
3.2.2. Experimental Conditions and Procedures 40
3.3. Observations 41
3.3.1. Pure Argon Plasma 41
3.3.2. Argon+Nitrogen Plasma 44
3.4. Discussion and Conclusions 46

PART 2: MODELING STUDY

4. DEVELOPMENT OF THE PHYSICAL MODEL 50
4.1. General Description and Assumptions 50
4.2. Current Transfer in the Cathode Sheath 54
4.2.1. Electron Emission Current 55
4.2.2. Ion Current 56
4.2.3. Back-Diffusing Plasma Electron Current 57
4.2.4. Poisson's Equation 58
4.2.5. Surface Electric Field Strength 58
4.3. Heat Transfer to the Cathode 59
4.3.1. Returning Ion Bombardment 60

4.3.2. Back-Diffusing Plasma Electron Bombardment 61
4.3.3. Energy Exchange Associated with Electron Emission (Nottingham Effect) 61
4.3.4. Heat Lost by Cathode Material Vaporization 63
4.3.5. Conduction Losses 63
4.4. Criteria for a Self-Sustaining Arc Operation 64
4.4.1. First Criterion 64
4.4.2. Second Criterion 65
4.5. Erosion 65
4.5.1. Erosion by Vaporization 66
4.5.2. Re-Deposition of Ions and Neutrals 66
4.5.3. Liquid Volume Formation 67
4.6. Boundary Conditions 67
4.6.1. Composition of a Two-Temperature Plasma 68
4.7. Calculation Procedure 70
4.8. Materials Properties 70

5. MODEL'S PREDICTIONS WITH CU, FE AND TI CATHODES 72
5.1. Introduction 72
5.2. Parametric Study for Cu: Influence of p and T_e^{sc} 72
5.2.1. Choice of the Cathode Sheath Voltage Drop 73
5.2.2. Minimum Plasma Pressure for a Self-Sustaining Arc 73
5.2.3. Plasma Properties 76
5.2.4. Current Transfer to the Cathode 80
5.2.5. Electron Emission Conditions 84
5.2.6. Internal Structure of the Cathode Sheath 88
5.2.7. Heat Transfer to the Cathode 92
5.2.8. Erosion by Vaporization 96
5.3. Model's Predictions with Fe and Ti Cathodes 98
5.4. Validity of the Collisionless Cathode Sheath Assumption 101

5.5. Influence of the Cathode Sheath Voltage Drop 103
5.6. Discussion and Conclusions 105

6. ELECTRON EMISSION FROM THE CATHODE: A COMPARATIVE STUDY 110
6.1. Introduction 110
6.2. Refractory W Arc Cathode 111
6.2.1. Influence of Temperature and Electric Field Strength 112
6.2.2. Influence of Work Function 113
6.2.3. Influence of Ambient Gas Pressure and Electron Temperature . 114
6.3. Non-Refractory Cu Arc Cathode 116
6.3.1. Ion Effects on Current Density Distribution 117
6.3.2. Ion Effects on Spot Conditions 119
6.3.3. Comparison with other Studies 123
6.4. Summary 124

7. LIQUID VOLUME FORMATION 127
7.1. Introduction 127
7.2. Description of the Heat Transfer Model 127
7.2.1. Mathematical Formulation 129
7.2.2. Solution Method 130
7.2.3. Discretization and Grid Definition 133
7.2.4. Boundary and Initial Conditions 134
7.3. Results 135
7.3.1. Simulation Conditions 135
7.3.2. Time Scale for Liquid Volume Formation 136
7.3.3. Maximum Erosion by Liquid Volume Ejection 138
7.4. Discussion and Conclusions 143

PART 3: CONCLUSIONS

GENERAL CONCLUSIONS 146

RECOMMENDATIONS FOR FUTURE STUDIES 148

NOMENCLATURE 151

APPENDICES 156

Appendix A: Solution of the Murphy and Good Equations in SI Units 156

Appendix B: Derivation of the Field-Enhanced Thermionic Equation 158

Appendix C: The NASA Method 160

REFERENCES 162

LIST OF FIGURES

FIGURE 2.1.1 General representation of a high pressure arc attachment region on a hot, thermionically emitting cathode (cathode region). 8

FIGURE 2.1.2 Schematic representation of the voltage, particle number density and temperature distributions in the cathode region of a high pressure arc on an emitting cathode (adapted from Roth 1995, fig. 9.21). 11

FIGURE 2.2.1 Schematic representation of the 1-dimensional potential experienced by the electrons outside the metal surface. Thermionic emission (short dashes), thermo-field emission (long dashes), and ion-enhanced thermo-field emission (continuous line). 14

FIGURE 2.2.2 Thermo-field emission electron current density predicted by the Murphy and Good equations (j_{T-F}^{MG}) in the T_s-log(E_s) plane for ϕ=4.5 eV (Based on our calculations). 16

FIGURE 2.2.3 Schematic representation of the electrostatic electric field establishment across a thin insulating (dielectric) film on the cathode and the electron emission process. 20

FIGURE 2.2.4 Time necessary to charge a Cu_2O dielectric (ε_r=7.1) until establishment of a film electric field of 2×10^9 V m^{-1} with f=0.01 and for several fractions p_{Cu}/p_{tot} in an Ar + Cu plasma (T_o=LTE plasma temperature) (Based on our calculations). 21

FIGURE 2.3.1 Calculated ratio of the flux of vaporized atoms (Γ_{vap}) to the flux of thermionic electrons (j_{RD}/e) as a function of the cathode surface temperature for different cathode materials. 25

FIGURE 2.3.2 Scanning electron micrograph (SEM) of a Cu cathode surface arced by an atmospheric pressure argon arc operating at 100 A for 30 sec. 27

FIGURE 2.3.3 Estimated total current density per spot j_{tot} on a Cu cathode arced by an atmospheric pressure Ar arc as a function of the observed crater radius r_s (spot radius) for several values of the current per spot I_s. Insert: Schematic of the arc attachment region. Shaded area: Estimated existence area for the current density (Based on

our calculations). 29

FIGURE 2.3.4 Schematic representation of the ignition process for a new arc attachment point on the cathode surface. (a) Heating of the protusion by Joule and Nottingham heating; field-emission of electrons. (b) Pressure build up; surface heating by ion bombardment, Joule and Nottingham heating; enhancement of electric field due to the ions. (c) Operating spot. 36

FIGURE 3.2.1 Schematic representation of the erosion test chamber and auxiliary equipment. 39

FIGURE 3.3.1 Surface morphology (SEM) of a Cu cathode having been exposed to a pure Ar plasma operating at 100 A for 30 s. 42

FIGURE 3.3.2 Surface morphology (SEM) of a Ti cathode having been exposed to a pure Ar plasma operating at 100 A for 30 s. 43

FIGURE 3.3.3 Surface morphology (SEM) of a Ti cathode having been exposed to a pure Ar plasma operating at 100 A for 2 hours. 44

FIGURE 3.3.4 Surface morphology (SEM) of a Cu cathode having been exposed to an Ar+1%vol N_2 plasma operating at 100 A for 5 min. 45

FIGURE 3.3.5 Surface morphology (SEM) of a Ti cathode having been exposed to an Ar+1%vol N_2 plasma operating at 100 A for 15 min. 45

FIGURE 4.1.1 Schematic representation of the attachment region of a high pressure arc on an emitting non-refractory cathode. 52

FIGURE 4.2.1 Detailed representation of the cathode region of an emitting cathode exposed to a high pressure arc. 55

FIGURE 4.3.1 Nottingham potential of the electron ε_N as a function of the cathode surface temperature T_s, and surface electric field strength E_s for ϕ=4.5 eV. Continuous line: equation (4.3.4) using fitting formula of Paulini *et al* (1993). Dashed line: equation (4.3.5). 62

FIGURE 4.8.1 Vapor pressure curve for Cu, Fe and Ti. Continuous line: data reported by Honig and Kramer (1969). Dotted line: fits of the data using equation (4.8.1). 71

FIGURE 5.2.1 Ratio $j_{ion}/j_{T\text{-}F}$ (criterion 4.4.2a) for a two-temperature Cu plasma as a function of p for V_c=15 V and $0.9 < T_e^{sat} < 2.0$ eV. 74

FIGURE 5.2.2. Ratio $e\Gamma_{vap}/j_{T\text{-}F}$ for a two-temperature Cu plasma as a function of p for V_c=15 V and 0.9< T_e^{sc} <2.0 eV. The corresponding cathode surface temperatures are indicated in parentheses (in K). 76

FIGURE 5.2.3 Electron density in a two-temperature Cu plasma as a function of T_e^{sc} and p. 77

FIGURE 5.2.4 Lowering of the ionization potential of the CuI species as a function of T_e^{sc} and p. 78

FIGURE 5.2.5 Pressure correction for a two-temperature Cu plasma as a function of T_e^{sc} and p. 79

FIGURE 5.2.6 Total spot current density as a function of p for V_c=15 V and 0.9< T_e^{sc} <2.0 eV. 81

FIGURE 5.2.7 Fraction j_{ion}/j_{tot} of the total spot current density carried by the ions as a function of p for V_c=15 V and 0.9< T_e^{sc} <2.0 eV. 83

FIGURE 5.2.8 Fraction $j_{T\text{-}F}/j_{tot}$ of the total spot current density carried by the emitted electrons as a function of p for V_c=15 V and 0.9< T_e^{sc} <2.0 eV. 84

FIGURE 5.2.9 Surface electric field strength E_s and cathode surface temperature under the spot T_s as a function of p for V_c=15 V. E_s is plotted for 0.9< T_e^{sc} <2.0 eV. T_s is independent of T_e^{sc}. 85

FIGURE 5.2.10 Cathode sheath thicknes x_c as a function of p for V_c=15 V and 0.9< T_e^{sc} <2.0 eV. 87

FIGURE 5.2.11 Distribution of the particle number densities and voltage in the cathode sheath as a function of the distance from the cathode surface for V_c=15 V, T_e^{sc} =1.0 eV and p=35 atm. λ_D~1.02x10^{-9} m and the corresponding total current density is j_{tot}=10^{10} A m^{-2}. 89

FIGURE 5.2.12 Space charge formation in the cathode sheath for V_c=15 V, T_e^{sc} =1.0 eV and p=35 atm. λ_D~1.02x10^{-9} m and the corresponding total current density is j_{tot}=10^{10} A m^{-2}. 90

FIGURE 5.2.13 Space charge n_{sc} as a function of the local potential in the cathode sheath $V(x)$ for V_c=15 V, T_e^{sc} =1.0 eV and for two values of p (35 and 50 atm). 91

FIGURE 5.2.14 Total incoming heat flux to the cathode spot surface q_{in} as a function of p for V_c=15 V and 0.9< T_e^{se} <2.0 eV. 93

FIGURE 5.2.15 Distribution of the different heat losses from the cathode spot surface as a function of p for V_c=15 V and 0.9< T_e^{se} <2.0 eV. 94

FIGURE 5.2.16 Heat flux lost by conduction q_{cond} as a function of p for V_c=15 V and 0.9< T_e^{se} <2.0 eV. 95

FIGURE 5.2.17 Calculated erosion rate by vaporization ($E_{r,vap}^{max}$) and erosion rate by vaporization considering ion redeposition ($E_{r,vap}^{min}$) for a clean Cu cathode as a function of p for V_c=15 V and 0.9< T_e^{se} <2.0 eV. The measured vacuum erosion rate for Cu (~ 65-115 μg C^{-1}) is represented by the shaded area. 97

FIGURE 5.3.1 Range of metallic plasma pressures needed for a self-sustaining operation of the arc spots as a function of the cathode material's boiling temperature T_v. 100

FIGURE 5.4.1 Evolution of the ratio $x_c / \lambda_{e-Cul}^{M}$ as a function of p for V_c=15 and T_e^{sc}=1.0 eV. 103

FIGURE 5.5.1 Total current density j_{tot} as a function of V_c and p for T_e^{sc}=1 eV. .. 104

FIGURE 5.5.2 Ratio $j_{ion}/j_{T\text{-}F}$ (criterion 4.4.2a) as a function of V_c and p for T_e^{sc}=1 eV. 105

FIGURE 6.2.1 Isocontours $j_{T-F}^{MG} / j_{T-F}^{FEE}$ = constant in the T_s-E_s (logarithmic scale) plane for ϕ=4.5 eV. Typical conditions encountered at the cathode surface of an atmospheric pressure argon arc on a W cathode are delimited. 113

FIGURE 6.2.2 Model's predictions in the p- T_e^{se} plane of the ratios $j_{T-F}^{MG} / j_{T-F}^{FEE}$ (long dashes) and $j_{T-F}^{MG-I} / j_{T-F}^{FEE}$ (continuous line) for a high pressure arc on a refractory W cathode with T_s=3 750 K, V_c=8 V and ϕ=4.5 eV. 116

FIGURE 6.3.1 Model's predictions of the ratios j_{T-F}^{FEE} / j_{tot}, j_{T-F}^{MG} / j_{tot} and j_{T-F}^{MG-I} / j_{tot} for a high pressure arc on a non-refractory Cu cathode as a function of j_{tot} with V_c=15 V, T_e^{sc}=1 eV (11 600 K) and ϕ=4.5 eV. 118

FIGURE 6.3.2 Model's predictions of the metallic plasma pressure within the cathode spot p for a high pressure arc on a non-refractory Cu cathode as a function of j_{tot} with V_c=15 V, T_e^{sc}=1 eV (11 600 K) and ϕ=4.5 eV. 120

FIGURE 6.3.3 Model's predictions of the cathode surface temperature under the spot T_s for a high pressure arc on a non-refractory Cu cathode as a function of j_{tot} with V_c=15 V, T_e^{sc}=1 eV (11 600 K) and ϕ=4.5 eV. 121

FIGURE 6.3.4 Model's predictions of the surface electric field strength E_s for a high pressure arc on a non-refractory Cu cathode as a function of j_{tot} with V_c=15 V, T_e^{sc}=1 eV (11 600 K) and ϕ=4.5 eV. 122

FIGURE 7.2.1 Geometry used for the heat transfer model. F_m=location of the moving boundary T=T_m. 128

FIGURE 7.2.2 Evolution of the continuous enthalpy function H of copper. Insert: Evolution of H around T=T_m (T_m=1356 K, T_v=2836 K, Δ=1 K, L_m=23.38 J kg^{-1} and L_v=536.4 J kg^{-1}). 131

FIGURE 7.2.3 Kirrchoff's transform of copper calculated with T_w=300 K. 132

FIGURE 7.3.1 Evolution of q_{cond} and r_s as a function of p. Points linked by letters A through E correspond to the simulation conditions. 136

FIGURE 7.3.2 Minimum time t_{min} needed to form a liquid volume underneath the arc attachment point on the cathode as a function of T_{ini} for cases A through E presented in figure 7.3.1. 137

FIGURE 7.3.3 Temporal evolution of the liquid mass formed underneath the arc attachment for the self-sustaining conditions corresponding to case B. 140

FIGURE 7.3.4 Temporal evolution of the temperature distribution within the cathode for the conditions corresponding to case B with 1) T_{ini}=500 K and 2) T_{ini}=700 K. 141

FIGURE 7.3.5 Temporal evolution of the maximum erosion rate by liquid volume ejection $E_{r,liq}^{max}$ for the self-sustaining conditions corresponding to case B. 142

LIST OF TABLES

TABLE 2.2.1 Calculated averaged ion-enhancement factor β for H^- ions (protons) slowly moving in the close vicinity of a Cu cathode with $E_s=10^9$ V m^{-1}. Values in parentheses were calculated for alpha particles*. 18

TABLE 2.3.1 Erosion results obtained for a magnetically rotated arc between two concentric electrodes. Anode material: Copper. 23

TABLE 2.3.2 Estimated conditions and behaviors of the arc attachment point(s) for refractory and non-refractory cathodes of high pressure arcs. 26

TABLE 5.2.1 Ion-enhancement factor β of the thermo-field emission current $j_{T\text{-}F}$ as a function of the conditions prevailing within the cathode spots. 86

TABLE 5.3.1 Model's predictions of the self-sustaining operating conditions for the arc spots on Cu, Fe and Ti cathodes. 99

TABLE 6.3.1 Comparison between the results obtained with the present model to the results of Benilov (1993) and Klein *et al* (1994) for the current transfer to the surface under a Cu cathode spot. 124

CHAPTER 1

GENERAL INTRODUCTION

In recent years there has been an increasing interest in modeling arc-electrode interactions. This interest is motivated by the primary desire of understanding the complex mechanisms governing the arc attachment on electrodes but also, by the need to develop plasma systems showing better performance. A problem of major concern still restraining the use of plasma systems over long periods of time is the phenomenon of electrode erosion. Typical examples of erosion by an electric arc are encountered in the development of high-enthalpy arc gas heaters and plasma torches for chemical processing and re-entry simulations (Milos and Shepard 1994), switch gears and circuit breakers (Guile 1971), magneto-plasma-dynamic (MPD) thrusters for space propulsion (Choueiri 1992, Satheesh *et al* 1992) and high intensity discharge (HID) lamps (Almeida and Benilov 1997).

In some other cases however, electrode consumption is essential and a better understanding of the complicated phenomena involved would help reaching better performances. One can think for instance of the electric arc welding process where the electrode material is used to join two workpieces, to any vacuum arc process such as arc ion-plating (AIP) where an electric arc is used to vaporize the cathode material for deposition on a remote substrate, or to the electrogun metal vapor plasma discharge used to produce vapors of different metals at a high rate (Raja *et al* 1997). A better understanding is crucial for the two last examples where the formation and emission of liquid droplets from the arc attachment points on the cathode must be avoided while maximizing the cathode material vaporization rates.

The arc-cathode interactions have been the subject of numerous studies for many years (Guile 1971) and are today even more studied due to the number of new plasma processes involving surfaces. The cathode region is however known as the least understood region of the arc (Zhou and Heberlein 1996). From a theoretical standpoint, the complexity of the phenomena involved still prohibits a detailed theory. From an experimental standpoint, the extremely small dimension of the arc attachment region on the cathode, and sometimes the movement of the arc foot itself, make the observation of any important quantity difficult or impossible. Some consequences of this are the few experimental data available, and the appearance in the literature of many incomplete studies and sometimes, contradictory results. This lack of knowledge is even more pronounced for the interactions of high pressure arcs with non-refractory cathodes where no microscopic model can be found in the literature.

1.1. Overall Objective

Over the last fifteen years, considerable efforts have been dedicated by the graduate students and professors of the *Plasma Technology Research Centre* (CRTP) of McGill University to study the erosion phenomena in high pressure plasma systems simulating thermal arc plasma torches with non-refractory cathodes (the terminology "high pressure" used in this study includes atmospheric and higher pressures, in contrast to vacuum arcs). The emphasis was put mainly on the reduction of the cathode erosion rate by contamination of the cathode surface (Szente 1989), on the search for low-erosion cathode materials (Kwak 1994), and on the optical monitoring of the plasma and cathode erosion products (Desaulniers-Soucy 1992). Simultaneously to atmospheric pressure erosion studies, experiments were carried to understand the characteristics and use the low pressure "cathodic arc" (vacuum arc) for deposition and erosion behavior in the transition between vacuum (10^{-6} torr) to atmospheric pressure arcs (Meunier and Drouet 1987, Meunier 1990, Kandah 1997). All these experimental studies have led to a considerable enhancement of our knowledge of such systems, but a detailed theoretical study is needed to provide qualitative and quantitative explanations for the experimentally observed phenomena. A theoretical study would also define the basis needed for the future

developments of cathode materials showing better characteristics such as lower erosion rates. This thesis work is aimed at developing a model for such systems.

1.2. Organization of the Thesis

In order to achieve this general objective, the present thesis was realized in three main parts.

In Part I, the problem of arc attachment on non-refractory cathodes is defined by reviewing the actual knowledge of the arc-cathode interactions, and by studying the limits of the actual models (Chapter 2). Chapter 2 not only consists of a literature review, but also of a presentation of some preliminary calculations necessary to define the basis of the model developed later in Chapter 4. To complete the problem definition, an analysis of the surface morphology of some non-refractory cathodes having been exposed to a high pressure electric arc is presented in order to define the mode of arc attachment that will be studied in this thesis.

Part II consists of the modeling study itself. The physical model describing the arc attachment on non-refractory cathodes is first developed in Chapter 4 and applied in Chapter 5 to three different cathode materials. These are respectively copper (Cu), iron (Fe) and titanium (Ti). The accent will be put mainly on copper since it represents the extreme case where the thermionic arc cathode model, which successfully explains the attachment of high pressure Ar arcs on refractory W cathodes, cannot be applied. The conditions necessary for the self-sustaining arc attachment will be first obtained by validation of two simple criteria based on particle and energy balance considerations, and the mechanisms of heat and current transfers to the cathode studied thereafter. It will become clear in Chapter 5 that the high erosion rates observed on such non-refractory cathodes are directly attributable to the necessity of having high local metallic vapor pressures in the cathode region for a self-sustaining operation of the arc. Such conditions expected to prevail in the cathode region force the cathode to emit electrons in the "thermo-field" emission regime. In such a situation, the use of the simple Richardson-

Dushman equation to describe the current of electrons emitted from the cathode is inappropriate, and the use of a more sophisticated model becomes necessary. At this point, a critical comparative study of the electron emission models found in the literature is carried out (Chapter 6). Chapter 7 concludes the modeling study and is dedicated to a brief study of liquid volume formation at the arc attachment point(s) on the cathode. The formation of liquid volumes is associated with the impossibility for the cathode to dissipate the strong heat flux coming from the arc root by conduction or radiation. Such liquid volumes are important since they represent a possible source of further erosion when microdroplets are ejected.

The last part of the thesis (Part III) consists of a general conclusion and some recommendations for further studies.

PART 1: PROBLEM DEFINITION

CHAPTER 2

BACKGROUND AND PRELIMINARY RESULTS ON ARC-CATHODE INTERACTIONS

In terms of modeling efforts dedicated to the arc-cathode interactions in high pressure arc systems (thermal arc plasmas), the attention has been almost only focused on refractory cathodes probably due to the extensive use of such systems in industry (e.g. Hsu and Pfender 1983, Lowke *et al* 1992, Zhou and Heberlein 1994, and Rethfeld *et al* 1996). Thanks to their refractory properties, such cathodes can sustain the high temperatures needed for a strong emission of electrons from the cathode (thermionic emission) without strong melting and vaporization which cause erosion. Considerable efforts are now made by several leading research groups to integrate such cathode models to the existing arc column models in order to describe the entire electric arc system in a self-consistent manner (Zhu *et al* 1992, Benilov and Marotta 1995 and references therein). This is however far from being the case for high pressure electric arcs interacting with non-refractory, highly vaporizing cathodes when only partial, and sometimes inadequate descriptions are reported. This thesis work attempts to enhance our knowledge of such systems by extending the actual models for high pressure arcs on refractory cathodes to non-refractory cathodes.

This chapter presents the necessary background information and some preliminary results needed to set the basis of the model developed in Chapter 4. A brief definition of the high pressure arc followed by a review of the principal characteristics of the cathode region are first presented in section 2.1. In section 2.2, a review is made of the mechanisms allowing electron extraction from the cathode. A presentation of the basic distinctions between the modes of arc attachment on both refractory and non-refractory cathodes

constitutes the first part of section 2.3. Following this are presented a discussion concerning the difficulties encountered when trying to explain the attachment of high pressure arcs on non-refractory cathodes using the actual models, and an introduction to the approach of high local pressure cathode spots that we favored as a solution to the problem. Chapter 2 terminates with a review of the actual models describing the formation of such spots.

2.1. Introductory Concepts

2.1.1. A Definition of the High Pressure Arc

"An arc is a discharge of electricity between electrodes, in a gas or in vapor from the electrodes, which has a voltage drop at the cathode of the order of the excitation potential of the electrode vapor ..." (Guile 1971). This general definition of the arc states explicitly the basic needs to sustain an arc: two electrodes, the anode (positively charged) and the cathode (negatively charged) and a medium filling the gap between the electrodes an allowing the current transfer between them. In vacuum arcs, where no filling gas is present, the medium corresponds to the vapors produced by erosion of the cathode. For high pressure arcs, this medium is composed of the ambient gas filling the chamber and to some extent, the electrode erosion products. On the universal voltage-current characteristic curve of the DC electrical discharge tube (Roth 1995, chap. 10), arcs correspond to the discharge regime carrying a current higher than 30 mA for a relatively low cathode voltage drop (~10-20 V). High pressure arcs are highly luminous and show relatively large current densities (>>1 A m^{-2}) explaining their use since more than 200 years for lighting purposes and as sources of energy for materials processing (Roth 1995).

The maintenance of a high pressure arc into a self-sustaining regime (regime avoiding from the spontaneous extinction) is strongly dependent on the conditions prevailing in the electrode regions; especially those prevailing at the cathode. These electrode regions assume the transition from the metallic conduction in the electrodes to the gaseous conduction in the high pressure arc column. The anode acts as the electron collector and the basic processes occurring in the anode region are relatively simple. On

the other hand, the cathode region shows much more complicated processes since the current transfer is in this case not only assumed by the electrons extracted from the cathode surface, but also by the ions accelerated by the cathode voltage drop and the plasma electrons retro-diffusing towards the cathode surface (Guile 1971).

2.1.2. Principal Characteristics of the Cathode Region

Figure 2.1.1 represents schematically the cathode region of a high pressure arc on a hot, thermionically emitting cathode (refractory cathode). For modeling purposes, the cathode region which connects the arc column to the cathode surface is generally described in terms of an ionization zone (or presheath) and a cathode sheath (or cathode space charge zone) (Benilov and Marotta 1995, Hsu and Pfender 1983, Lowke *et al* 1992, Rethfeld *et al* 1996, and Zhou and Heberlein 1994). The presheath is responsible for the formation of charged particles while the cathode sheath is responsible for the important electric phenomena of the cathode region. The overall thickness of the cathode region is of the order of 10^2-10^3 Debye lengths (λ_D is ~10^{-8} m in an Ar plasma at atmospheric pressure).

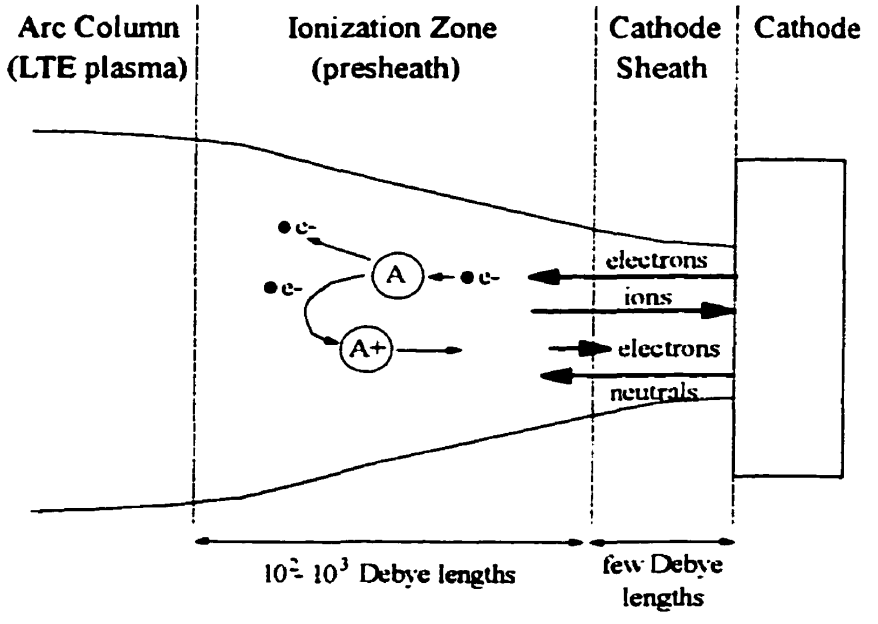

FIGURE 2.1.1. General representation of a high pressure arc attachment region on a hot, thermionically emitting cathode (cathode region).

The establishment of the self-sustaining arc column from the emission of electrons from the cathode surface can be described by the following scenario. The electrons extracted from the cathode (beam electrons) under the action of the high surface temperatures and electric field strengths travel without collision in the cathode sheath, and start to ionize the filling gas atoms (and ions), or vapors emitted from the cathode, in the presheath. Further collisions inducing ionization, charge exchange, recombination, energy exchange, occur among charged and neutral particles in the presheath, and an electrically charged volume is maintained in kinetic (collisional) equilibrium. Radial diffusion (ambipolar diffusion) occurs towards to cold walls of the discharges causing losses of charged particles from the hot core of the discharge. If the strength of the electron source at the cathode is high enough to maintain the sufficient ionization in the presheath needed to assume the current transfer in between the two electrodes and to compensate for the radial diffusion losses, the arc discharge will be self-sustaining. Obviously, the cathode plays the important role of maintaining the sufficient electron emission but, the plasma of the presheath plays, on the other hand, the important role of maintaining the favorable conditions for strong electron emission from the cathode. It is on the way to achieve the self-sustaining operating conditions that refractory and non-refractory cathodes exposed to a high pressure arc differ strongly as will be seen in this thesis.

In terms of current transport, the following important charge carriers can be identified in the cathode region: 1) The electrons emitted from the cathode. 2) The ions formed in the presheath and accelerated towards the negative cathode surface. These ions are responsible for the maintenance of a high cathode surface temperature upon ion bombardment. 3) Some plasma electrons reach the cathode surface by retro-diffusion in the adverse potential gradient and contribute only weakly to the current transfer. The attraction of the ions by the negative cathode (with respect to the plasma potential), and the repulsion of the plasma electrons induce the formation of a net positive charge in the cathode sheath (so-called 'space charge'). Such a space charge is responsible for the establishment of the high surface electric field strengths.

The cathode region shows an important constriction due to the gradual change from gaseous conduction in the arc column to metallic conduction of electricity in the cathode. The current densities in the arc column are of some 10^3 A m^{-2} and considerably increase to values larger than 10^7 A m^{-2} at the arc foot on the cathode. Important gradients of all quantities occur in the cathode region as it can be seen with the schematic representation of figure 2.1.2. The temperatures, particle number densities and voltage show important drops as one gets closer to the cathode. The voltage drop in the presheath is usually low in comparison to the one in the cathode sheath (1 to 2 V in comparison to 8-15 V in the cathode sheath, e.g. Zhou and Heberlein 1994, fig. 11). As a result, it is sometimes assumed that all the cathode voltage drop occurs in the cathode sheath (e.g. Hamilton and Guile 1968).

The important decrease of the potential in the cathode region is responsible for the formation of large electric field gradients; the electric field strength is ~10^3 V m^{-1} in the LTE plasma and exceeds 10^7-10^8 V m^{-1} at the cathode surface. Due to the increasing local electric field observed as one goes towards the cathode (increasing ratio E/p, Boulos *et al* 1994, chap. 1), deviations from LTE appear and the plasma conditions are no longer defined by a unique temperature. Even closer to the cathode, the concept of temperature losses its sense due to the assumption of a collisionless cathode sheath. In terms of these temperatures, the heavy species temperature strongly decreases in the cathode region to accommodate the cathode surface temperature, while the beam electrons, all emitted with a single energy, thermalize after collisions with the different components of the plasma gas forming the presheath (electron beam relaxation).

The respective boundaries separating the important zones of the cathode region are defined as follows: The boundary shared by the cathode sheath and the presheath (so-called 'cathode sheath edge') is located at a distance x_c from the cathode surface where the electron (n_e) and ion (n_i) densities start to differ, while the boundary shared by the LTE plasma of the arc column and the presheath is defined where the electron (T_e) and heavy species (T_h) temperatures start to differ.

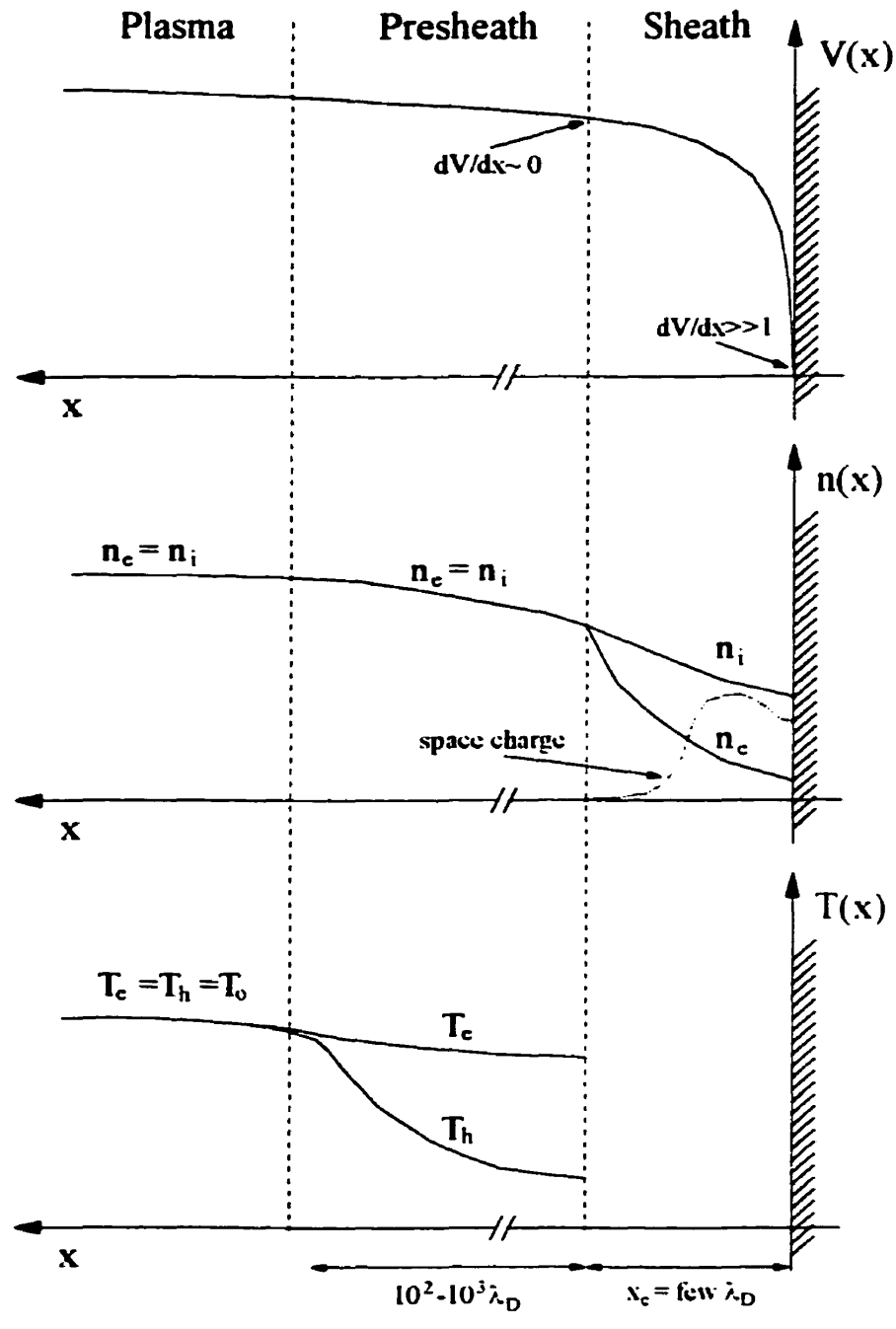

FIGURE 2.1.2. Schematic representation of the voltage, particle number density and temperature distributions in the cathode region of a high pressure arc on an emitting cathode (adapted from Roth 1995, fig. 9.21).

Depending on the electric field strengths and temperatures that are maintained at the cathode surface mainly by the ions bombarding the cathode and maintaining the space

charge, the electrons will be extracted from the cathode in the thermionic (10^7-10^8 V m^{-1}), thermo-field (10^8-10^{10} V m^{-1}) or field emission regime (>10^{10} V m^{-1}) as is discussed in the next section (section 2.2).

2.2. Electron Emission from the Cathode

The accurate calculation of the flux of electrons emitted from the cathode surface is crucial since these electrons carry a dominant fraction of the total current to the cathode surface. However, after almost 100 years of research in the field (starting with Richardson 1901), the theory of electron emission from the cathodes of electric arcs is still incomplete due to the complexity of the phenomena involved in the cathode region. For instance, Guile (1971) reported at least eight mechanisms allowing electron transfer from the conduction band of the metal to the arc. Fortunately, not all of them are dominant.

For a clean metallic cathode, only three parameters govern the electron emission processes from its surface: 1) its temperature (T_s), 2) the macroscopic surface electric field strength (E_s), and 3) the presence of ions in the cathode region. The geometry of the emitter and the presence of a thin film covering the surface, microimpurities embedded in the cathode surface and adsorbates will also influence the electron emission, but to a negligible extent for the conditions prevailing under the attachment point on the cathode (reasons discussed in section 4.1). When only the temperature effect is concerned (low surface electric field and low ion density and charge), the electron current is accurately predicted by the Richardson-Dushman equation for thermionic emission which reads:

$$j_{RD}(T_s,\phi) = \frac{4\pi e m_e (k_B T_s)^2}{h^3} \exp\left(-\frac{e\phi}{k_B T_s}\right) \qquad (2.2.1)$$

where ϕ is the cathode material work function. Electron emission by a pure electric field effect is described by the Fowler-Nordheim equation for field emission (Fowler and Nordheim 1928). When thermal and electric field effects combine, the electrons are being emitted in the so-called 'thermo-field' (T-F) regime (Lee 1959). The theory of T-F

electron emission has been developed by Murphy and Good (1956) and Christov (1966) and proved valid for a wide range of temperatures and electric field strengths by Christov and Vodenicharov (1968). In arc-cathode systems, the high temperatures and high electric field strengths needed for thermo-field emission are mainly maintained by the ions present in the cathode region. Such ions heat up the cathode by bombardment and generate the important electric field at the cathode surface by formation of a space charge (previous section).

Until recently, the local modification of the potential 'experienced' by the electrons outside the metal surface due to the presence of a high density of ions was not considered. As it was shown theoretically by Gayet *et al* (1996) and Spataru *et al* (1997), the thermo-field emission current is further enhanced when a density of ions n_i larger than $\sim 10^{24}$ m^{-3} is present in the cathode region. Such high densities of ions are encountered in cathode spots (Jüttner 1987), but also in the cathode region of high pressure arcs on refractory cathodes when $p>>1$ atm (Schmidt and Speckhofer 1996).

The respective effects of these three main parameters on the emission processes can be visualized with the help of figure 2.2.1 which shows the one-dimensional potential energy curve for an electron outside the metal surface for three cases: 1) thermionic emission (dotted line), 2) thermo-field emission (long dashes), and 3) ion-enhanced thermo-field emission (continuous line). The respective equations allowing to calculate the emitted electron current density for the three cases are now presented in the next three sections (sections 2.2.1-2.2.3). The effects of protusion, adsorbates and thin films are discussed in sections 2.2.4 and 2.2.5.

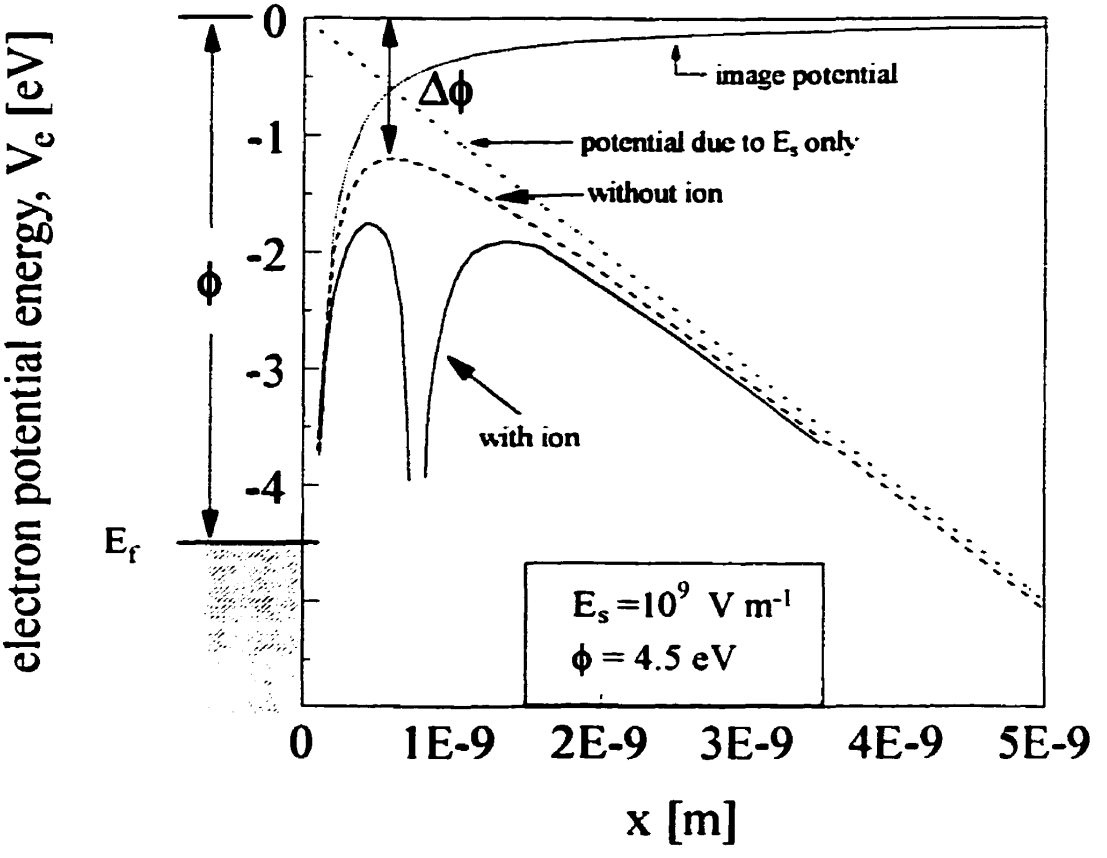

FIGURE 2.2.1. Schematic representation of the 1-dimensional potential experienced by the electrons outside the metal surface. Thermionic emission (short dashes), thermo-field emission (long dashes), and ion-enhanced thermo-field emission (continuous line).

2.2.1. Field-Enhanced Thermionic Emission

Thermionic emission from the surface occurs when an electron from the top of the conduction band (Fermi level, E_f) gains enough energy by thermal agitation to overcome the classical potential barrier at the surface. The height of the potential barrier corresponds to the material work function ϕ. The potential energy of the electron at a distance x outside the metal surface is described by the classical image potential:

$$V_e(x) = -\frac{e^2}{16\pi\varepsilon_o x} \qquad (2.2.2)$$

and the current density of thermionic electrons calculated using the Richardson-Dushman relation (equation (2.2.1)). High surface electric fields induce a reduction of the height of the potential barrier at the metal surface by an amount $\Delta\phi=(eE_s/4\pi\varepsilon_o)^{1/2}$, allowing an easier thermal promotion of the electrons above it. This effect is known as the Schottky effect. In the presence of a macroscopic surface electric field E_s, the electron potential outside the metal surface takes the form:

$$V_e(x) = -\frac{e^2}{16\pi\varepsilon_o x} - eE_s x \tag{2.2.3}$$

and the Richardson-Dushman equation for thermionic emission once corrected for the Schottky effect reads:

$$j_{T-F}^{FEE}(E_s, T_s, \phi) = \frac{4\pi e m_e (k_B T_s)^2}{h^3} \exp\left(-\frac{e(\phi - \Delta\phi)}{k_B T_s}\right) \tag{2.2.4}$$

The last equation, more commonly called the field-enhanced thermionic equation, is generally used in modeling the arc-cathode interactions with refractory cathodes where the surface temperatures are high (T_s>3500 K) and the surface electric field strengths relatively low (E_s<10^8 V m^{-1}) (e.g. Benilov and Marotta 1995, Lowke *et al* 1992, Rethfeld *et al* 1996, and Zhou and Heberlein 1994). Its simplicity makes its treatment easy.

2.2.2. Murphy and Good Formalism for Thermo-Field Emission

When the surface electric field strengths become higher than ~10^8 V m^{-1}, the field-enhanced thermionic equation becomes inappropriate since the electrons are now being emitted not only by thermal promotion above the potential barrier of height $\phi-\Delta\phi$ at the metal surface, but also by quantum tunneling across the barrier. According to Murphy and Good (1956), the thermo-field emission current density j_{T-F}^{MG} is related to the temperature of the emitter T_s, the surface electric field strength E_s, and emitter work function ϕ by:

$$j_{T-F}^{MG}(E_s, T_s, \phi) = e \int_{-W_a}^{\infty} D(E_s, W)\, N(W, T_s, \phi)\, dW \qquad (2.2.5)$$

where $-W_a$ is the effective potential of the electrons inside the metal surface ($-W_a$ ~10 eV), $D(E_s, W)$ the electron tunneling probability across the barrier, and $N(W, T_s, \phi)\, dW$, the number of Fermi-Dirac distributed electrons having energies between W and $W+dW$ and incident on the barrier per unit of time and surface area. The result of the numerical integration of equation (2.2.5) using the technique presented in Appendix A for ϕ=4.5 eV is presented in figure 2.2.2.

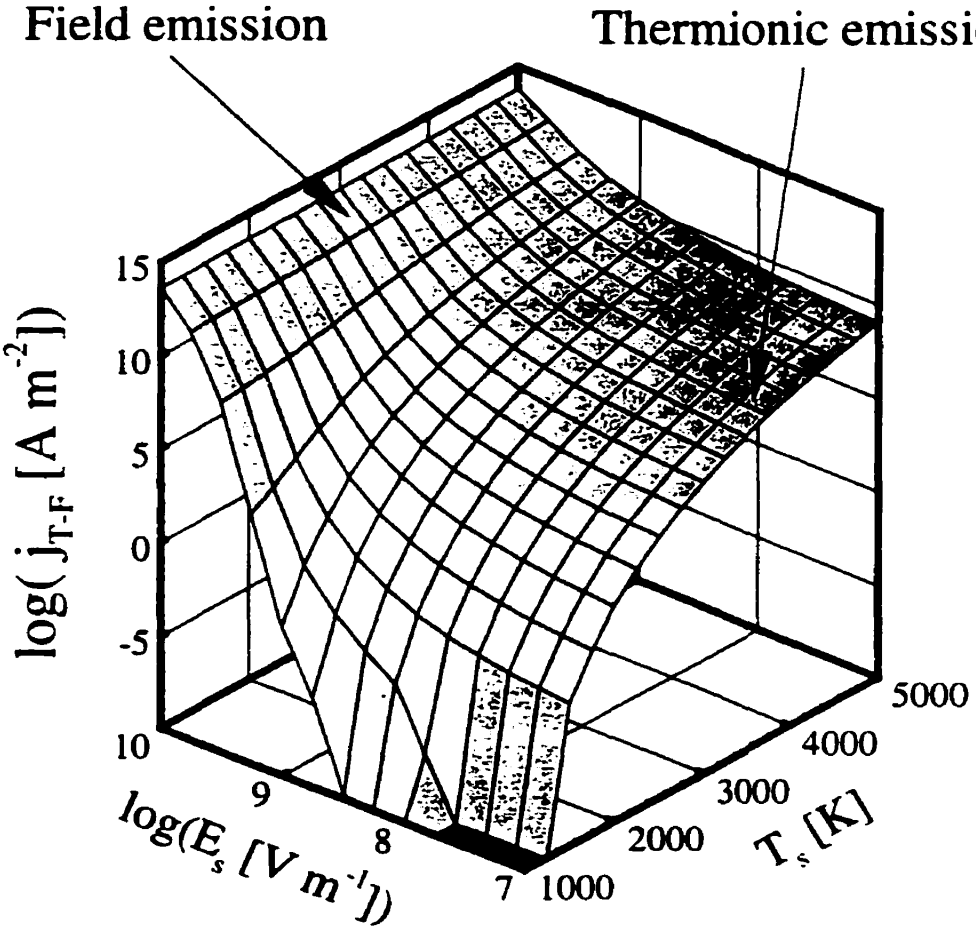

FIGURE 2.2.2. Thermo-field emission electron current density predicted by the Murphy and Good equations (j_{T-F}^{MG}) in the T_s-log(E_s) plane for ϕ=4.5 eV.

The thermo-field emission current density tends to become independent from the electric field E_s for small fields (thermionic emission) and independent from the temperature T_s for large fields (field or cold emission). The formalism of Murphy and Good (1956) accounts accurately for the thermo-field emission current for electric field strengths up to 10^{10} V m^{-1} (Miller and Good 1953), but its treatment is much more complex than the simple field-enhanced thermionic equation due to the number of numerical integrals necessary to perform. Note finally that equation (2.2.1) is a limiting case of equation (2.2.5) for $E_s \rightarrow 0$ (Appendix B).

2.2.3. Effects of Slowly Moving Ions

The approach of slowly moving ions (free moving) in the close vicinity of the metal surface (few angstroms) favors two mechanisms of ion-assisted electron emission by modification of the surface potential barrier (concept schematically represented in figure 2.2.1 by the potential well): 1) A non-resonant process which is simply the enhancement of the tunneling probability across the barrier due to the reduction of the barrier height, and 2) a resonant process attributable to the formation of a quasi-stationary bound state for the electron outside the metal surface upon temporary neutralization with the incoming ion (Gayet *et al* 1996 and Spataru *et al* 1997). In this process, the potential barrier formed by the macroscopic electric field is momentarily split into two thinner barriers having much higher transition probabilities for electron tunneling. These two electron extraction processes were known to occur in the cathode region of arcs since the 60's (Guile 1971 and references therein), but to our knowledge, no accurate calculations of their mean enhancement effects on the electron current density have been carried out until recently by Gayet *et al* (1996) and Spataru *et al* (1997).

Gayet *et al* (1996) defined a convenient mean ion-enhancement factor β as the ratio of the thermo-field emission current in the presence of ions to the thermo-field emission current in the absence of ions (equation (2.2.5)). Taking into account this ion-enhancement effect, the thermo-field emission current density is now defined as:

$$j_{T-F}^{MG-I}(E_s,T_s,\phi,n_i,z_i)=\beta(E_s,T_s,n_i,z_i)\,j_{T-F}^{MG}(E_s,T_s,\phi) \qquad (2.2.6)$$

Calculations made by Gayet *et al* (1996) for H^- and H^{2+} ions approaching a Cu cathode exposed to a macroscopic electric field strength $E_s=10^9$ V m^{-1} suggest that the enhancement of the T-F emission current sets for cathode surface temperatures below 4000 K or ion densities above 10^{24} m^{-3} (Table 2.2.1). This enhancement factor is shown to depend strongly on the surface temperature T_s, ion density n_i and charge z_i, and weakly on the nature of the metal (at least for Al, W and Cu), the nature of the ion incident on the surface, and the surface electric field E_s for values ~10^9 V m^{-1}.

TABLE 2.2.1. Calculated averaged ion-enhancement factor β for H^- ions (protons) slowly moving in the close vicinity of a Cu cathode with $E_s=10^9$ V m^{-1}. Values in parentheses were calculated for alpha particles*.

	Temperature [K]			
ion density, n_i ($\times 10^{24}$ m^{-3})	2000	2500	3000	3500
81	212 (12769)	38.6 (849)	15 (162.5)	8.6 (55.5)
8.6	30 (1828)	6 (115)	3 (22.6)	2 (8.5)
2.5	9.8 (543)	2.6 (35)	1.7 (7.6)	1.4 (3.4)
1.1	4.8 (230)	1.7 (15)	1.3 (4)	1.2 (2)

*: data taken from Gayet *et al* (1996)

2.2.4. Effects of Protusions

Sharp asperities and protusions present at the surface of the cathode are known to enhance the electron emission current due to local enhancement of the surface electric field (Farrall 1980). Field-enhancement of the electron emission current by 10^2 to 10^3 are commonly encountered with needle-shaped tip of field-emission electron guns used for instance in FEGSEM (field-emission gun scanning electron microscope). This enhancement phenomenon has an important effect during the cathode spot ignition processes (section 2.3.7), but becomes negligible under a burning spot where the surface is relatively plane (Hull 1962).

2.2.5. Effects of Adsorbates, Microimpurities and Thin Films

Adsorbates present at the metal surface have almost the same effect as the slowly moving ions on the electron emission current: they make available energy states for the electrons outside the metal surface which favor electron emission by the tunneling effect (Duke and Alferieff 1967). The adsorbates are generally weakly bound to the surface and easily desorbed by the thermal action of the arc. Therefore, adsorbates probably play an important role only during the ignition process of the cathode spot (section 2.3.7).

Semiconducting and insulating microimpurities embedded in the cathode surface along cracks or grain boundaries (Allen *et al* 1979) and thin films covering large areas of the cathode surface significantly enhance the electron emission (Guile and Hitchcock 1975). Such enhancement effects have been thoroughly studied in the context of vacuum insulation where they are considered harmful since they reduce the minimum electric field strengths needed for breakdown on pure metals ($\sim 10^6$ V m^{-1} rather than $\sim 3 \times 10^9$ V m^{-1}) (Latham 1983 and Halbritter 1985). Like the adsorbates, such coatings are also thought to play an important role in the cathode spot ignition process (Haworth 1950, Hancox 1960). However, since films are generally more strongly bound to the surface than adsorbates, the arc might be attached to the metallic cathode through these films, at least for a while.

The theory of electron emission across metal-semiconductor barriers (so-called Schottky barriers) was developed in the 60's (e.g. Crowell and Sze 1966 and Padovani and Stratton 1966) and its complex description is far beyond the scope of this thesis. For metal-insulator barriers, the mechanism leading to electron emission is schematically represented in figure 2.2.3 (inspired from Guile and Hitchcock 1975). An insulating layer of some nm (<10 nm) covering the cathode surface is being charged by the positive ions drifting from the plasma. These unneutralized positive ions charge the oxide surface and are responsible for the establishment of an electrostatic electric field across the oxide film (dielectric) causing electron emission by tunneling.

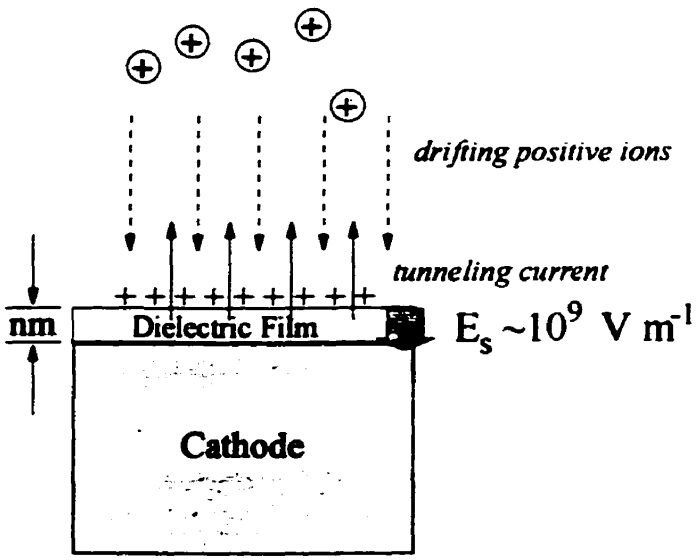

FIGURE 2.2.3. Schematic representation of the electrostatic electric field establishment across a thin insulating (dielectric) film on the cathode and the electron emission process.

The high electric field strengths necessary for strong field electron emission across the dielectric (>10^9 V m^{-1}) are established in a relatively short period of time when exposed to the ions drifting from a plasma. Actually, the time τ necessary to establish a field E across the dielectric film is (equation obtained assuming a constant electrid field across the dielectric):

$$\tau = \frac{E\varepsilon_o\varepsilon_r}{j_{ion} f} \qquad (2.2.7)$$

where f is the fraction of the ion flux j_{ion} that sticks on the surface of the dielectric and ε_r, the dielectric constant of the film. Taking for example a Cu_2O dielectric exposed to an atmospheric pressure Ar + Cu plasma of temperature T_o and assuming that 1% of the ions stick on the surface (f=0.01), the typical time scale required to charge the dielectric surface until a field E=2x10^9 V m^{-1} is less than 10 ms as it can be seen with figure 2.2.4. For the regions containing an important amount of Cu vapors (lets say 1-10 %), this time scale is less than a ms. Such a time scale is less than the typical residence time of the arc at

a given location for magnetically driven arcs rotating on non-refractory cathodes (point discussed later in section 2.3).

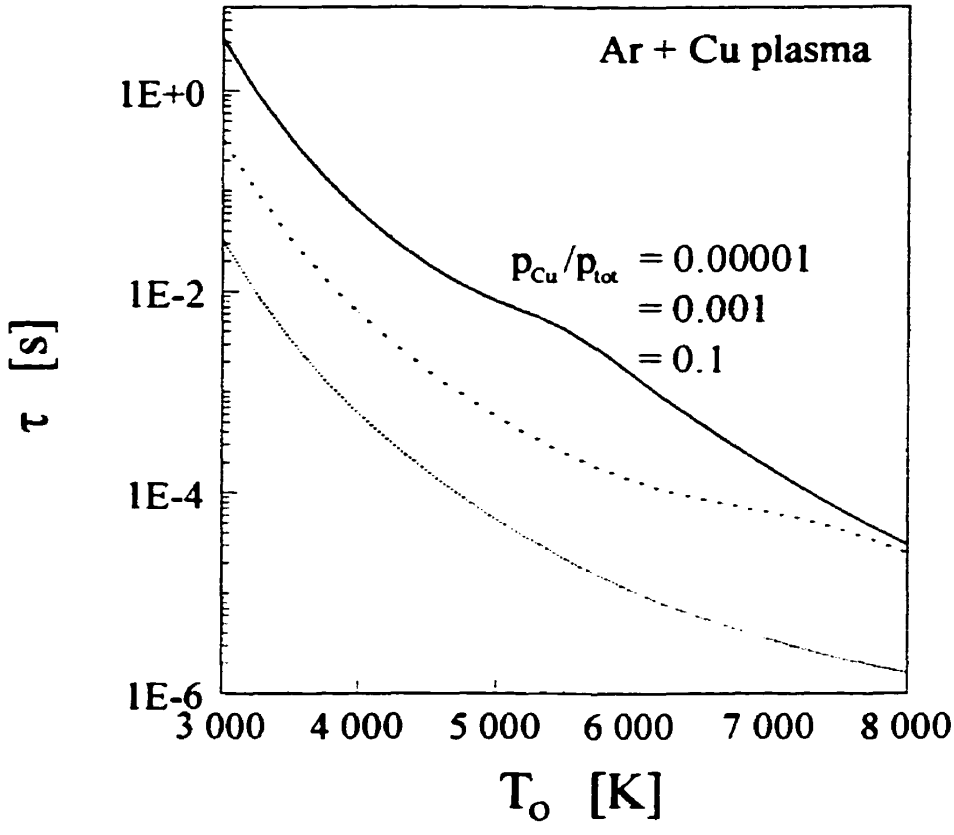

FIGURE 2.2.4. Time necessary to charge a Cu_2O dielectric (ε_r=7.1) until establishment of a film electric field of $2x10^9$ V m^{-1} with f=0.01 and for several fractions p_{Cu}/p_{tot} in an Ar + Cu plasma (T_o=LTE plasma temperature) (Based on our calculations).

2.2.6. Nottingham Effect

The emission of electrons from the cathode surface is associated with an energy exchange with the lattice; depending whether the energy of the emitted electron is higher or lower than the energy of the replacing electron coming from the external circuit, the electron emission is associated with a cooling or heating effect (Nottingham effect, Nottingham 1941; the equations necessary to calculate the Nottingham energy exchange term are presented later in section 4.3.3). Under the conditions encountered at the cathode surface of electric arcs, the emission of electrons results in a cooling effect for the cathode.

Only during the iniation phase of an arc on an initially cold cathode is the Nottingham heating observed. This phenomenon is fundamental in the arc ignition process as it will be discussed in section 2.3.7.

2.3. Attachment of High Pressure Arcs on Non-Refractory Cathodes

2.3.1. General Observations

High pressure arcs burning on non-refractory cathodes such as copper show the emission of metallic vapor bursts which induce fluctuations of the arc parameters such as the arc voltage, temperature and species densities (Desaulniers-Soucy and Meunier 1995b). The erosion of copper cathodes is important as shown by the measurement using the cathode weight loss method (Szente 1989 and Kwak 1994). An important quantity of copper fume entrained by the plasma gas condenses on the reactor walls as a powder (Kwak 1994). Due to the high erosion rates observed, the arc root of such systems is usually put into rotation to reduce the local thermal loads which cause erosion (Munz *et al* 1992).

At atmospheric pressure, the arc root moves by a succession of random jumps in the direction induced by the external magnetic field (Amperian motion) as observed with rapid photography (Szente 1989). For a pure Cu cathode in a pure argon plasma, the arc root remains at a given location on the cathode for a long period (some ms) before making a jump over a large distance to another site. It is shown that the ease at which the arc root is moved to a new attachment region on the cathode is related to the cathode ability to emit electrons (Munz *et al* 1992). As studied by Szente (1989), the addition of reactive molecular gases such as CO and N_2 to the inert plasma gas (e.g. argon) results in a smoother and faster movement of the arc and a lower erosion rate. The same phenomenon was observed by Kim *et al* (1995) where the addition of N_2 to a low pressure argon arc moving on a Ti cathode resulted in an abrupt reduction of the cathode erosion rate when a TiN film formed. Such reactive gases are thought to form adsorbates, microimpurities or possibly thin films upon contact (or reaction) with the cathode and become sites showing a high probability of arc ignition. As it was calculated in section 2.2.5, such films charge

quickly when exposed to the ions drifting from the plasma, and become high electron emission sources where new arc attachment points are ignited.

Some typical results obtained for copper cathodes in a magnetically rotated arc system (system illustrated in figure 3.1.1.) by Szente *et al* (1994), Desaulniers-Soucy and Meunier (1995a) and Kwak and Munz (1996) are reported in Table 2.3.1. For all these experiments the arc current was set equal to 100 A, the external magnetic field to 0.1 T, and the total gas flow rate to 20 L min^{-1}. The electrode spacing was 4 mm.

TABLE 2.3.1. Erosion results obtained for a magnetically rotated arc between two concentric electrodes. Anode material: Copper.

Cathode Material	Gas	V_{arc} [V]	v_{arc} [m s^{-1}]	E_r [µg C^{-1}]	n_{CuI} [2] [m^{-3}]
Cu [1]	Ar	44	2	13.5	n.d.
Cu [1]	Ar+0.3%vol. N_2	38	34	3.0	$6x10^{21}$
Cu [1]	Ar+0.1%vol. CO	22	75	0.4	$5x10^{20}$
Cu+10%W [1]	Ar	30	50	6.0	n.d.
Cu+10%Nb [1]	Ar	26	60	0.6	n.d.
Cu+10%Ni [3]	Ar	44	7.1	4.8	n.d.

[1]: from Szente *et al* (1994)
[2]: Desaulniers-Soucy and Meunier (1995a) at 1 mm from the cathode.
[3]: from Kwak and Munz (1996)

A few important remarks have to be made concerning the results presented in Table 2.3.1 since they will be discussed later in the thesis:

i) There exists a direct relationship between the cathode erosion rate and the number density of Cu atoms (CuI) present in the plasma close to the cathode (Meunier and Desaulniers-Soucy 1994). This suggests that erosion is an atomic process such as vaporization.

ii) The value of 22 V for the arc voltage in an Ar+0.1%vol. CO plasma mixture on Cu electrodes is slightly lower than the value of 23 V for the sum of the cathode and anode voltage drops obtained by Hamilton and Guile (1968) using a similar setup but with a pure Ar plasma on Cu electrodes. This observation suggests that the voltage drops at the electrodes are reduced when oxide layers are formed. It is however most probably the cathode region which sees its voltage drop decreasing due to an easier electron emission process (section 2.2.5). This phenomenon is not observed with N_2 since copper does not form strong nitride films like TiN on Ti cathodes. Electronically excited or dissociated nitrogen chemisorbs on copper as an atomic species to form a stable Cu_3N structure (observed on Cu(110) by Baddorf and Zehner 1990) which is however completely desorbed at 800 K.

iii) Copper composite cathodes show lower erosion rates and burning arc voltages, and higher arc root velocities when compared to copper cathodes. The wide range of melting temperatures of the alloying element (1726 K for Ni, 2740 K for Nb and 3680 K for W) suggests that the reduction of the erosion rate is not due to the formation of a more refractory surface. It is probably more related to the presence of microimpurities embedded at grain boundaries and local enhancement of electric field which lead to an easier electron emission process (Allen *et al* 1979 and Hamilton and Guile 1968).

2.3.2. Fundamental Distinctions between Refractory and Non-Refractory Cathodes

Cathodes of high pressure electric arc systems are either classified as thermionic or nonthermionic electron emitters. Thermionic cathodes are made of refractory materials such as tungsten and can sustain the high temperatures needed for strong thermionic emission without strong melting or vaporization. On the other hand, nonthermionic cathodes made of non-refractory materials such as copper cannot sustain such high temperatures and a severe erosion is observed. The name nonthermionic comes from the fact that such cathodes are expected to emit electrons rather in the thermo-field or field emission regime. This distinction made between the two types of arc cathodes is clearly seen with figure 2.3.1 which presents the amount of atoms vaporized from the cathode

(equation (2.3.1)) per thermionic electron emitted (equation (2.2.1)) as a function of the cathode surface temperature. This ratio would represent the cathode 'ability' to operate in the thermionic range (the lower is the ratio $e\Gamma_{vap}/j_{RD}$, the higher is the 'ability').

The equation that relates the rate of vaporization to the cathode material vapor pressure reads (Zhou and Heberlein 1994):

$$\Gamma_{vap,i} = \frac{p_i}{4(m_i k_B T_s / 3)^{1/2}} \tag{2.3.1}$$

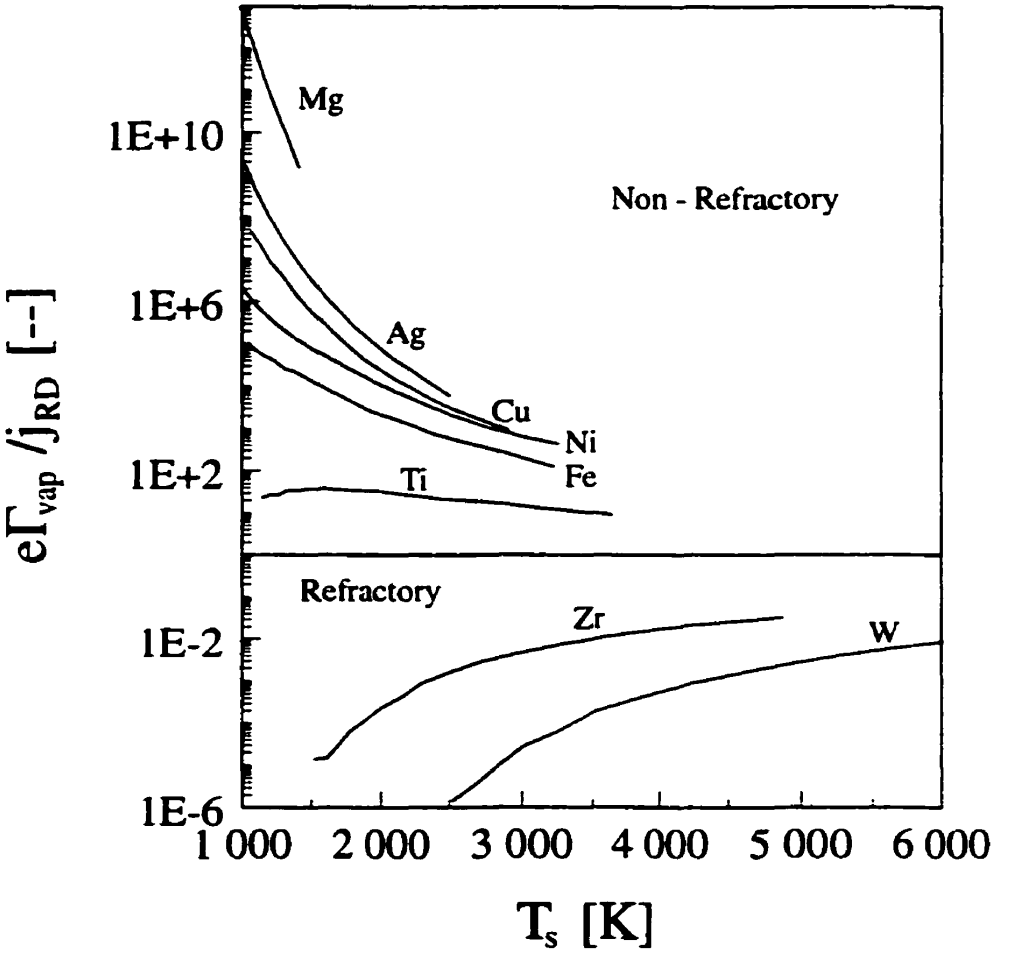

FIGURE 2.3.1. Calculated ratio of the flux of vaporized atoms (Γ_{vap}) to the flux of thermionic electrons (j_{RD}/e) as a function of the cathode surface temperature for different cathode materials.

According to figure 2.3.1, tungsten and copper which are commonly used as high pressure arc cathode materials, clearly represent the two extremes and therefore, considerably different behaviors for the arc attachment point(s) on the cathode are theoretically expected and experimentally observed. These different behaviors are summarized in Table 2.3.2.

TABLE 2.3.2. Estimated conditions and behaviors of the arc attachment point(s) for refractory and non-refractory cathodes of high pressure arcs.

Type of Cathode	Refractory	Non-Refractory
Other names	- Hot cathode - Thermionic cathode - High-boiling point cathode	- Cold cathode - Nonthermionic cathode - Low-boiling point cathode
Operating temperature[1]	>3500 K	Wide range, generally below 3000 K (if field emission prevails)
Current density[1]	10^{7}-10^{8} A m^{-2}	~10^{10}-10^{11} A m^{-2}
Mechanism of electron emission	Thermionic emission	Field or thermo-field emission
Number of attachment points	One and diffuse over some mm	Several and constricted over 5-20 μm
Movement of the arc attachment point(s)[1]	Fixed or limited displacement	Rapid
Excess pressure above the cathode[1]	No evidence	Evidenced by depression of liquid metal

[1]:data taken from Guile (1971), Table 2.

2.3.3. Crater Formation: Time Scale and Current Density

Another basic feature that differentiates the arc attachment on non-refractory cathodes from refractory cathodes is the formation of craters which suggest an important constriction of the arc foot. Indeed, the characteristic trace left by the arc foot on a refractory cathode is rather a gross melting of the surface (Zhou *et al* 1996). Figure 2.3.2 shows a scanning electron micrograph (SEM) of the surface of a copper cathode arced by

a magnetically rotated, atmospheric pressure argon arc operated at a current of 100 A for 30 sec (schematic of the arc chamber represented in figure 3.1.1). Observation of the cathode surface reveals an important number of craters of ~5-10 μm-diameter and some of up to 25 μm-diameter uniformly distributed along the trace left by the arc (arc groove) showing that liquid volumes are formed and displaced to some extent forming craters with rims and splashes with sharp edges. Overlapping of the craters is due the numerous passages of the arc root at the same location (~600 rotations in 30 sec).

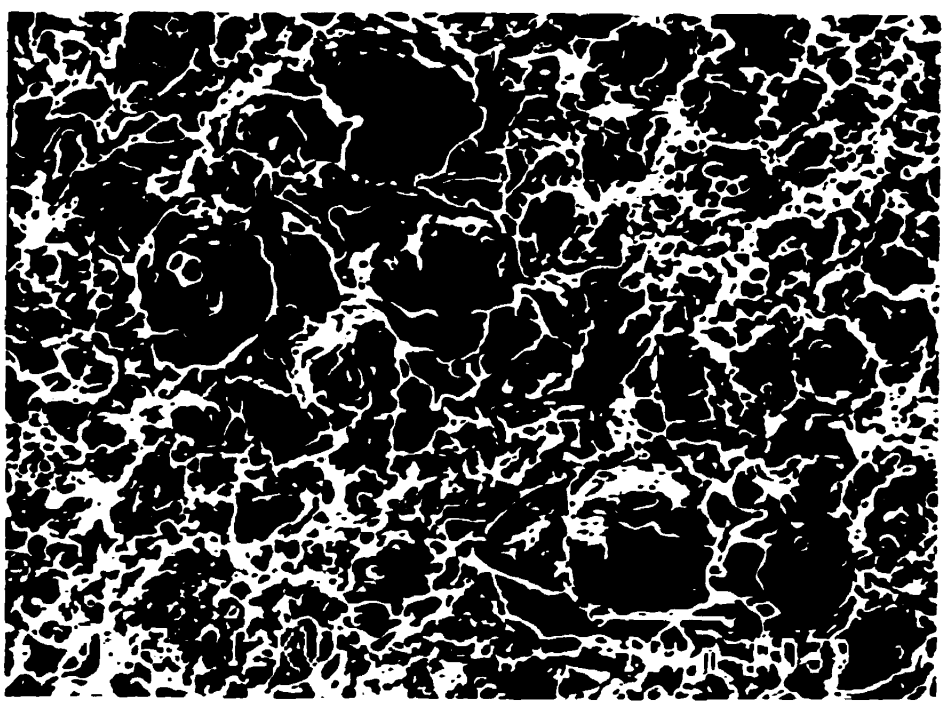

FIGURE 2.3.2. Scanning electron micrograph (SEM) of a Cu cathode surface arced by an atmospheric pressure argon arc operated at 100 A for 30 sec.

Contrary to refractory cathodes which show a relatively stable and diffuse attachment of the arc, the attachment of high pressure arcs on non-refractory cathodes is made of several highly constricted and dynamic structures 'dancing' over the surface (so-called 'cathode spots'). The voltage fluctuations of the arc are associated with the ignition and extinction of such structures (burst emission of metallic vapors, Desaulniers-Soucy

and Meunier 1995b). The craters left on the cathode are being formed in a time much less than the ms scale (probably at the μs scale, Tioursi and Haug 1997). Knowing that a heat flux of $2x10^9$ W m^{-2} brings a copper cathode to the vaporization temperature in about 10 ms (based on our calculations), considerably higher values for the heat flux are expected to form the craters. Liquid volume displacement from the crater is thought to be due to thermo-capillary convection within the liquid bath (Kharin 1992) or ion plasma pressure release (if any) upon extinction of the cathode spots (Gray and Pharney 1974). Thermo-capillary flows however require a minimum time to set on.

Indirect estimations of the current density at the arc foot of an atmospheric pressure argon arc on a copper cathode reveal values of j_{tot} ranging from $\sim 10^8$ A m^{-2} (Szente *et al* 1991) to $\sim 10^9$ A m^{-2} (Marotta and Sharakhovsky 1996) when the measurement method does not allow a resolution of the internal structure of the attachment region (resolution >100 μm). Actually, these values for the current density are representative of the arc root itself. Measurements allowing a resolution of the internal structure of the arc attachment region (e.g. voltage fluctuations combined with crater size estimations, Tioursi and Haug 1997) reveal current densities per cathode spot of $8x10^{10}$ and $6.4x10^{11}$ A m^{-2}, respectively for non-refractory Ag and Au cathodes. Such high current densities per cathode spot were also estimated, but not to the same degree of accuracy, by Szente *et al* (1991) who obtained values ranging from 10^{10} to 10^{11} A m^{-2} for Cu cathodes (same range reported by Guile 1971). Estimations of the current carried per each copper cathode spot at atmospheric pressure range from 0.7 A (Drouet 1985 and references therein) to 2-20 A (Guile 1971). According to these estimations for Cu, an arc carrying a total current of 100 A would have 5-150 active cathode spots. It is generally assumed that the crater corresponds to the current transfer region and that the current density is constant over the crater radius. There is however no definitive proof of these assumptions (this discussion will be continued in chapter 6).

The concept of an internal structure for the arc attachment region on the cathode surface is represented on figure 2.3.3. which shows the estimated existence area for the

cathode spot traces left on the copper cathode of figure 2.3.2. The arc attachment is made of macrospots carrying a current density of the order of 10^8-10^9 A m^{-2} which themselves are composed of several cathode spots (or subspots) of 5-10 μm-diameter. The number of momentary active macrospots for this system is 1-2 as observed with a high speed camera (Szente 1989). As it can be seen with figure 2.3.3, the current density per cathode spot under those conditions ranges approximately from $5x10^9$ to 10^{11} A m^{-2}. The existence time of a macrospot or simply, the residence time of the arc at a given location, is much higher than the typical existence time of a cathode spot (ms compared to μs). Thus, the number of cathode spots forming the arc attachment is constantly changing in time.

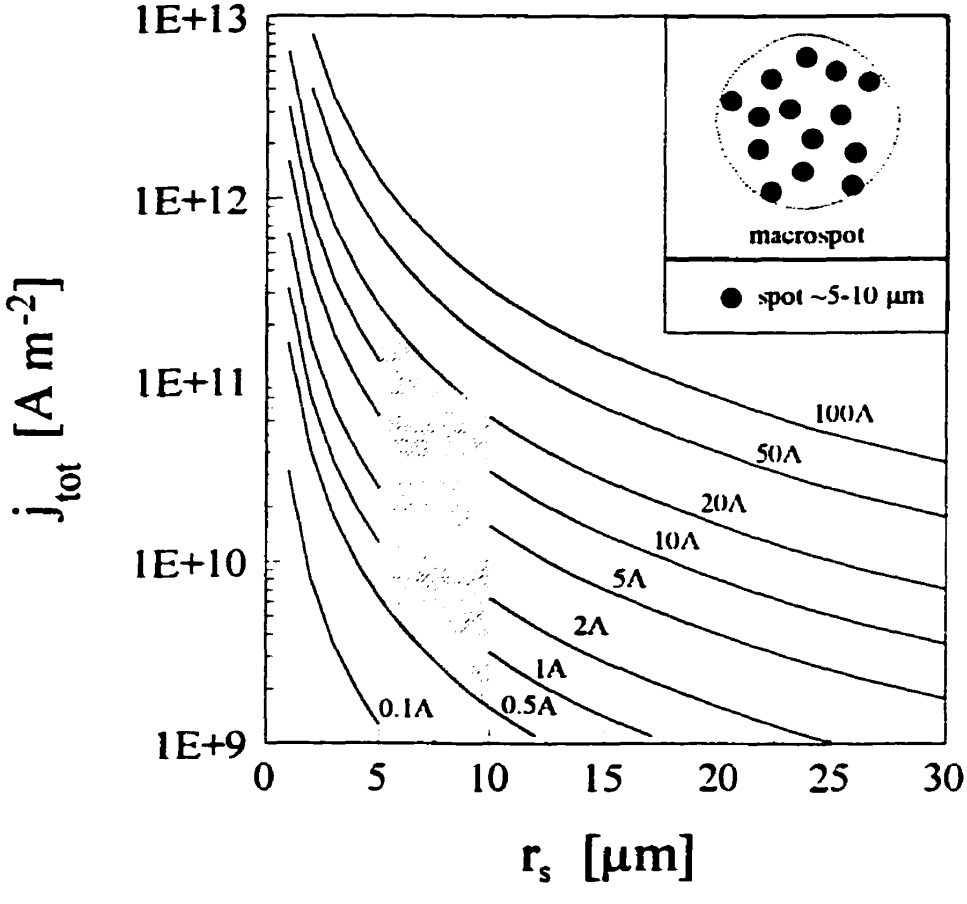

FIGURE 2.3.3. Estimated total current density per spot j_{tot} on a Cu cathode arced by an atmospheric pressure Ar arc (figure 2.3.2) as a function of the observed crater radius r_s (spot radius) for several values of the current per spot I_s. Insert: Schematic of the arc attachment region. Shaded area: Estimated existence area for the current density (Based on our calculations).

2.3.4. Limitations of the Actual Models

Any model attempting to describe the interactions of a high pressure arc with a non-refractory copper cathode must successfully explain the following experimental observations:

1) Current densities per cathode spot exceeding $5x10^9$ A m^{-2} for pure copper cathodes.

Such high current densities cannot be accounted for by the actual models developed for refractory cathodes even if one assumes that the cathode surface is boiling. For instance, a boiling copper cathode operating at atmospheric pressure would have a surface temperature T_s=2836 K and a vapor pressure p_{Cu}=1 atm (101325 Pa). Simple calculations using the Murphy and Good equation for thermo-field emission (equation (2.2.5) or figure 2.2.2) show that, for such a surface temperature, the surface electric field strength needed to account for a current density of $5x10^9$ A m^{-2} by electron emission alone is E_s=$2.8x10^9$ V m^{-1}. Such a high value for E_s would induce field emission of electrons which is inconceivable at atmospheric pressure due to a too low ion density in the cathode region. Indeed, a solution of the Poisson's equation in the cathode sheath using the method described by Prewett and Allen (1976) allows to obtain a value for E_s which is barely of $2.8x10^8$ V m^{-1} for V_c=15 V (estimated cathode sheath voltage drop on a Cu cathode. Kesaev 1965).

The other solution is to assume that all the current is carried by the ions. Simple calculations using equation (2.3.1) and assuming that all the atoms vaporized from the cathode surface are ionized and accelerated back towards the cathode by the cathode voltage drop allow to obtain a maximum ion current density j_{ion} of $\sim 10^8$ A m^{-2}, which value is by far too low. Indeed, even if the ion current had been sufficient, this idea would be still debatable since one cannot justify such a high flux of ions without a high flux of electrons (the beam electrons are responsible for the generation of ions by ionization in the presheath). Furthermore, calculations of the total incoming heat flux to the cathode surface using a standard model for refractory cathodes (e.g. Rethfeld *et al* 1996 and Zhou and

Heberlein 1994) show that the predicted incoming heat flux (mainly due to ion bombardment) is too low ($\sim 10^9$ W m^{-2}) to maintain the cathode surface at its boiling temperature (T_s=2836 K) under steady state conditions due to the important conduction losses in a copper cathode. A solution would be to have a cathode voltage drop much larger than 15 V (close to 100 V), but it is known that an atmospheric pressure argon arc burning between two copper electrodes is self-sustaining for an arc voltage of 23 V only (Hamilton and Guile 1968).

2) The formation of liquid volumes and craters on a copper cathode in a μs-time scale.

Heat fluxes larger than 10^{10} W m^{-2} are necessary to form liquid volumes in the μs time scale (based on our own calculations reported in Chapter 7). Such high values are around one order of magnitude larger than what is predicted at atmospheric pressure using the refractory arc cathode models. Also, the formation of depressions within the craters by expulsion of liquid matter cannot be attributed only to the onset of important liquid movements by the thermo-capillary forces for the time scale considered (Kharin 1992). The possibility of a local excess pressure must be considered.

Due to these experimental observations and the simple calculations just mentioned, the application without modifications of the models developed for refractory cathodes to non-refractory cathodes is doubtful. Previous attempts to do so showed difficulties such as predictions of cathode surface temperatures exceeding 4900 K for copper (Durgapal 1993) or showed the impossibility of predicting the conditions prevailing in the cathode region when vaporization can no longer be neglected. For instance, Morrow and Lowke (1993) limited their study to the calculation of the current density necessary to bring a copper cathode to its melting temperature. Most of the other studies related to the arc attachment on non-refractory cathodes were oriented towards a macroscopic description of the arc movement and/or heat transfer to the cathode, and therefore, no information relating the conditions prevailing within the cathode region could be inferred (e.g. Milos and Shepard 1994, Testé *et al* 1995 and Marotta and Sharakhovsky 1996).

2.3.5. The Concept of High Local Pressure

As concluded by Guile (1971), it seems that the self-sustaining operation of an high pressure arc on a non-refractory cathode is possible only if some destruction of the cathode surface occurs. The presence of a high density of metallic vapors in the cathode region would have the effect of maintaining a high ion bombardment and a high surface electric field which in turn, would allow a high current density (both ion and electron emission currents). In such a scenario a pressure build up would naturally occur upon cathode spot ignition (Schwirzke *et al* 1993) and would be maintained by the synergetic effects of high ion bombardment heating, and high vaporization. Like the vacuum arc cathode spot, the cathode region of a high pressure arc on a non-refractory cathode would be composed of a high density metallic vapor plasma formed by vaporization of the cathode. The conditions within the cathode region allowing a self-sustaining operation of the arc would be those satisfaying the energy balance at the cathode surface and allowing the emitted electrons to maintain sufficient ionization in the cathode region (so-called 'conditions for a self-sustaining arc' discussed in Chapter 4).

The concept of pressure excess was also introduced to explain the high current densities observed in the cathode region of high intensity arcs where the current is of some kA's (Maecker 1955, Cobine and Burger 1955 and Lee 1959). However, in such high current arcs, the pressure excess (build up) is created by the self-magnetic pinch effect (Maecker effect, Maecker 1955) associated with the high current and high current densities at the arc foot, and not by the cathode vaporization process itself. For instances, a high current, atmospheric pressure arc (1 atm) operating at 10 000 A and having a current density of 10^9 A m^{-2} at a refractory cathode would induce a self-magnetic pinch pressure p_M ($p_M = \mu_o I_s j_{tot} / 4\pi$, Boulos *et al* 1994) of ~10 atm (1 Mpa) balanced out by the kinetic plasma pressure in the cathode region. In such a case, the self-magnetic pinch pressure is the source of a high local pressure above the cathode. On the other hand, for a low current, atmospheric pressure arc (1 atm) on a non-refractory Cu cathode, even if one assumes high values for the current and current density per cathode spot of respectively 50 A and 10^{10} A m^{-2}, the pressure excess associated with the self-magnetic pinch remains low

(p_M ~0.5 atm (50 kPa)). Model calculations assuming a metallic plasma pressure of 1.5 atm allow a current density of barely $3x10^8$ A m^{-2}, which is almost two orders of magnitude below the current density associated with p_M=0.5 atm. In such a case, the self-magnetic pinch pressure cannot be responsible for the high local pressure.

2.3.6. Similarities with Vacuum Arc Cathode Spots

The concept of high local pressure in the cathode region is well-known to people investigating the vacuum arc cathode spots. Local metallic vapor pressures exceeding 10 atm are estimated for copper (Jüttner 1985) and it is known that the self-maintenance of the unipolar vacuum arc is assumed by this dense plasma region.

The vacuum cathode spots are usually grouped under two categories (Anders and Anders 1991): Type 1 spots show a rapid movement (10-100 m s^{-1}), a low erosion rate (0.1-10 μg C^{-1}), small crater radii (<1 μm), and low current per spot (<<1 A). Such spots occur on contaminated surfaces (oxide layers). Type 2 spots show a slower movement (0.1-1 m s^{-1}), a much higher erosion rate (30-100 μg C^{-1}), large craters radii (5-20 μm), and a high current per spot (2-20 A, Siemroth 1995). Such spots occur on clean metallic surfaces. The cathode spots of high pressure arcs on clean non-refractory cathodes (figure 2.3.2) have strong similarities with vacuum cathode spots of type 2. The erosion rate for type 2 cathode spots is however higher than what is observed at atmospheric pressure, but some effects that are not present under vacuum could have to be considered (neutral redeposition for instance). Typical current densities per spot reported in the literature show a broad range from 10^8 to 10^{12} A m^{-2} (Siemroth 1995).

These similarities were also observed by Kimblin (1974) and Emtage (1975) while studying the cathode spot structure in the transition from vacuum to atmospheric pressure. The explanation of Kimblin (1974) was that, since the local pressure within the cathode spot is high (several atmospheres), the internal spot behavior is not likely to be disturbed for ambient pressures up to atmospheric. Indeed, the behavior of the cathode spots on clean copper cathodes seem not to be affected until an ambient gas pressure of around 11

atm is reached (Guile 1971 and references therein). The radius of the plasma ball forming the cathode spot is however strongly reduced as the ambient gas pressure increases (Meunier and Drouet 1987).

This concept of a correspondence between the vacuum arc cathode spots and high pressure arc cathode spots suggests that their behavior can be described for the whole ambient pressure range by a unique model. It is known that the diffuse attachment of an atmospheric pressure arc on a tungsten cathode does not show any excess pressure. Therefore, for tungsten, the transition from constricted high pressure cathode spot in vacuum to the diffuse attachment at atmospheric pressure must occur somewhere between vacuum and 1 atm (0.1 MPa). For copper, this ambient gas pressure where the transition occurs is probably well above atmospheric, if such a transition occurs.

2.3.7. Cathode Spot Ignition

This last section of the chapter is a review of the actual knowledge of the mechanisms leading to the ignition of new arc attachment points on the cathode surface, or simply the cathode spot ignition processes. Figure 2.3.4 is used for the following description.

The ignition of an arc discharge between two electrodes requires an electrical breakdown; the formation of an electrically conducting channel between the two electrodes (concept valid at any pressure). This breakdown occurs when an electron flux emitted from the cathode is maintained for a sufficiently long time to allow the onset of ionization of the filling gas and the establishment of a self-sustaining arc. For the first ignition event of the discharge, the cathode is cold (300 K) and no significant thermionic emission from the surface occurs (see figure 2.2.2). Field emission of electrons is then induced by generating a giant voltage pulse across the interelectrode gap which momentary establishes a large surface electric field at the cathode. Onset of field emission on pure metal cold cathodes (300 K) occurs for $E_s \sim 3 \times 10^9$ V m^{-1}, but due to the presence of impurities at the surface, field emission is observed for much lower values of E_s ($\sim 10^6$ V

m^{-1}) (Latham 1983). Practical experiences show that a pulse of ~20 kV is sufficient to ignite an electric arc in argon with an interelectrode gap of 4 mm (E ~$5x10^6$ V m^{-1}).

Under vacuum conditions, where no filling gas is present in the chamber, a microvolume underneath the cathode surface heats up by resistive Joule heating and by the Nottingham heating associated with the field emission of electrons (He and Haug 1997) until it explodes within some tens of ns forming a high density metallic plasma, or cathode spot (Schwirzke *et al* 1993). This mechanism of spot ignition by microexplosion of cathode material or the 'ecton' formation mechanism was described by Mesyats (1995). Light emission from localized spots on the cathode (cathode spot formation) is observed prior to the electric breakdown confirming this idea of a high density plasma (Hurley and Dooley 1978, Mentel *et al* 1994 and Nachtigall and Mentel 1991). The breakdown events occur at localized areas on the cathode surface showing insulating impurities or sharp protusions (field-enhancement effects).

When ions are already present in the interelectrode gap (ions produced by a burning spot in the close vicinity of the new ignition site), the ignition of a new conducting channel is easier and less destructive (Schmoll and Hartmann 1997 and He and Haug 1997). These ions heat up the cathode by bombardment allowing thermionic emission of electrons. Due to this thermionic emission, the intensity of the electric field required for cathode spot ignition decreases with the increasing ion current. These ions also charge up insulating layers present at the cathode surface favoring electron emission (section 2.2.5).

As discussed by Schmoll and Hartmann (1997), two limiting cases can then be identified for the onset of breakdown and formation of cathode spots: 1) the non-stationary, fast explosive destruction of the emitter corresponding to the field emission-dominated ignition (time scale of some tens of ns), and 2) the quasi-stationary thermionic emission with slow evaporation and pressure buildup induced by a high ion current (time scale > μs). The regime of breakdown and new spot formation in the close vicinity of a

burning spot will be located in between these two extremes depending on the conditions external to the burning spot (plasma density).

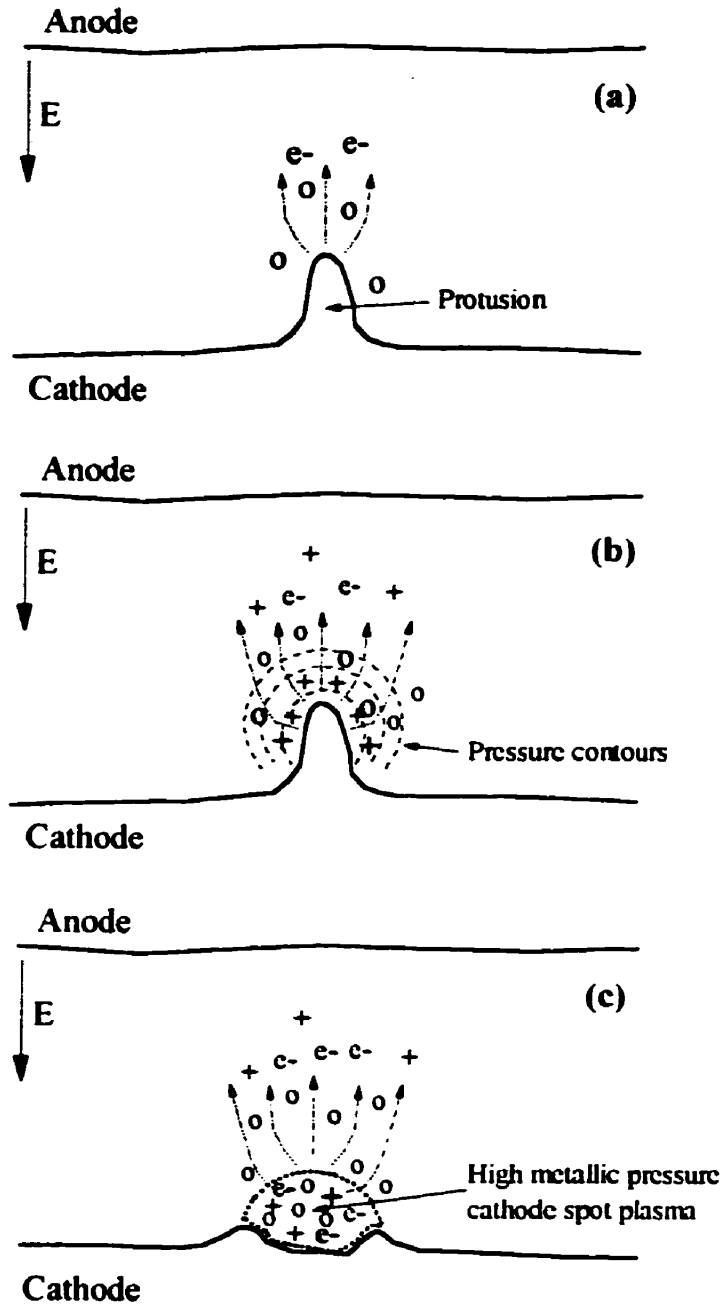

FIGURE 2.3.4. Schematic representation of the ignition process for a new arc attachment point on the cathode surface. (a) Heating of the protusion by Joule and Nottingham heating; field-emission of electrons. (b) Pressure build up; surface heating by ion bombardment, Joule and Nottingham heating; enhancement of electric field due to the ions. (c) Operating spot.

Desorbed neutral atoms from the cathode are also thought to play an important role under vacuum conditions since they provide material which, upon ionization, help establishing the discharge channel (Schwirzke *et al* 1993). At high chamber pressures, the adsorption of gas atoms on the cathode rather helps forming a high surface density of localized regions showing high probability for spot ignition (Szente 1989).

CHAPTER 3

SEM SURFACE ANALYSIS

3.1. Introduction

In this chapter, the surface morphology of Cu and Ti cathodes having been exposed to a high pressure electric arc (1.1 atm) was analyzed in order to identify the different modes of arc attachment on the cathode and to estimate the size of the arc attachment points. Two different arc attachment modes are observed on such cathodes: 1) constricted arc attachment on impurities and/or surface layers made of oxides or nitrides giving rise to small crater diameters (<μm-size) and low erosion rates, and 2) constricted arc attachment on clean metallic surfaces which gives rise to the formation of large craters (>μm-size) and high erosion rates. The transition from one mode of attachment to the other is discussed and some general comments are made concerning the relationship that exists between the mode of arc attachment and the erosion rate.

3.2. Preparation of the Cathodes

3.2.1. Equipment and Materials

The electric arc system used in this study is essentially the same as the one used by Kwak (1994) for cathode erosion studies and is schematically represented in figure 3.1.1. It basically consists of a non-transferred arc in a cylindrical geometry simulating conventional cold electrode plasma torches. The arc is put into rotation with the help of a magnetic coil surrounding the arc chamber. The electrodes and reactor walls are strongly water-cooled. The spacing between the two electrodes is 4.0 mm. The plasma gases are injected through the bottom of the chamber at low velocity in order not to deflect the arc, and collected at the top of the chamber before being re-directed to an exhaust. The arc is struck at the nearest distance between the two electrodes. An alumina paste covers the

anode water leads in order to prevent arcing elsewhere. The cathode assembly was designed to accommodate standard 38.1 mm-OD tubing for convenience.

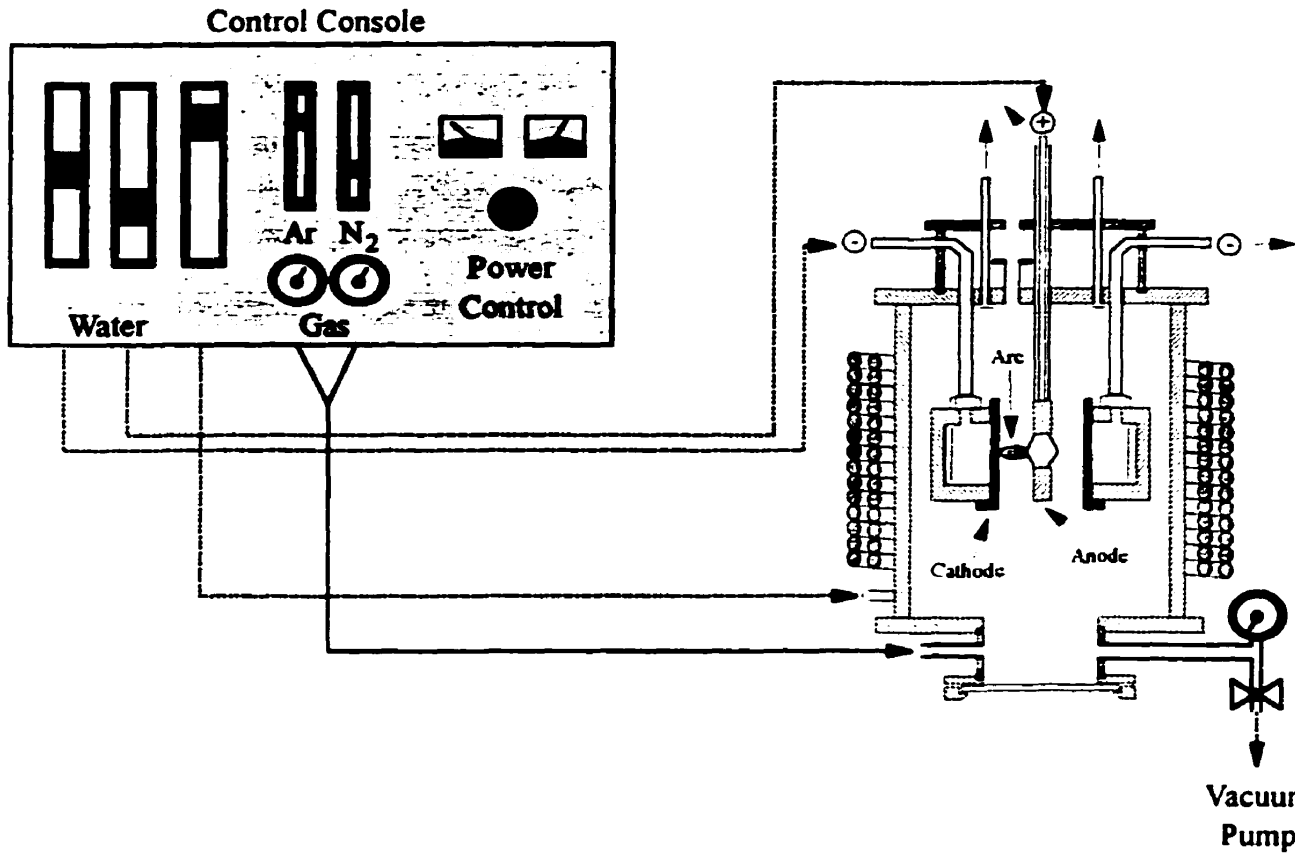

FIGURE 3.2.1. Schematic representation of the erosion test chamber and auxiliary equipment.

Electric power is delivered to the arc using a series of 4 Miller SRH-444 power supplies giving an open circuit voltage of 320 V and a maximum power of 80 kW. The arc is ignited by adding a high frequency pulse (MHz) of several kV to the open circuit voltage using a Miller HF-250-1 arc starter. The current delivered to the arc is monitored by measuring the voltage drop across a calibrated 50Ω-500A resistor connected in series with the grounded cathode. A Syntron P0063 DC power supply is used to deliver the current to the water-cooled magnetic coil surrounding the arc chamber.

High purity argon (99.999%) was used as the main plasma gas. High purity nitrogen was used for the experiments involving contamination of the cathode material. Two cathode materials have been used: OFHC copper and welded ASME SB338 titanium 38.1 mm-OD tubings. The anode was made of electrolytic copper.

3.2.2. Experimental Conditions and Procedures

Before any experiment, the top-flange assembly holding the cathode was disassembled from the reactor for cleaning and installation of a new cathode. At that time, all the powder and dust deposited on the reactor walls were taken off. The new cathodes were cleaned for 10-15 min in a dilute nitric acid solution in order to remove the oxides and other surface contaminants. The test cathodes were finally rinsed with water after the acid treatment and dried with a lint free paper before being mounted on the cathode holder. The cathode holder was then inserted in the reactor assembly and bolted. As soon as all the water and gas leads were connected, a mechanical pump was used to vacuum the reactor chamber from air. The time elapsed between mounting a clean cathode and pumping down the reactor was kept under 10 min to minimize oxide reformation. Water was then allowed to circulate in the reactor assembly and the rotameters adjusted to supply enough cooling. All the power supplies were then turned on and the current to the magnetic coil adjusted to generate a magnetic field strength on the axis of the cathode holder of 0.1 T. The mechanical pump was turned off and an argon flow of 20 L min^{-1} was maintained in the reactor by adjusting a regulation valve. The chamber pressure was adjusted to 1.1 atm to avoid air entrance from leaks (contamination). The water cooling indicators were all checked again and finally, the arc was ignited. The arc current was adjusted within less than 5 sec to its desired value of 100 A. At this moment, the flow of the contaminant gas, if any needed, was allowed and adjusted to the desired value. During the experiments, the arc current and water flow indicators were constantly checked for safety.

The arc was run for a determined period of time and extinguished by turning off the safety switch on the control panel. The flow of contaminant gas was quickly turned off

and the argon flow maintained during the cooling down period (~5 min) in order to maintain an oxygen-free atmosphere. After having turned off the power supplies, the cathode holder was disassembled from the reactor and the cathode taken off and stored.

Two plasma gas compositions were used in the present study: 1) pure argon and 2) argon contaminated with nitrogen (1% vol. N_2). The experiments in pure argon allow to observe the arc attachment in the transition from an initially contaminated cathode (native surface oxides) to a clean cathode. Indeed, even though great cares are taken during cleaning, one cannot eliminate reoxidation of the test cathodes during reassembling. Therefore, once ignited, the arc in pure argon is initially burning on a contaminated surface that progressively cleans up due to the thermal action of the arc. When the plasma gas is contaminated with nitrogen, contamination of the cathode surface is maintained. Indeed, both Cu and Ti are shown to react with activated nitrogen to form most probably layers of Cu_3N and TiN, respectively (most stable nitrides).

3.3. Observations

The observations of the cathode surface morphology after arcing were carried out using a JEOL JSM-840A scanning electron microscope (SEM). No special preparation of the sample was carried out except for drying and dust removal. Metallization of the surface was not necessary.

3.3.1. Pure Argon Plasma

The experiments carried out in pure argon plasmas showed an interesting behavior that was also observed by Kwak (1994). The time needed to reach steady state operation of the arc was ~30 sec for Cu and ~20 min for Ti, respectively. As discussed by Kwak (1994), this time scale needed to reach steady state operation is related to the time scale needed for a change in the mode of arc attachment; at and shortly after ignition, the arc is burning on an oxidized surface while after a given arcing period, the oxide is taken away by the thermal action of the arc root. The important difference between the time scales observed for Cu and Ti is probably related to the differences in the properties of the most

stable oxides formed. Indeed, the most stable oxide of Cu is Cu_2O with a formation energy ΔG of -350 kJ mol^{-1} and a melting temperature of 1500 K while these properties for the most stable oxide of Ti, Ti_3O_5, are respectively -3000 kJ mol^{-1} and 2450 K (Kwak 1994). Therefore, the arc attachment on an oxidized cathode surface is thought to be maintained for a longer period on Ti than on Cu. This is clearly shown in figures 3.3.1 through 3.3.3 giving the surface morphology of Cu and Ti cathodes as obtained with a scanning electron microscope (SEM). Figure 3.3.1 corresponds to the surface morphology of a Cu cathode having been exposed to the arc for 30 s; Figure 3.3.2. to a Ti cathode having been exposed for 30 s., Figure 3.3.3. to a Ti cathode having been exposed for 2 hours.

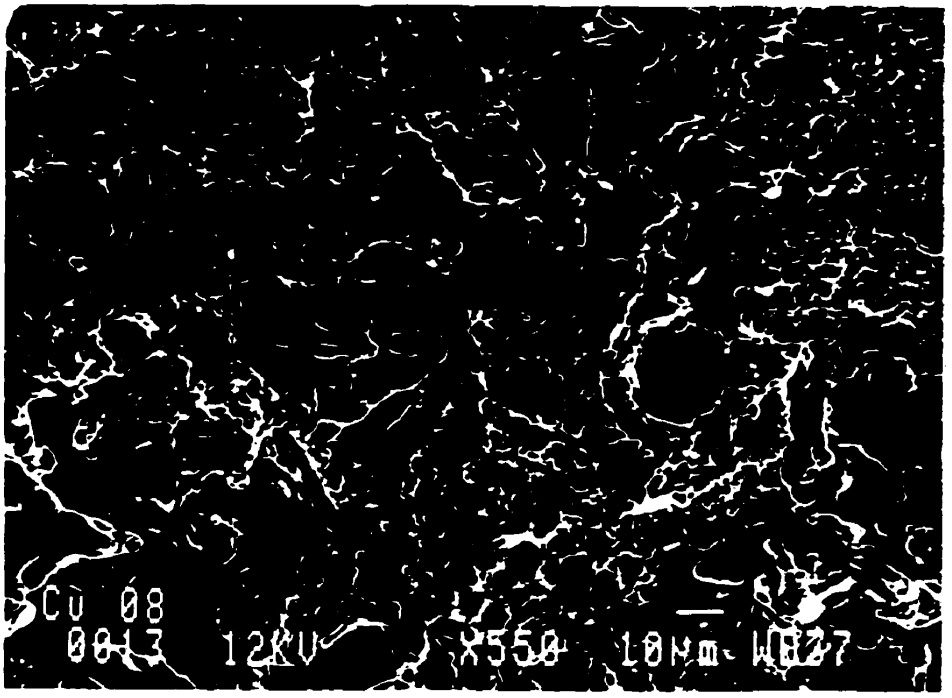

FIGURE 3.3.1. Surface morphology (SEM) of a Cu cathode having been exposed to a pure Ar plasma operating at 100 A for 30 s.

An important quantity of large craters is observed on the Cu cathode of figure 3.3.1. Displacements of liquid volumes are also observed. Typical crater radii range from 5 to 15 μm. It is however difficult to estimate their size accurately due to their overlapping.

Indeed, the arc made more than 500 rotations within this 30 s period at an average velocity of 2 m s^{-1} (Kwak 1994). An analysis of the cathode surface at a higher resolution revealed only a limited number of craters of dimension less than the μm-size. The large craters are characteristic of an arc burning on a clean cathode.

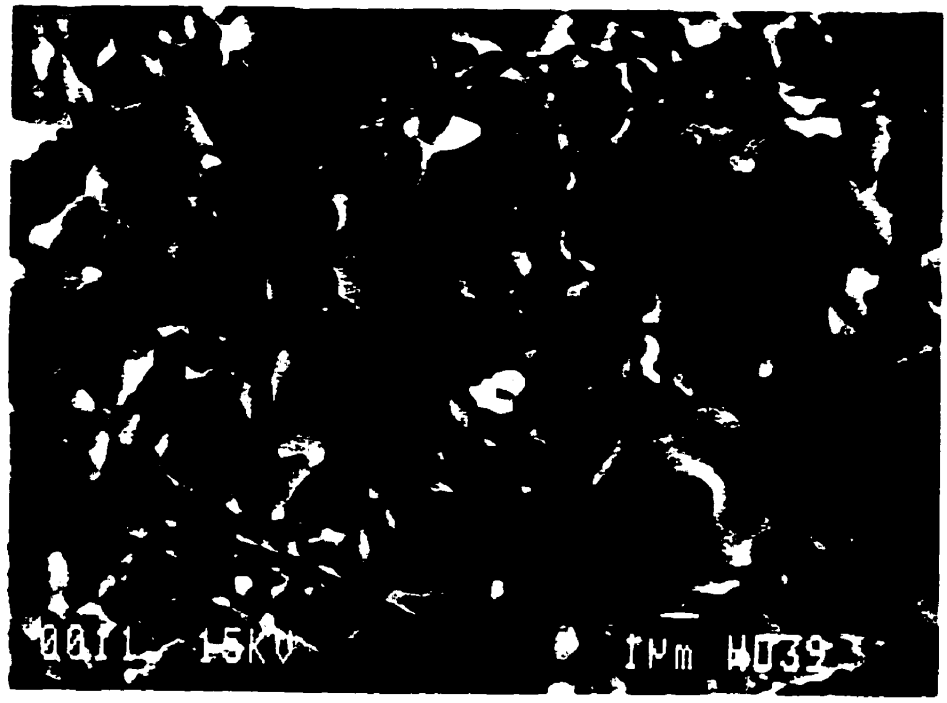

FIGURE 3.3.2. Surface morphology (SEM) of a Ti cathode having been exposed to a pure Ar plasma operating at 100 A for 30 s.

For Ti, the crater radii are less than 1 μm for a cathode having been exposed to the arc for 30 s (figure 3.3.2). No large craters are observed suggesting that the arc had burned on a contaminated surface for all that time. For much longer time periods, characteristic traces of an arc burning on a pure metallic surface start to appear as it can be seen with figure 3.3.3 where large craters are observed (10-20 μm-radius). However, small crater radii are still observed showing the presence of surface contaminants even after 2 hours of operation in a pure Ar plasma. As discussed by Kwak (1994), this might be due to the ppm concentration of oxygen in an Ar cylinder and the high reactivity of Ti with oxygen.

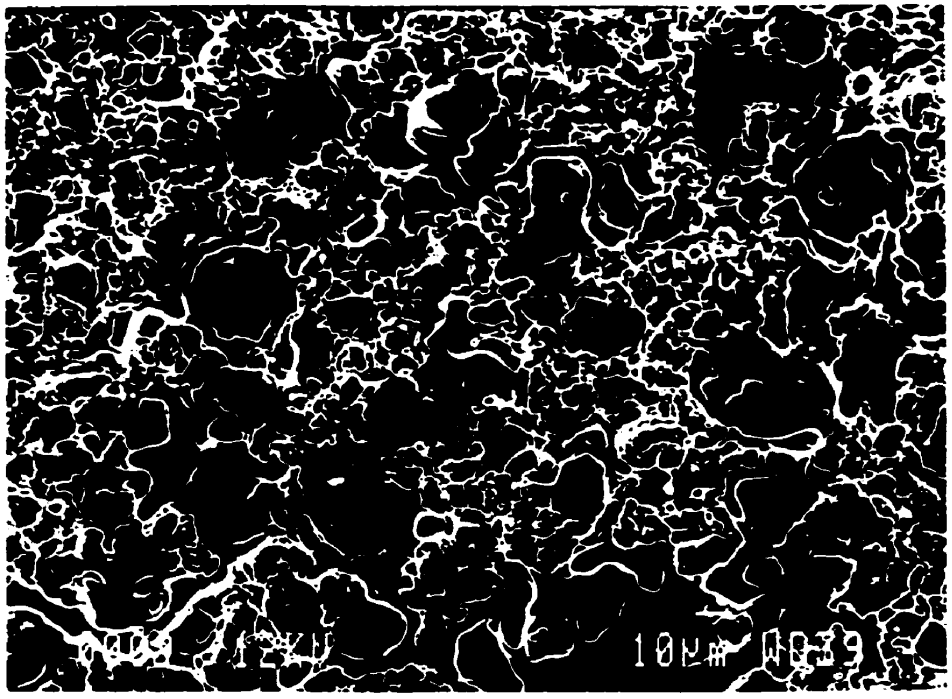

FIGURE 3.3.3. Surface morphology (SEM) of a Ti cathode having been exposed to a pure Ar plasma operating at 100 A for 2 hours.

3.3.2. Argon+Nitrogen Plasma

When low concentrations of a reactive gas is added to the inert plasma gas, surface contaminants appearing in the form of adsorbates, inclusions or thin films are permanently formed and taken off the cathode surface. The arc attachment on the cathode leaves small radius craters of dimension less than the μm-range, these being closely spaced as it can be seen with figures 3.3.4 and 3.3.5.

The arc behavior in the case of a Cu cathode exposed to an Ar+1%vol N_2 plasma was shown to remain stable for a long period of time showing that a dynamic equilibrium of formation and removal of the contaminants was achieved. In the case of Ti however, the arc became unstable after about 20 min of operation due to the formation of an insulating TiN layer (also observed by Kwak 1994) which is stable at high temperatures.

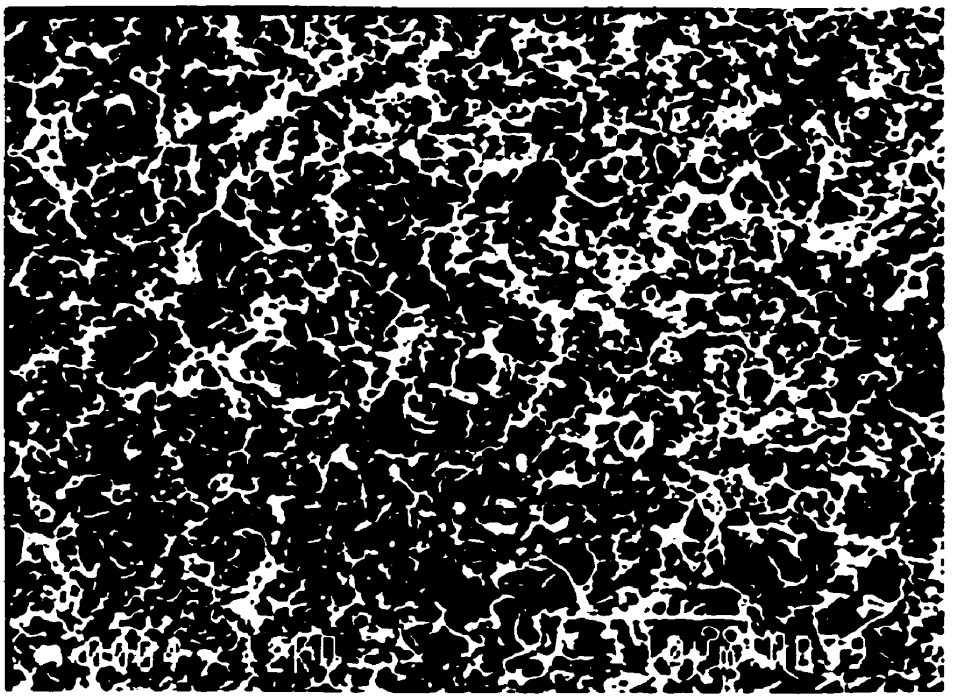

FIGURE 3.3.4. Surface morphology (SEM) of a Cu cathode having been exposed to an Ar+1%vol N_2 plasma operating at 100 A for 5 min.

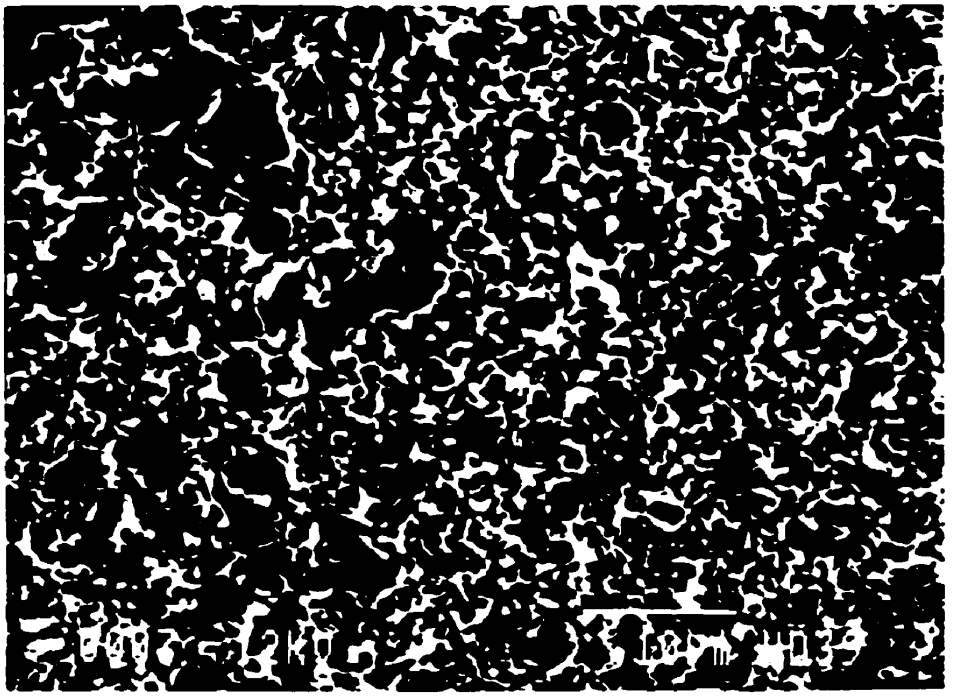

FIGURE 3.3.5. Surface morphology (SEM) of a Ti cathode having been exposed to an Ar+1%vol N_2 plasma operating at 100 A for 15 min.

3.4. Discussion and Conclusion

Two different types of arc attachment are observed for non-refractory cathodes exposed to high pressure arcs depending on the presence or not of surface contaminants. When contaminants are present, small craters of radius less than the μm-scale are left on the cathode while much larger craters are left on clean metallic cathodes (>5-10 μm). Such a behavior is also observed with vacuum arc cathode spots (Rakhovskii 1976). Arc attachment leaving small craters is associated with a low erosion rate. Actually, as reported in Table 2.3.1, the erosion rate of a Cu cathode is around 13.5 μg C^{-1} when exposed to an atmospheric pressure argon arc while this erosion rate decreases respectively to 3.0 and 0.4 μg C^{-1} when 1%vol of N_2 and CO is added to the inert argon gas (Table 2.3.1). The high density of small-radius craters left on the cathode surface lets suggest that the arc is maintained by a high frequency ignition of new cathode spots on contaminated sites. Such a mechanism of arc attachment leading to the formation of small-radius craters can be described by a three steps scenario:

1) As it was discussed in section 2.3.7, a high emission of electrons is possible from these contaminated sites without the need for the formation of the cathode spot plasma (high pressure plasma). The density of plasma ions coming from the ionization of the ambient gas atoms is sufficient to charge the dielectric surface within a time scale less than the residence time of the arc at a given location (see figure 2.2.4) and therefore, to allow the sufficient electron emission current. As long as no cathode spot plasma is formed, the erosion of the cathode is negligible since no vapors coming from the cathode erosion are needed for the current transfer.

2) The current transfer through the impurity sites is however associated with a high dissipation of heat by Joule heating due to the non-conductive nature of the dielectric impurities. Therefore, after a short period of time of high current transfer, the destruction of the emission sites might occur according to two scenarios: i) Explosion of the impurity inclusion or film due to an excessive Joule heating, or ii) by dielectric breakdown across the impurity layer that occurs due to the formation of charge carriers

at elevated temperatures. In both cases, an electrically-conducting channel is formed between the arc column and the metallic cathode.

3) A cathode spot plasma is formed. A large amount of vapors is then produced and liquid volume displacements occur. Once formed, the cathode spot burns for a short period only since much higher emission sites are present all around it and new emission centers are formed.

An estimation of the number of craters left on the Ti cathode of figure 3.3.2 allows to roughly calculate the number of arc attachment points that were active during an arc rotation. Indeed, the surface density of craters is ~0.2 μm^{-2} and the arc trace left on the cathode surface was about 5 mm-wide giving rise to approximately 10^8 craters on the surface (cathode inner radius of 34 mm). The velocity of the arc was about 8.7 m s^{-1} (Kwak 1994) and therefore, approximately $4x10^4$ craters were formed per arc rotation during the first 30 s of the arc establishment. This number is probably higher since the overlapping of the craters prevented an accurate calculation of their surface density. The same kind of calculations for the Cu cathode of figure 3.3.1 give roughly 10^3 craters per rotation during the first 30 s of the arc establishment. Such numbers, even though they are approximate in nature, give a rough idea of the dynamics of the arc attachment points on the surface of non-refractory cathodes. An interesting phenomenon is observed here: the number of craters formed on a Ti cathode is much larger than on a Cu cathode for the first 30 s of arcing in Ar. As it was said before, impurities are present at the surface of the Ti cathode for a long period of time comparatively to the Cu cathode which is cleaned in a time period probably much less than 30 s. Therefore, like for the vacuum arc on a contaminated surface, the attachment of a high pressure arc on a contaminated cathode surface is assumed by an important number of small cathode spots carrying a small current. As the surface gets cleaner, a transition in the arc attachment mode occurs from the mode characterized by numerous small cathode spots burning on impurity sites to a mode with only a limited number of cathode spots burning on a pure metallic surface. Such cathode spots cause a high cathode erosion and leave large craters on the cathode surface upon

extinction. The remaining of this thesis is dedicated to the development of a physical model of such cathode spots of high pressure arcs and on a theoretical estimation of their properties.

Note finally that surface contamination also plays an important role with refractory cathodes. For instance, zirconium (Zr) is known to be a low-erosion cathode for air plasma applications (Marotta 1991). This is probably due to the formation of a stable zirconium oxide at the cathode surface that helps electron emission according to the scenario discussed in section 2.2.5. Furthermore, Zr is probably a better material than W for such an application, even though the curves presented in figure 2.3.1 let suggest the contrary, since W makes a volatile oxide when reacting with oxygen (WO_3). Another example where contamination plays an important role is the voluntary addition of ThO_2 inclusions to W in order to form high emission sites on the cathode surface (so-called 'thoriated tungsten cathodes').

PART 2: MODELING STUDY

CHAPTER 4

DEVELOPMENT OF THE PHYSICAL MODEL

4.1. General Description and Assumptions

Due to the parallel made between the attachment of high pressure arcs on a non-refractory cathodes and the vacuum arc cathode spots (sections 2.3.5 and 2.3.6), the present model was inspired from the existing models of such cathode spots. The model combines the quasi-stationary vacuum arc model (Ecker 1980) for the concept of high local pressure, the snow-plow expansion model (Meunier 1990) for radius estimation, and the collisionless cathode sheath model developed for high pressure arcs interacting with non-vaporizing, refractory cathodes for the current and heat transfer to the cathode surface (Rethfeld *et al* 1996 and Zhou and Heberlein 1994). For the first time in such modeling studies, the enhancement of the thermo-field electron emission current induced by the presence of slowly moving ions in the cathode region was taken into account using the formalism of Josso (1997).

An electric arc is attached to a low boiling point cathode by one or several cathode spots which number depends on the arc current (figure 4.1.1). Each cathode spot has been ignited according to the scenario described in section 2.3.7 and expands into the ambient gas. During the expansion (initial expansion velocities of the plasma/gas boundary up to 10^4 m/s, Jüttner 1985), the state of the material within the cathode spot changes gradually from solid metal to liquid metal ($\sim 10^{28}$ m^{-3}), to a high pressure, two-temperature metallic plasma, and to a LTE metallic plasma at the hemisphere boundary (Anders *et al* 1992). Mass conservation of the expanding plasma suggests that the density of material in the cathode spot decreases with the square of the distance to the surface, i.e. $n(r)=n'/r^2$ (Jüttner 1985 and Meunier 1990). After its ignition period, the cathode spot plasma remains confined by the ambient gas within an hemisphere of radius smaller than the

millimeter scale until favorable conditions for the creation of a new one are encountered. The final radius of the hemispherical cathode spot can be calculated using the 'snow-plow' expansion model described by Meunier and Drouet (1987) and Meunier (1990). According to this model, a cathode spot plasma carrying a current of 10 A and expanding from a copper cathode into an atmospheric pressure argon plasma would have a final radius of ~0.37 mm.

The following assumptions are made in order to describe the cathode spot plasma region:

1) A quasi-stationary description is made for the cathode spot. After ignition of the spot (time scale < ns), it is assumed that the cathode spot plasma properties remain unchanged during the spot lifetime. Typical time scales for plasma processes ($\tau=\lambda_D/v_{th,e}$) for p=35 atm (3.5 MPa) and T_e=1 eV (11 600 K) are ~10^{-15} s, which values are considerably less than the time scales of spot existence (> ns to μs). On the other hand, the heat transfer within the cathode has to be treated in the fully time-dependent regime (Chapter 6) due to much larger time scales (same time scales as spot existence).

2) The ambient background gas has no effect on the internal cathode spot properties (Emtage 1975 and Jüttner 1987). Therefore, the conditions prevailing within the cathode spot and necessary for a self-sustaining arc attachment are independent of the conditions external to the spot. This is expected to be true for ambient gas pressures up to 11 atm (Guile 1971) for copper cathodes in an ambient argon atmosphere.

3) The liquid metal surface is in equilibrium with its vapor. Therefore, the cathode surface temperature under the spot is related to the metallic plasma pressure via a vapor-pressure curve, i.e. $T_s=T_s(p)$. This assumption allows to decouple the cathode sheath model describing the current and heat transfers from the plasma to the cathode surface from the heat transfer model in the cathode bulk.

4) The cathode spot might form on an impurity or a protusion according to the scenarios discussed in section 2.3.7 but, once it is formed, the cathode spot is burning on a pure metallic surface showing no curvature (Hull 1962).

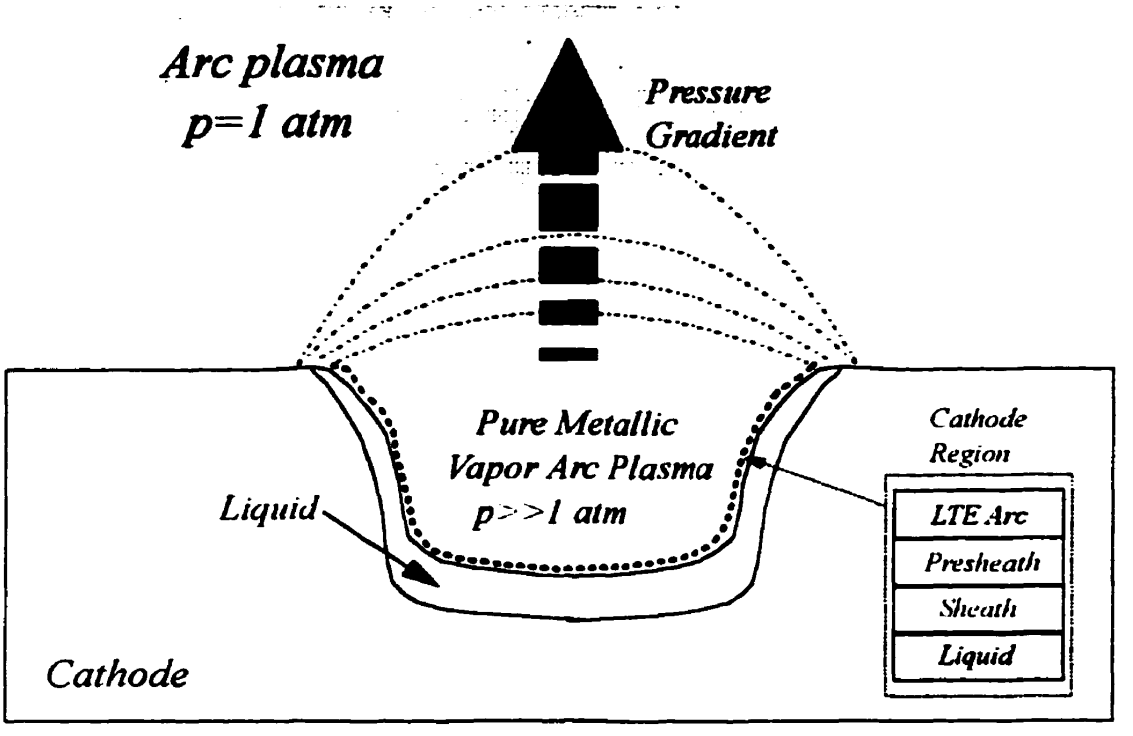

FIGURE 4.1.1. Schematic representation of the attachment region of a high pressure arc on an emitting non-refractory cathode.

5) The cathode region is described using the usual approach used for high pressure arcs interacting with refractory, non-vaporizing cathodes (Hsu and Pfender 1983, Zhou and Heberlein 1994, and Rethfeld *et al* 1996). This cathode region is composed of a cathode sheath and an ionization zone or presheath (figure 4.2.1).

6) A net positive space charge (cathode sheath) is formed in front of the cathode surface due to the presence, in different amounts, of three types of charge carrier: 1) the thermo-field electrons emitted by the cathode surface and carrying a current density $j_{T\text{-}F}$, 2) the ions generated by ionization in the presheath of the atoms vaporized from the cathode surface, these are accelerated back towards the cathode, and carry a current

density j_{ion}, and 3) the plasma electrons retro-diffusing towards the cathode surface and carrying a current density j_{bde}.

7) The cathode sheath is 1-dimensional since its thickness (a few λ_D) is much less than the cathode spot radius.

8) The cathode sheath is collisionless. No collisions involving momentum exchange among particles nor ionization, recombination or charge transfer occur in the cathode sheath. Thus the heavy species temperature is constant and equal to the cathode surface temperature throughout the cathode sheath (i.e. $T_s=T_s(p)=T_h^{sc}$), and the individual current densities are conserved. The collisionless assumption implies that the thickness of the cathode sheath x_c is smaller than any inelastic collision mean free paths involving particularly charged species:

$$\lambda_D < x_c < \lambda_{io} \text{ or } \lambda_{eo} \text{ or } \lambda_{ee} \text{ or } \lambda_{ei} \text{ or } \lambda_{ii} \qquad (4.1.1)$$

where the mean free path for collisions among particles a and b (o=neutral, i=ion, e=electron) is calculated using the relation:

$$\lambda_{ab} = \frac{1}{n_b \sigma_{ab}} \qquad (4.1.2)$$

9) The cathode sheath is described using the Bohm's model (Riemann 1991) which implies as a necessary and sufficient condition for the ions produced in the presheath to enter the cathode sheath at the local sound velocity, i.e. $v_i^{se} = C_s^{se}$ (Bohm velocity).

10) The primary role of the presheath (ionization zone) is to provide charged species by ionization of the vaporized metal atoms that will in this way contribute to the current transfer in the cathode spot. The ionization of neutrals is mostly assumed by the beam electrons close to the cathode sheath edge, which mechanism is progressively replaced

by thermal ionization by the plasma electrons as the distance in the presheath increases. The beam electrons are efficient in terms of ionization at their entrance in the presheath, even though their density is low, due to their relatively high energy (~10-20 eV). For larger distances to the cathode, the beam electrons become plasma electrons upon inelastic collisions (beam relaxation), and the ionization state is maintained by the few plasma electrons occupying the highest energy states of the Maxwell-Boltzmann electron distribution function. Since an increasing ratio E/p is observed as one goes towards the cathode (figure 2.1.2), departures from LTE exist in the presheath. The plasma of the presheath consists then of a two-temperature, electrically neutral plasma mixture in collisional (kinetic) equilibrium. At the boundary shared with the cathode sheath (cathode sheath edge), the electrons assume a much higher temperature than the heavy species temperature which is assumed to be equal to the cathode surface temperature (i.e. $T_e^{sc} >> T_h^{sc} = T_s(p)$).

The physical model is restrained to the description of the cathode sheath only (sections 4.2 to 4.4). The cathode sheath voltage drop V_c that is usually calculated by resolution of the equations for the presheath is therefore specified. Proper boundary conditions (section 4.6) are specified at the cathode sheath ends for the resolution of the model's equations.

4.2. Current Transfer in the Cathode Sheath

In this section, the equations necessary to calculate the individual current densities in the cathode sheath are developed. These include the equations for the respective particle number densities and velocities as a function of the local potential $V(x)$ in the cathode sheath, and the equations for the current densities themselves. The detailed schematic representation of the cathode region presented in figure 4.2.1 will be used for this discussion.

According to the assumptions, the total electric current density in the cathode sheath is conserved and is defined as:

$$j_{tot} = j_{T-F} + j_{ion} + j_{bde} \tag{4.2.1}$$

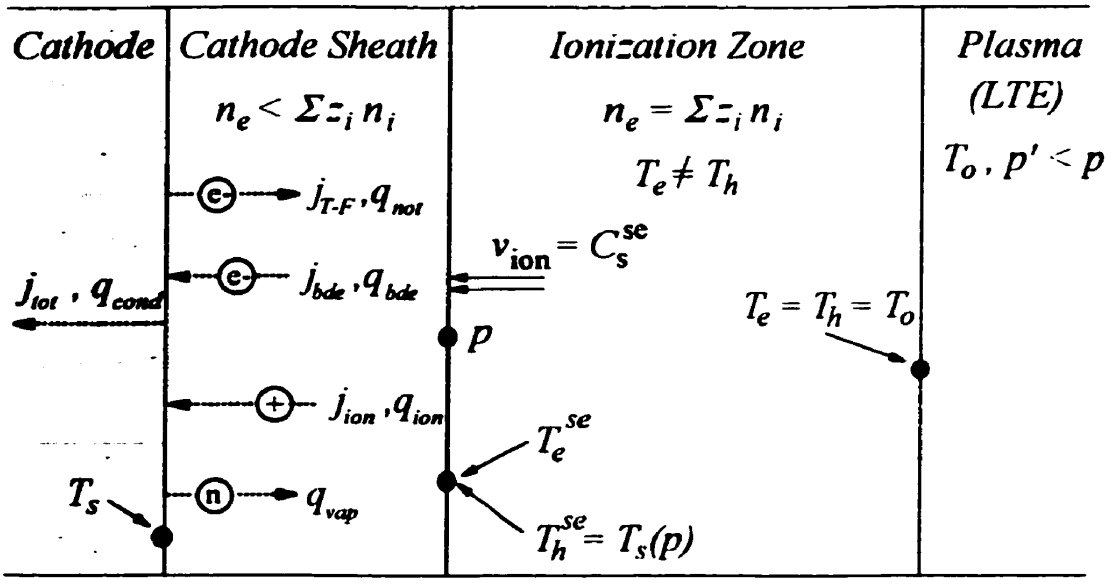

FIGURE 4.2.1. **Detailed representation of the cathode region of an emitting cathode exposed to a high pressure arc.**

4.2.1. Electron Emission Current

Due to the combined action of the high cathode surface temperatures (T_s), high surface electric field strengths (E_s), and high densities of ions in the cathode region (n_i), a strong thermo-field current of electrons is emitted from the cathode surface at a rate given by equation (2.2.6). Once in the cathode sheath, these emitted electrons of density $n_{T\text{-}F}$ are accelerated by the cathode sheath voltage drop to a velocity $v_{T\text{-}F}$ giving rise to a current density in the sheath:

$$j_{T-F} = en_{T-F}v_{T-F} \tag{4.2.2}$$

Unless specified, $j_{T-F} = j_{T-F}^{MG-I}$ (equation 2.2.6). Since the cathode spot is assumed to burn on a pure metallic cathode showing no curvature (assumption 4), the effects of geometry (section 2.2.4) and contamination (section 2.2.5) on the electron emission

current are not considered here. The thermo-field electrons are emitted from the cathode with a mean kinetic energy K_e defined by (Benilov and Marotta 1995):

$$K_e = 2k_B T_s, \tag{4.2.3}$$

and accelerated by the local potential in the cathode sheath $V(x)$ to a velocity:

$$v_{T-F}(V) = \left[\frac{2e}{m_e}\left(\frac{K_e}{e} + V\right)\right]^{1/2}, \tag{4.2.4}$$

giving rise to a density $n_{T\text{-}F}$ of thermo-field emitted electrons in the cathode sheath defined by:

$$n_{T-F}(V) = \frac{j_{T-F}}{e}\left[\frac{2e}{m_e}\left(\frac{K_e}{e} + V\right)\right]^{-1/2} \tag{4.2.5}$$

4.2.2. Ion Current

Each ion species carries a current density j_i in the cathode sheath which once summed up, give rise to a total ion current density defined by:

$$j_{ion} = \sum_i j_i = \sum_i e z_i n_i^{se} C_s^{se} \tag{4.2.6}$$

where the local sound velocity is:

$$C_s = \left[\frac{k_B}{m_c}\left(T_h^{se} + \frac{n_e}{\sum_i z_i n_i} T_e^{se}\right)\right]^{1/2} \tag{4.2.7}$$

At the cathode sheath edge where electrical neutrality still prevails ($n_e = \sum_i z_i n_i$), equation (4.2.7) resumes to the Bohm velocity (assumption 9):

$$C_s^{se} = \left[\frac{k_B}{m_c}\left(T_h^{se} + T_e^{se}\right)\right]^{1/2} \tag{4.2.8}$$

Once in the cathode sheath the ions are accelerated to a velocity v_i by the voltage drop V_c-V:

$$v_i(V) = \left[\frac{2e}{m_c}\left(V_h + z_i(V_c - V)\right)\right]^{1/2} \tag{4.2.9}$$

where their Volt-equivalent initial velocity V_h is defined by:

$$V_h = \frac{m_c (C_s^{se})^2}{2e} \tag{4.2.10}$$

Applying the conservation of current density for each individual ion species allows to obtain the ion density distributions in the cathode sheath:

$$n_i(V) = \frac{n_i^{se} C_s^{se}}{v_i(V)} = n_i^{se}\left[\frac{V_h}{V_h + z_i(V_c - V)}\right]^{1/2} \tag{4.2.11}$$

4.2.3. Back-Diffusing Plasma Electron Current

A fraction $\exp(-eV_c/k_B T_e^{se})$ of the Maxweli-Boltzmann distributed plasma electrons present at the cathode sheath edge have sufficient energy to reach the cathode surface with their thermal velocity giving rise to a negative contribution to the total current density:

$$j_{bde} = -\frac{1}{4} e n_{bde}^{se} \exp\left(-\frac{eV_c}{k_B T_e^{se}}\right) v_{bde}^{se} \tag{4.2.12}$$

where the thermal velocity for the back-diffusing plasma electrons at the cathode sheath edge is:

$$v_{bde}^{se} = \left(\frac{8 k_B T_e^{se}}{\pi m_e}\right)^{1/2} \tag{4.2.13}$$

Since the back-diffusing plasma electrons are repelled by the cathode sheath electric field, their density decays as the distance to the sheath edge increases according to an electrostatic Boltzmann's distribution:

$$n_{bde}(V) = n_{bde}^{se} \exp\left(\frac{e(V - V_c)}{k_B T_e^{se}}\right) \tag{4.2.14}$$

where the density of back-diffusing plasma electrons at the cathode sheath edge is given by the difference between the density of plasma electrons and the density of incoming thermo-field electrons:

$$n_{bde}^{se} = n_e^{se} - n_{T-F}^{se} \tag{4.2.15}$$

4.2.4. Poisson's Equation

The particle number densities in the cathode sheath are related to the local potential via the Poisson's equation. When ions, emitted and back-diffusing plasma electrons are present in the cathode sheath, the one-dimensional Poisson's equation takes the form:

$$\frac{d^2V}{dx^2} = -\frac{e}{\varepsilon_o}\left(\sum_i z_i n_i - n_{T-F} - n_{bde}\right) \tag{4.2.16}$$

Once the value of E_s is known (E_s appears in $n_{T\text{-}F}$), the distributions of potential and particle densities can be obtained by integration of equation (4.2.16) from (x=0, V=0) to (x, $V(x)$). This integration for the whole cathode sheath is straightforward when both sides of equation (4.2.16) are multiplied by $(dV/dx)dx$ since the right-hand side depends then only on the local potential V, while the left-hand side can easily be integrated by parts using $E = -dV/dx$. The determination of E_s from equation (4.2.16) is now discussed.

4.2.5. Surface Electric Field Strength

The analytical expression for the surface electric field strength necessary to calculate the density of thermo-field electrons $n_{T\text{-}F}$ appearing in equation (4.2.16) is obtained using the method originally developed by Mackeown (1929) considering the ions

and emitted electrons, and later extended by Prewett and Allen (1976) to include the back-diffusing plasma electrons. This method consists of the integration of the Poisson's equation over the entire cathode sheath thickness (x_c) using the boundary conditions:

$$\left.\frac{dV}{dx}\right|_{x=0} = E_s \tag{4.2.17a}$$

$$\left.\frac{-dV}{dx}\right|_{x=x_c} = 0 \tag{4.2.17b}$$

and allows to obtain the following analytical expression for E_s when equations (4.2.5), (4.2.11) and (4.2.14) are taken for the species densities:

$$\frac{E_s^2}{2} = \underbrace{\frac{2eV_h}{\varepsilon_o}\sum_i\left(\frac{n_i^{se}}{z_i}\right)\left[\left(\frac{V_h + z_i V_c}{V_h}\right)^{1/2} - 1\right]}_{\text{contribution from ions}} + \ldots$$
$$\ldots \underbrace{-\frac{j_{T\text{-}F}}{\varepsilon_o}\left(\frac{2m_e}{e}\right)^{1/2}\left[\left(\frac{K_e}{e} + V_c\right)^{1/2} - \left(\frac{K_e}{e}\right)^{1/2}\right]}_{\text{contribution from thermo-field electrons}} + \ldots \tag{4.2.18}$$
$$\ldots \underbrace{\frac{k_B T_e^{se}}{\varepsilon_o}\left(n_e^{se} - n_{T\text{-}F}^{se}\right)\left[1 - \exp\left(-\frac{eV_c}{k_B T_e^{se}}\right)\right]}_{\text{contribution from plasma electrons}}$$

Strictly speaking, the boundary condition 4.2.17b is not valid since the local electric field strength at the cathode sheath edge is not zero, but of the order of 10^3 V m^{-1}. However, such a value is low in comparison with the value taken at the cathode surface (E_s~10^8-10^9 V m^{-1}) and therefore, the use of boundary condition 4.2.17b introduces only a small error on E_s (as also observed by Klein *et al* 1994).

4.3. Heat Transfer to the Cathode Surface

The principal contribution to the incoming heat flux from the cathode spot plasma to the cathode area under the spot is the bombardment by the returning ions (q_{ion}), and

back-diffusing plasma electrons (q_{bde}). Energy is lost by emission of thermo-field electrons (Nottingham effect, q_{not}), by conduction through the cathode bulk (q_{cond}), and by vaporization of the cathode material (q_{vap}). Radiative heat losses from the cathode area under the spot is negligible in comparison with the other heat fluxes. Radiation from the metallic vapor plasma to the surface is not considered. The expression for the net heat flux from a momentary stationary cathode spot plasma to the cathode surface area under the spot then reads:

$$q_{ion} + q_{bde} = q_{in} = q_{not} + q_{vap} + q_{cond} \tag{4.3.1}$$

which expression is a simplification of the equation proposed by Cobine (1941).

Since the cathode sheath is assumed collisionless, the hydrodynamic transport equations for heat transfer are not applicable in this region (Knudsen layer). Thus one has to describe the particle fluxes to the cathode in terms of the free-molecular flow approach (directed transport by individual particles).

4.3.1. Returning Ion Bombardment

Each ion accelerated in the cathode sheath which bombards the cathode surface liberates upon impact the sum of its initial enthalpy, its translational energy gained in the cathode sheath, and its neutralization energy with electrons of the cathode surface giving rise to a net heat flux:

$$q_{ion} = \sum_i \left(\frac{j_i}{z_i}\right)\left(\underbrace{\frac{5k_B T_h^{se}}{2e}}_{initial} + \underbrace{z_i V_c}_{translational} + \underbrace{\sum_{j=1}^{i} E_{ion}^{j-1} - z_i \phi_{eff}}_{neutralization}\right) \tag{4.3.2}$$

Equation (4.3.2) slightly underestimates the actual heat flux brought to the surface by the ions since their possible condensation after neutralization has not been taken into account. For copper, the condensation energy of an atom on the surface is ~3.15 eV/atom which is comparable to the neutralization energy of a singly charged copper ion (~3.22 eV

when $E_s = 0$). Indeed, this phenomenon can not be taken into account since the values of the accommodation coefficient for copper at elevated temperatures are not known. The usual assumption that all the ions are backscattered after neutralization (Klein *et al* 1994) was therefore made.

4.3.2. Back-Diffusing Plasma Electron Bombardment

The back-diffusing plasma electrons liberate upon impact with the cathode surface the sum of their condensation energy and initial enthalpy giving rise to a heat flux:

$$q_{bde} = j_{bde}\left(\underbrace{\phi_{eff}}_{\text{neutralization}} + \underbrace{\frac{5k_B T_e^{se}}{2e}}_{\text{initial}}\right) \tag{4.3.3}$$

4.3.3. Energy Exchange Associated with Electron Emission (Nottingham Effect)

The emission of electrons from the cathode surface is accompanied by an energy exchange ε_N (so-called 'Nottigham potential'); the electrons are promoted outside the potential barrier at the metal surface by taking their energy from the lattice. The net energy exchange with the cathode, the so-called 'Nottingham potential' is defined as (Swanson *et al* 1966):

$$\varepsilon_N = \frac{e}{j_{T\text{-}F}(E_s, T_s, \phi)} \int_{-\infty}^{\infty} W P(W, E_s, T_s, \phi) dW + \phi \tag{4.3.4}$$

where $P(W,E_s,T_s,\phi)\,dW$ is the total energy distribution for the electrons. Equation (4.3.4) involves a double integration on the electron energy which complicates its resolution ($P(W,E_s,T_s,\phi)$ is obtained from an integration over the electron energy from 0 to W). Fitting formula of equation (4.3.4) were obtained by Paulini *et al* (1993) for $10^8 < E_s < 10^{10}$ V m^{-1} and $2 < \phi < 5$ eV, respectively, were used in this study to reduce the calculation efforts. As reported by the authors the use of these fitting formula introduces an average error of 1.1% and a maximum error of 4.56% when compared to the exact calculations.

The results of calculation of ε_N using the fitting formula are represented in figure 4.3.1. and compared with the values predicted using:

$$\varepsilon_N = \phi_{eff} + \frac{2kT_s}{e} \tag{4.3.5}$$

which equation is the limit of equation (4.3.4) when field emission across the barrier becomes negligible (thermionic emission).

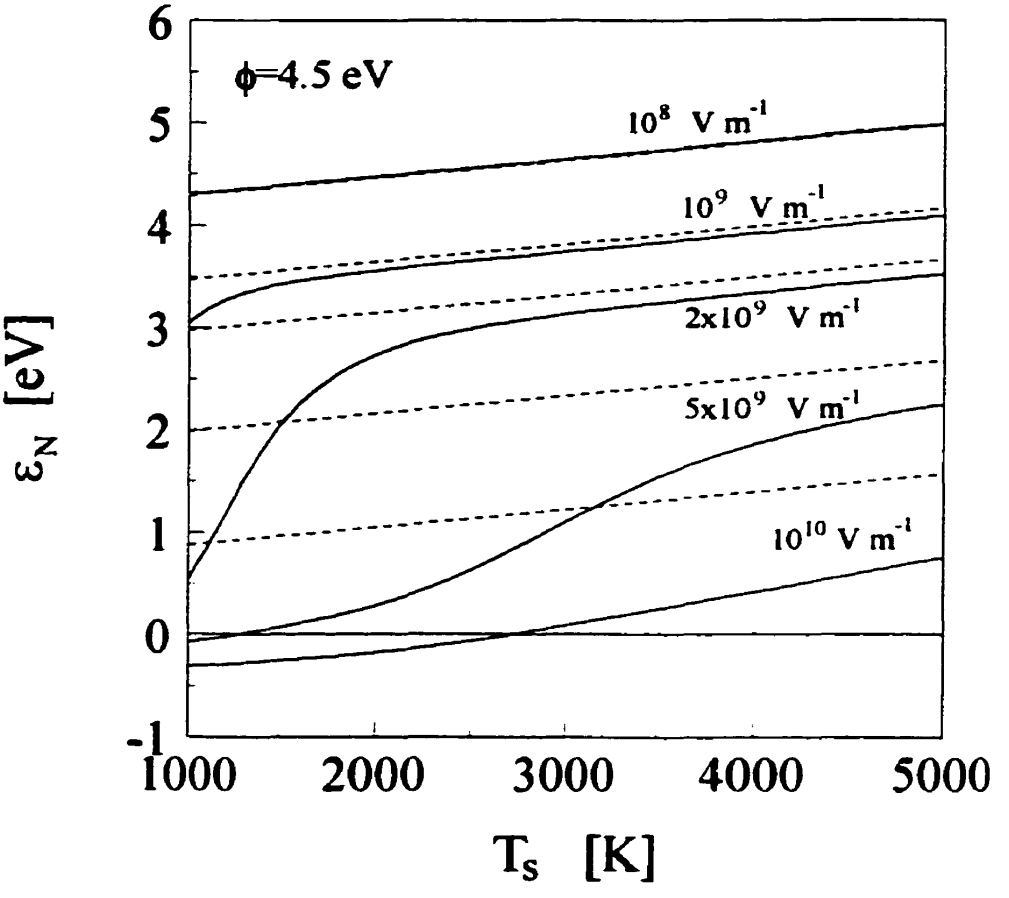

FIGURE 4.3.1. Nottingham potential of the electron ε_N as a function of the cathode surface temperature T_s, and surface electric field strength E_s for ϕ=4.5 eV. Continuous line: equation (4.3.4) using fitting formula of Paulini *et al* (1993). Dashed line: equation (4.3.5).

Equation (4.3.5) is commonly used in modeling the interactions between thermal arcs and refractory cathodes (e.g. Benilov and Marotta 1995 and references therein). One

can observe an increase of the discrepancy between the two predictions (fitting formula for equation (4.3.4) vs equation (4.3.5)) as the emission conditions favor field emission (high values of E_s and low values of T_s) due to electron tunneling across the barrier which induces a lower energy exchange; the electrons pass directly through the barrier without having to be promoted above it.

When a flux $j_{T\text{-}F}$ of electrons is emitted from the cathode surface, the Nottingham energy flux takes the form:

$$q_{not} = j_{T-F}\varepsilon_N \tag{4.3.6}$$

A positive value for ε_N corresponds to cathode cooling upon electron emission, while a negative value corresponds to a cathode heating upon electron emission. Such a heating effect appearing for high surface electric field strengths and low temperatures (see for example figure 4.3.1 for E_s=10^{10} V m^{-1} and T_s<2700 K) plays a fundamental role in the arc ignition process on initially cold cathodes (section 2.3.7). The temperature at which the cooling effect changes to a heating effect for a given electric field strength is called the 'inversion temperature'.

4.3.4. Heat Lost by Cathode Material Vaporization

The net heat loss due to the cathode material vaporization can be estimated using the expression for the flux of vaporized atoms (equation 2.3.1):

$$q_{vap} = \eta\Gamma_{vap} \tag{4.3.7}$$

where η is the condensation energy of the cathode material atoms.

4.3.5. Conduction Losses

Since radiative heat losses are negligible, the remaining of the energy flux brought to the cathode surface under the spot is dissipated to the cathode bulk by conduction:

$$q_{cond} = q_{in} - q_{not} - q_{vap} \tag{4.3.8}$$

4.4. Criteria for a Self-Sustaining Arc Operation

Essentially two criteria must be validated in order for the arc attachment on the cathode to be self-sustaining. The first criterion (equation 4.4.2a) is based on a particle balance for the ionization process, while the second (equation 4.4.2b) is based on a requirement for a minimum heat flux to maintain the cathode surface at its boiling temperature.

4.4.1. First Criterion

The principal role of the cathode of an electric arc is to provide a sufficient flux of electrons to maintain the discharge. These electrons (beam electrons) are emitted from the cathode under the combined actions of the high surface temperatures and electric fields maintained mainly by the ions flux bombarding the cathode surface and forming the cathode sheath. Once emitted from the cathode, the electrons are accelerated through the cathode sheath without collisions to the ionization zone where inelastic collisions with neutrals producing ions result in the formation of an electrically-conducting channel between the two electrodes (arc column formation). According to this scenario, it is obvious that the self-sustaining operation of the arc discharge is possible only if the conditions prevailing in the cathode region are those favoring a sufficient thermo-field emission of electrons.

The fraction f_{bi} of the beam electrons that are left for ionization after collisions can be defined as:

$$f_{bi} = \frac{\nu_{bi}}{\nu_{bi} + \nu_{be}} = \frac{\sigma_{bi}}{\sigma_{bi} + \sigma_{be}} < 1 \qquad (4.4.1)$$

where i stands for ionization and e for excitation, the ν's are the frequencies of the collision processes and the σ's, the collision cross sections. Obviously, f_{bi} is less than unity since all the σ's are positive. The maximum energy taken by the beam electrons before to start colliding corresponds to the cathode sheath voltage drop, and is therefore less than 10-20 eV for high pressure arcs. For this energy range, only single-ionization occurs upon

electron impact (Freund *et al* 1990). This observation and the condition defined by equation (4.4.1) allow to define the most restraining criterion for the self-sustaining operation of an arc discharge maintained by a beam of electrons emitted from the cathode ($j_{T\text{-}F}$):

$$\frac{j_{ion}}{j_{T-F}} < 1 \qquad (4.4.2a)$$

This criterion states that the flux of ions produced by ionization of the neutrals by the beam electrons cannot be higher that the flux of beam electron that generates it.

4.4.2. Second Criterion

The second criterion that must be validated is that the net heat flux brought in by the plasma to the cathode surface and left for conduction in the cathode must be larger than zero since the plasma is the only source of heat (i.e. $-\partial T / \partial z > 0$ at the cathode surface). Such criterion reads:

$$q_{cond} > 0 \qquad (4.4.2b)$$

The case $q_{cond}=0$ would correspond to a situation where all the incoming heat flux is lost by cathode material vaporization and electron emission cooling. If Joule heating in the cathode volume underneath the arc attachment point became important in comparison with the incoming heat flux from the plasma, it would become possible to have $q_{cond}<0$. Indeed, in this situation the heated volume underneath the cathode surface would become a source of heat flux across the plasma-cathode interface. As reported by Marotta and Sharakhovsky (1996), such a situation is possible for total current densities at the cathode surface much larger than 10^{11} A m^{-2}. Such values are however not likely to be observed (Chapter 5).

4.5. Erosion

Erosion is the phenomenon by which cathode material is lost under the action of the electric arc. It is commonly expressed in units of mass lost per unit charge passing through the cathode. The erosion rate expressed this way is independent of the arc current

and arcing time. This allows to make comparisons among different experiments. Three main mechanisms are responsible for the erosion of pure metal cathodes exposed to an electric arc (Kharin 1992): 1) The vaporization of the cathode material at an atomic rate Γ_{vap}, 2) the ejection of microdroplets due to the ion pressure release upon spot extinction, and 3) the ejection of microdroplets due to the onset of important thermo-capillary flows within the molten bath. There may be other causes of microdroplets and/or macro "chunks" ejection for example from gas dissolution in the high temperature cathode followed by explosure-like destruction of the surface after the arc passage. For instance, Munz and Habelrih (1992) observed that arc operation in $Ar+H_2$ over a Cu cathode resulted in the formation of a 100-200 μm powder composed of melted flakes or agglomerates. All these examples show that the calculation of the erosion rate E_r requires a fluid dynamics-heat transfer model of the cathode region under the spot coupled with a model of the cathode region.

4.5.1. Erosion by Vaporization

When liquid microdroplets ejection can be neglected, the erosion is due to the cathode material vaporization only and can be estimated using the following expression (in unit of mass per unit of charge):

$$E_{r,vap}^{max} = \Gamma_{vap}\, m_c / j_{tot} \qquad (4.5.1)$$

4.5.2. Re-Deposition of Ions and Neutrals

Equation (4.5.1) corresponds to the maximum erosion rate by vaporization since the redeposition of returning ions or neutrals diffusing back towards the cathode has not been taken into account. Under vacuum, one can assume that all the neutral atoms expand into the chamber and do not recondense on the cathode. Thus, only the ions accelerated back towards the cathode by the cathode voltage drop may possibly condense on its surface (within the spot or in the close vicinity). The vacuum erosion rate by vaporization

stands then between a maximum value $E_{r,vap}^{max}$, and a minimum value $E_{r,vap}^{min}$ reached when all the ions incident on the surface condense upon impact:

$$E_{r,vap}^{min} = \left(\Gamma_{vap} - \sum_i j_i / z_i e \right) m_c / j_{tot} < E_{r,vap}^{vacuum} < E_{r,vap}^{max} \qquad (4.5.2)$$

4.5.3. Liquid Volume Formation

The heat flux brought by the cathode spot plasma that cannot be dissipated by electron emission q_{not} and vaporization q_{vap} is dissipated by conduction in the cathode volume underneath the cathode spot (q_{cond}). When the arc stays a sufficient time at a given location, liquid volume formation occurs and the erosion process due to vaporization might be enhanced by the ejection of microdroplets (Gray and Pharney 1994). Once ejected these microdroplets are taken by the gas stream and leave the arcing zone or are redeposited on colder sections of the electrodes or on the reactor walls, causing a net cathode erosion. Liquid volume displacement is not considered as a source of erosion since the displaced cathode material stays as an integral part of the cathode. It however causes damages to the cathode surface. The liquid volume formation process will be studied in details in Chapter 7 by a transient heat transfer analysis of the cathode region under the spot considering the solid-liquid phase change.

4.6. Boundary Conditions

The model's equations presented in sections 4.2 through 4.5 form a self-consistent set of equations for the cathode spot plasma that is solvable if the conditions at both ends of the cathode sheath edge are specified. These conditions include the plasma conditions at the cathode sheath edge (p and T_e^{se}) and the cathode sheath voltage drop V_c. The cathode surface temperature does not have to specified for a non-refractory cathode since according to the assumptions made, this temperature is related to the metallic vapor pressure within the cathode spot plasma, i.e. $T_s=T_s(p)$. The method used to calculate the plasma composition at the cathode sheath edge knowing p, T_e^{se} and $T_h^{se} = T_s(p)$ is discussed in the next section.

4.6.1. Composition of a Two-Temperature Plasma

In the plasma out of LTE present in the cathode region, the electron temperature T_e is much higher than the heavy species temperature T_h. A consequence of this gap between the two temperatures is the higher densities of charged particles achieved in comparison to the densities encountered under LTE conditions at the same pressure. The plasma composition in such a case is calculated using the two fluids approach; an electron fluid at temperature T_e and a heavy species fluid at temperature T_h.

For the case considered in this study, no reaction among molecules is involved. The only possible reactions among the species are the forward reaction of electron impact ionization and its reverse reaction, the three-body recombination. The reactions proceed according to:

$$A + e^- \rightleftharpoons A^+ + e^- + e^- \tag{4.6.1}$$

where A is either a neutral atom or an ion. The equation of reaction equilibrium implies that the ratio of the forward (k_f) to the reverse (k_r) rate coefficients is given by:

$$\frac{k_f(T_h, T_e)}{k_r(T_h, T_e)} = \frac{n_{A^+}\, n_e}{n_A} \tag{4.6.2}$$

This ratio is function of both the electron and heavy species temperatures and therefore, it is not likely that a simple expression involving the ratio of the species partition functions evaluated at their own temperatures as often seen with equilibrium constants can be obtained. However, since the reaction rate is a measure of the velocity at which the reactants approach each other and since both reactions of ionization and recombination are rate-controlled by the electrons, it is assumed that both reactions occur at the electron temperature. By making the assumption that $k_f(T_h, T_e) \sim k_f(T_e)$ and $k_r(T_h, T_e) \sim k_r(T_e)$, Richley and Tuma (1982) obtained an expression relating n_A, n_{A^+} and n_e to T_e which takes the form:

$$\frac{n_{A^-} n_e}{n_A} = K_n(T_e) = 2\left(\frac{2\pi m_e k_B T_e}{h^2}\right)^{3/2}\left[\frac{Q_{A^-}(T_e)}{Q_A(T_e)}\right]\exp\left(-\frac{E_\infty^A - \Delta E_\infty^A}{k_B T_e}\right) \qquad (4.6.3)$$

where $K_n(T_e)$ is the equilibrium constant for the reaction based on the particle number densities (since a unique temperature is defined). Q_A and Q_{A^-} are respectively, the electronic partition function for the species A and A^-. Note here that this development based on a kinetic approach yields the generalized Saha equation obtained using the mass action law (Zemansky and Dittman 1981) at a single temperature T_e. However, this is only due to the fact that both the forward and reverse reactions occur at a rate imposed by the same species (electrons in this case).

The calculation of the two-temperature plasma composition is performed using the NASA method based on the equilibrium constants (Appendix C). In this method, a set of Z equations (Z being the number of species in the plasma) relating the different number densities of species n_i to p, T_e and T_h is solved iteratively from an initial guess of the plasma composition. These Z equations are respectively the equation expressing the electrical quasi-neutrality in the plasma:

$$n_e = \sum_i z_i n_i \ , \qquad (4.6.4)$$

the Dalton's law for the total pressure:

$$p = n_e k_B T_e + \sum_i n_i k_B T_h - \Delta p \ , \qquad (4.6.5)$$

and a set of Z-2 equations expressing the equilibrium constants for the ionization/ recombination reactions (equation (4.6.3)). The presence of a high density of charged particles in the cathode region induces a lowering of the ionization potentials and an increase of the total plasma pressure (Griem 1964) given respectively by:

$$\Delta E_{\infty}^{z} = \frac{(z+1)e^2}{4\pi\varepsilon_o\lambda_D} \tag{4.6.6}$$

and

$$\Delta p = \frac{k_B T_e}{24\pi\lambda_D^3} \tag{4.6.7}$$

where the Debye length λ_D is:

$$\lambda_D^{-2} = \left(\frac{e^2}{\varepsilon_o k_B}\right)\left(\frac{n_e}{T_e} + \sum_i z_i^2 \frac{n_i}{T_h}\right) \tag{4.6.8}$$

4.7. Calculation Procedure

For a given set of boundary conditions (p, T_e, V_c) and an initial guess for the surface electric field strength E_s, equation (4.2.18) for E_s is first solved by iteration by recalculating the thermo-field emission current at every step. Knowing the value of E_s, the Poisson's equation (4.2.16) is integrated over the entire cathode sheath from V=0 to V=V_c using a spatial step $\Delta x = \lambda_D^{ze}/50$ in order to obtain ~1000 data points representing accurately the spatial distributions of V(x) and of the different particle densities (equations (4.2.5), (4.2.11) and (4.2.14)). The value of x_c is then determined when V=V_c. The different contributions to the current and heat transfers to the cathode surface under the spot are finally calculated. All the calculations are repeated for a wide range of metallic plasma pressures and electron temperatures in order to perform a parametric study.

4.8. Materials Properties

The electronic partition functions $Q_i(T_e)$ necessary for the calculation of the plasma composition were taken from Tamaki and Kuroda (1987) and Drawin and Felenbok (1972). The vapor pressure curves were fitted from the experimental data reported by Honig and Kramer (1969) according to the general relation:

$$\log(p) = \frac{a}{T_s} + b\log(T_s) + cT_s + dT_s^2 + e \tag{4.8.1}$$

and extrapolated to pressures higher than atmospheric. Such an extrapolation is thought to not introduce a significant error since the fits of equation (4.8.1) were obtained considering fifteen orders of magnitude for the vapor pressure (10^{-14}-10^{0} atm) and extrapolated over less than two orders of magnitude ($p<10^{2}$ atm). Figure 4.8.1 shows the vapor pressure data reported by Honig and Kramer (1969) for the three metallic elements that are studied in Chapter 5 (Cu, Fe and Ti), and the extrapolations for $p>10^{0}$ atm (101325 Pa) obtained using the fitting formula (4.8.1). One can see that the trends of the experimentally obtained data are maintained by the fits for surface temperatures below 4500 K.

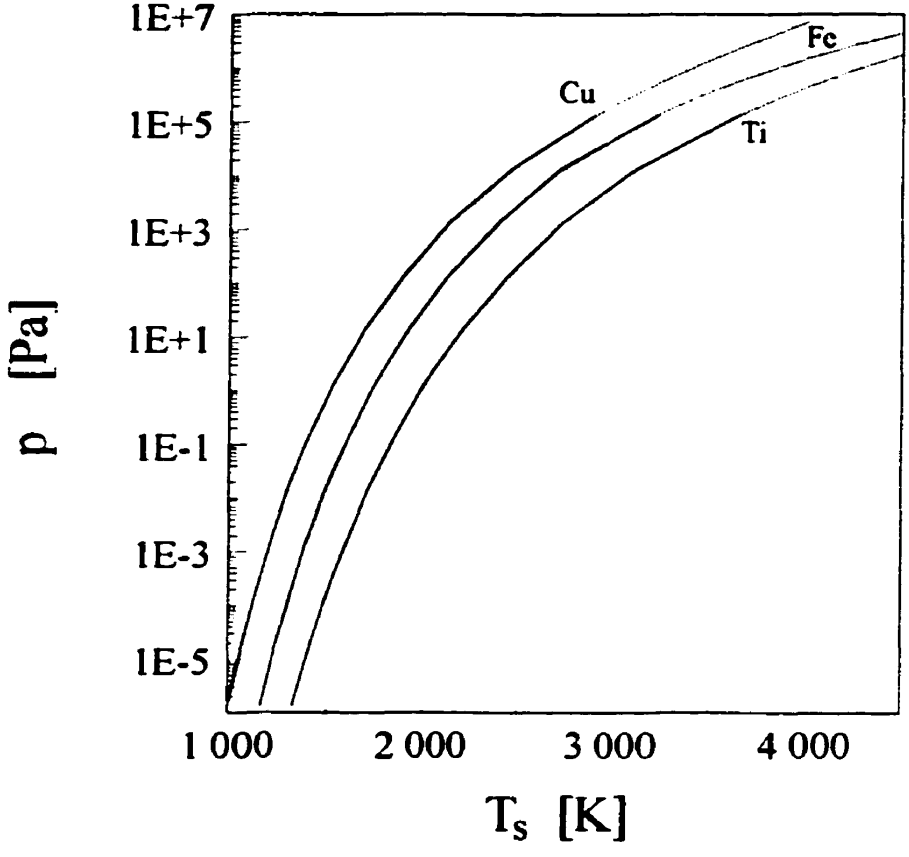

FIGURE 4.8.1 Vapor pressure curve for Cu, Fe and Ti. Continuous line: data reported by Honig and Kramer (1969). Dotted line: fits of the data using equation (4.8.1).

CHAPTER 5

MODEL'S PREDICTIONS WITH CU, FE AND TI CATHODES

5.1. Introduction

This chapter presents the predictions of the model developed in Chapter 4 when applied to Cu, Ti and Fe cathodes. The goal of the study is to determine the conditions prevailing within the cathode region of a high pressure arc on a non-refractory cathode which allow a self-sustaining attachment of the arc. The attention is put mainly on Cu because this element is one of the most commonly used cold-cathode materials. The mechanisms of current and heat transfers to the cathode surface, the distributions of voltage and particle densities in the cathode sheath, and the cathode material consumption rate (erosion rate) are first studied by making a parametric study with two of the three independent parameters of the model (section 5.2). These parameters are the metallic plasma pressure p, and the electron temperature T_e^{se}. The third independent parameter, the cathode sheath voltage drop V_c, is set equal to a specific value and the effects of slight deviations from this value are discussed later (section 5.5). The study is then extended in section 5.3 to include Ti and Fe, which elements show a more refractory behavior than Cu, in order to generalize the concept of high local pressure with several elements. The validity of the collisionless cathode sheath assumption is discussed in section 5.4. A general discussion of the results and a summary conclude the chapter (section 5.6).

5.2. Parametric Study with Cu: Influence of p and T_e^{se}

The metallic plasma pressure p and the electron temperature T_e^{se} at the cathode sheath edge are the two parameters affecting the most the properties in the cathode sheath. The cathode sheath voltage drop V_c is less determinant as it will be seen in section 5.4. For this first parametric study, and as discussed in section 2.3.5 indicating that a high local

plasma density is expected to prevail in the cathode region, p was allowed to vary from 1 to 70 atm (0.1 to 7 MPa) and T_e^{sc} from 0.9 to 2 eV (10 440 to 23 200 K). For some reasons related to the calculation of the plasma composition, it was impossible to extend the parametric study beyond 70 atm. The reasons for this are discussed in section 5.2.3.

5.2.1. Choice of the Cathode Sheath Voltage Drop

For this parametric study, the cathode sheath voltage drop V_c was set equal to 15 V. A number of studies relating the properties of vacuum arc cathode spots on copper cathodes used a value of 15 V after the measurements of Kesaev (1965). As shown by Kesaev, this value for V_c is expected to remain the same at atmospheric pressure. A value of 23 V was determined by Hamilton and Guile (1968) for the minimum operating voltage (V_{arc}^{min}) of an argon arc operating at atmospheric pressure on copper electrodes. A value of 15 V for V_c lets 8 V for the sum of the voltage drops in the ionization zone (1-2 V), in the anode sheath (4-6 V, ~ of the order of $e\phi$ (4.5 V)), and in the electrodes (1-2 V), which values are all reasonable. A value of V_c significantly lower than 15 V would mean a larger anode sheath voltage drop, which is not likely. A larger value is hardly conceivable taking into account the minimum arc voltage of ~23 V. The effects of slight deviations from V_c=15 V will be discussed in section 5.5.

5.2.2. Minimum Plasma Pressure for a Self-Sustaining Arc

As discussed in section 4.4, criteria 4.4.2a and 4.4.2b based on particle and energy balance considerations have been defined to determine the conditions for which the cathode spots forming the arc attachment on the cathode are self-sustaining. The criterion 4.4.2b is validated for the whole range of electron temperatures investigated when p<70 atm as discussed later in section 5.2.7. Figure 5.2.1 shows the evolution of the ratio $j_{ion}/j_{T\text{-}F}$ (criterion 4.4.2a) as a function of p and T_e^{sc}. This ratio shows a strong dependency on p and T_e^{sc}. It is shown that the criterion $j_{ion}/j_{T\text{-}F}$ <1 is validated only for p >19 atm (p_{min}~19 atm) showing the necessity of having high local metallic plasma pressures in the cathode region for a self-sustaining operation and therefore, a strong vaporization of the cathode surface. It is shown also that the closer is the electron temperature to 1 eV, the lower is

the minimum metallic plasma pressure needed for a self-sustaining operation. This observation will be discussed later in the section related to the current transfer to the cathode surface (section 5.2.4). As discussed previously in section 4.4.1, the conditions prevailing in the cathode region and for which $j_{ion}/j_{T\text{-}F}=1$ are not likely and one must rather look for ratios $j_{ion}/j_{T\text{-}F}$ smaller than unity for a representative view of the actual conditions.

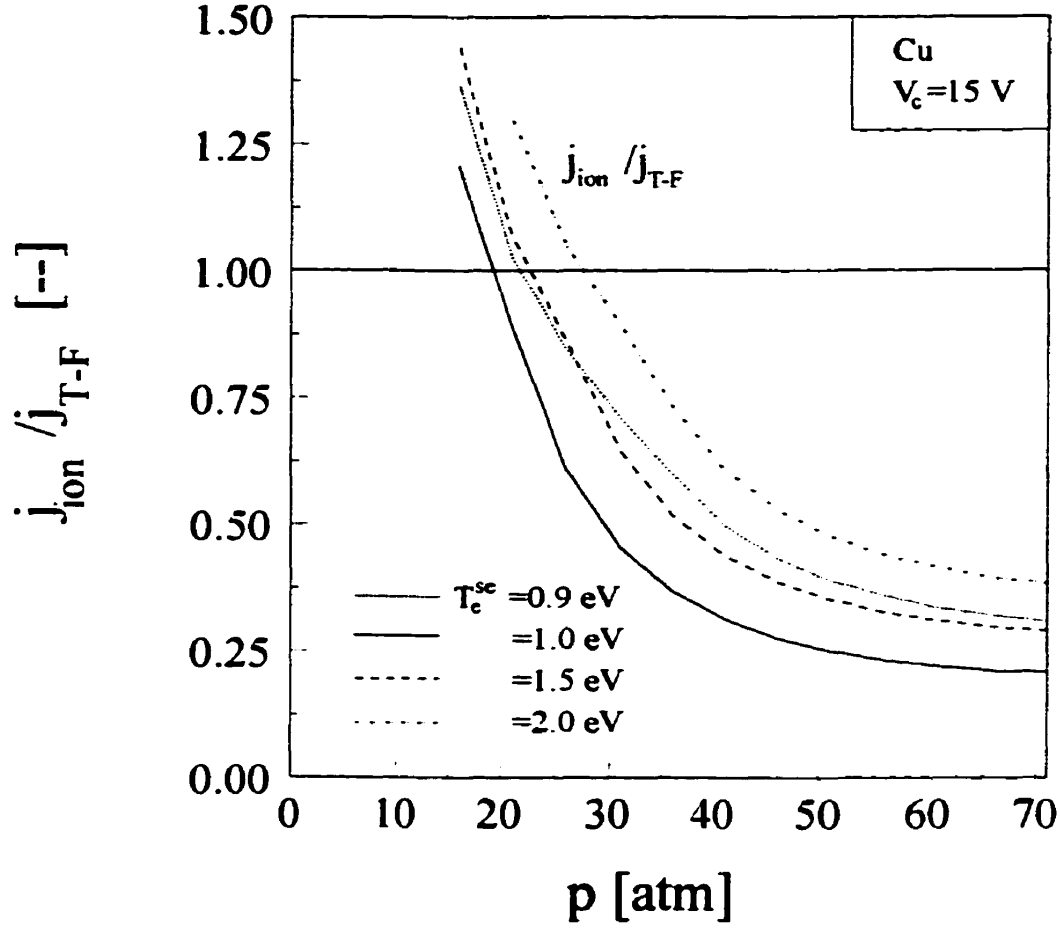

FIGURE 5.2.1. Ratio $j_{ion}/j_{T\text{-}F}$ (criterion 4.4.2a) for a two-temperature Cu plasma as a function of p for V_c=15 V and $0.9<T_e^{se}<2.0$ eV.

It is interesting to note that this ratio tends towards a limit as the metallic plasma pressure gets high (p>50 atm) and for all the electron temperatures considered. This limit ranges from $j_{ion}/j_{T\text{-}F}$ ~0.25 to ~0.4, the lowest value being for T_e^{se}=1 eV. This range for $j_{ion}/j_{T\text{-}F}$ is the same as the one theoretically predicted by Zhou and Heberlein (1994, figure 5) for the self-sustaining operation of a high pressure argon arc on a refractory W cathode,

but under conditions where no vaporization occurs. As shown by this limiting behavior, the current transported by the ions to the cathode surface is at least of 25% of the electron current, and this seems to be true for both refractory and non-refractory cathode cases.

One very important result of the model presented in this study is that for high metallic plasma pressures within the cathode region, the non-refractory copper cathode starts to behave like a refractory cathode according to the classification made with figure 2.3.1; i.e. the flux of emitted electrons becomes higher than the flux of vaporized cathode material atoms for a given surface temperature. Figure 5.2.2 shows this behavior where the ratio $e\Gamma_{vap}/j_{T\text{-}F}$ (not $e\Gamma_{vap}/j_{RD}$ as with figure 2.3.1) is plotted as a function of the plasma parameters within the cathode spot. Due to the high temperatures associated with the strong ion bombardment at high pressures, but also due to the important surface electric field strengths established by the ions, the flux of electrons emitted from the cathode becomes higher than the flux of atoms being vaporized. The results of figure 5.2.2 are extremely interesting in view of the complexity of the arc-cathode interaction system. They indicate that both refractory (hot) and non-refractory (cold) cathodes effectively behave in a similar way provided the criteria for a self-sustaining operation of the arc are validated. Indeed, for refractory materials, strong thermionic emission is achieved without a strong vaporization of the cathode surface while for non-refractory materials, a pressure build up in the cathode region resulting in the emission of electrons in the strong thermo-field emission regime is necessary. Such a symmetry in the arc behavior also puts forward the importance of a proper calculation of the electron current being emitted by the cathode surface. This will the subject of a comprehensive investigation in Chapter 6.

This simple analysis of the minimum metallic plasma pressure (p_{min}) needed for the self-sustaining operation of an electric arc on a non-refractory Cu cathode brings two preliminary conclusions: 1) Vaporization of the cathode in such a case is not only a consequence of the strong heat input from the arc that cannot be dissipated by conduction into the cathode bulk; the strong vaporization of the cathode is a *necessary condition* for the establishment of a self-sustaining arc attachment. The pressure build up in the cathode

region is a consequence of this strong vaporization and is necessary for the maintenance of surface conditions allowing strong electron emission. 2) Since the minimum metallic vapor pressure is much higher than the ambient gas pressure (reference made to 1 atm), the nature of the ambient gas has, a priori, no effect on the description of the arc attachment on such cathodes. The nature of this external gas would however affects the confinement of the arc spots (Meunier 1990) and their dynamics (Szente 1989, Jüttner 1997).

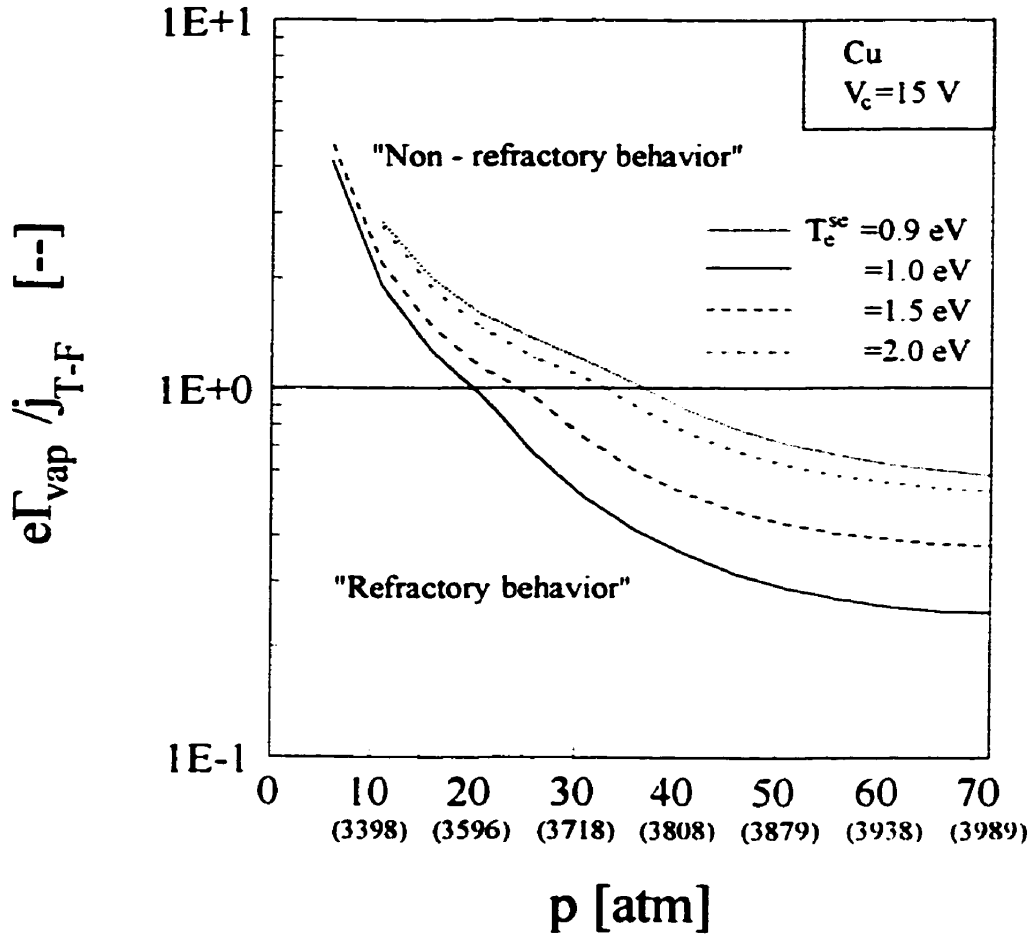

FIGURE 5.2.2. Ratio $e\Gamma_{vap}/j_{T\text{-}F}$ for a two-temperature Cu plasma as a function of p for V_c=15 V and $0.9<T_e^{se}<2.0$ eV. The corresponding cathode surface temperatures are indicated in parentheses (in K).

5.2.3. Plasma Properties

Before going further in the analysis of the current transfer to the cathode, it is necessary to know the behavior of the plasma mixture at high metallic pressures (p>19 atm), low heavy species temperatures (T_h^{se}~3500-4000 K), and low electron temperatures

(T_e^{se}=0.9-2 eV). Such conditions introduce important reductions of the ionization potentials, especially for the low-ionization species present here, and deviations from the ideal gas behavior. The relevant plasma properties are plotted as a function of the electron temperature and metallic plasma pressure in figures 5.2.3 through 5.2.5. Figure 5.2.3. shows the electron density at the cathode sheath edge (n_e^{se}), figure 5.2.4 the lowering of the ionization potential of Cu atoms ($\Delta E_{\infty,CuI}$, see equations 4.6.6 and 4.6.8), and figure 5.2.5, a parameter characterizing the deviation of the plasma mixture from the ideal gas behavior ($\Delta p/p$, see Dalton's law (4.6.5) and equation (4.6.7)).

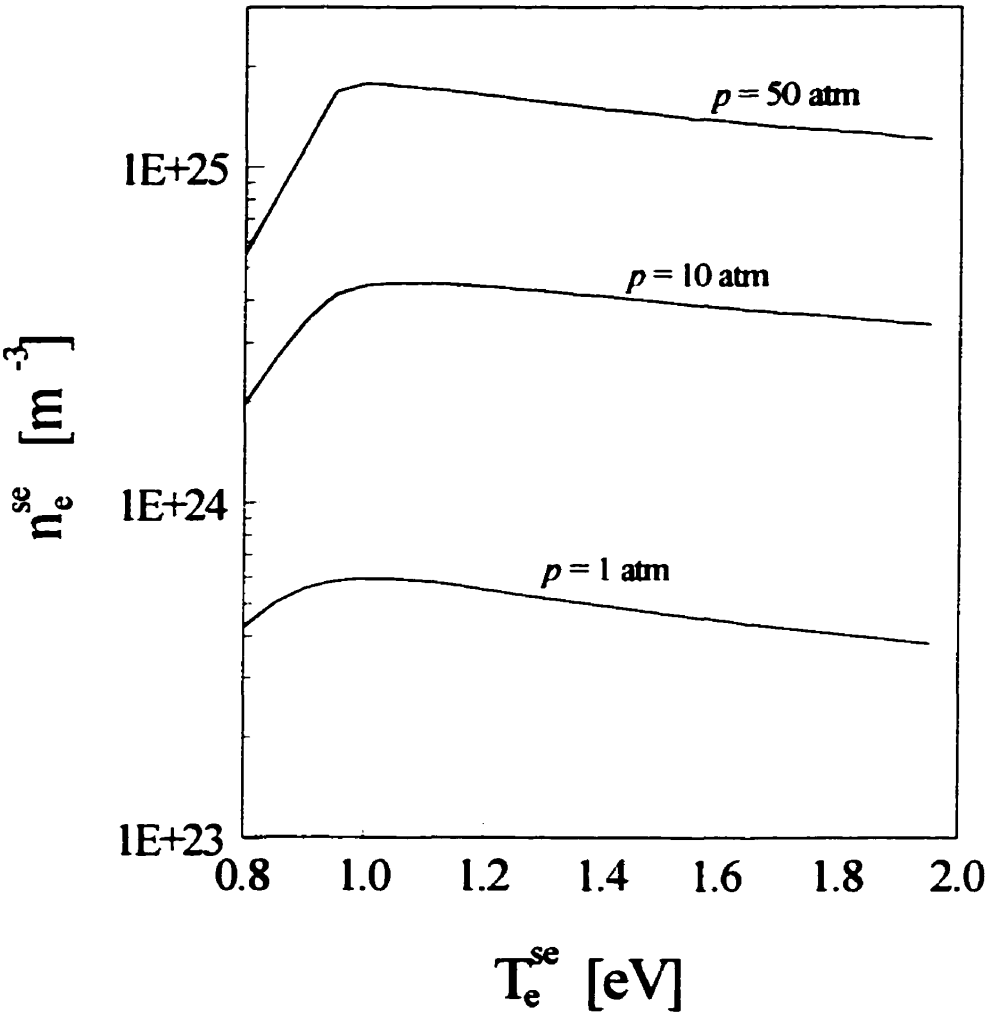

FIGURE 5.2.3. Electron density in a two-temperature Cu plasma as a function of T_e^{se} and p.

As shown in figure 5.2.3, the electron density n_e^{se} (and therefore the ion density n_i^{se}), peaks for an electron temperature T_e^{se} of ~1 eV, and this for any pressure. The increasing trend at low electron temperatures is attributable to the increase of the ionization rate of the Cu atoms with the increase of the electron energy (or temperature). The decreasing trend observed for higher electron temperatures is mainly due to the overall decrease of the particle number densities with the increasing electron temperature (Dalton's law). The lowering of the ionization energy of the copper atoms ($\Delta E_{\infty,CuI}$) shows the same behavior since it is directly related to the electron density (figure 5.2.4).

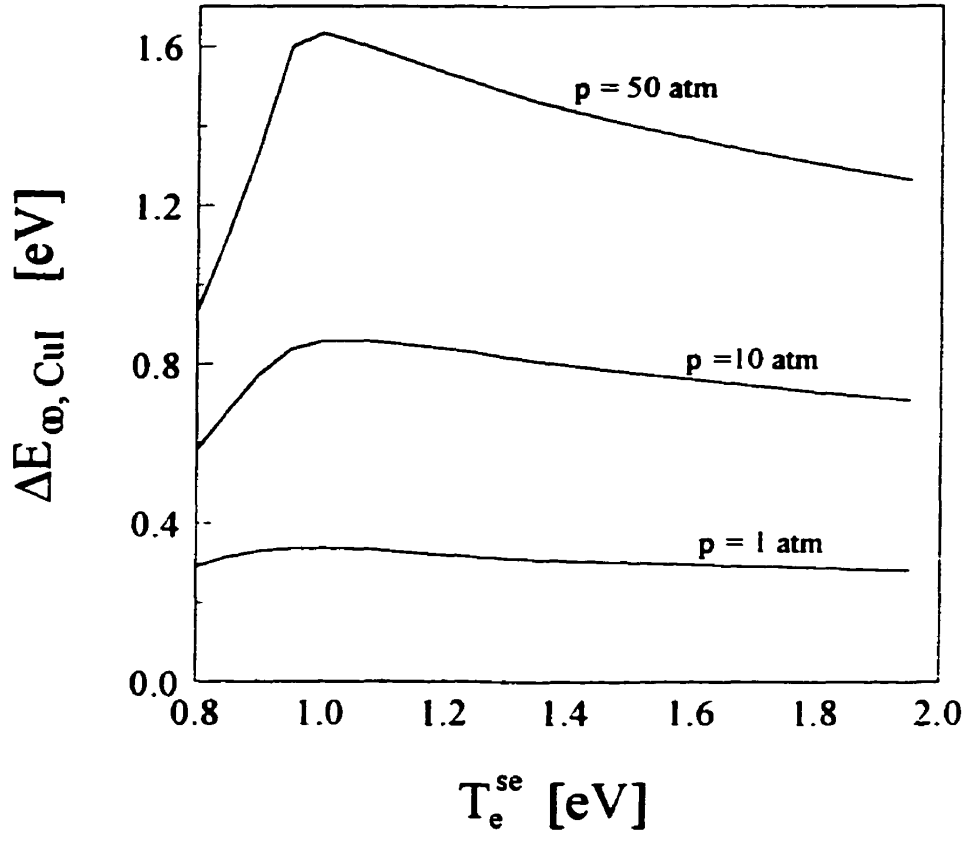

FIGURE 5.2.4. Lowering of the ionization potential of the CuI species as a function of T_e^{se} and p.

Remembering that the ionization potential of CuI is 7.72 eV, one can see that the lowering of the ionization potential becomes considerable as the electron density increases. Thus, the densities of charged particles calculated while taking into account the

electrostatic effects are higher that those that would be calculated considering an ideal plasma at a pressure p.

Figure 5.2.5 shows how far from the ideal gas behavior the metallic plasma mixture deviates. As expected, this deviation follows the electron density since an increase in this density means higher electrostatic interactions. Indeed, a high density of charged particles within a given volume induces an excess pressure build up due to the repulsive forces among particles carrying the same charge. The approximation of an ideal gas involving no Coulombic (electrostatic) interactions starts then to lose its accuracy, and therefore a positive correction Δp to the total pressure must be made to the Dalton's law (equation (4.6.5)). In such a scenario, the higher is the metallic plasma pressure p the higher are the electrostatic effects, and therefore the higher is the pressure correction Δp.

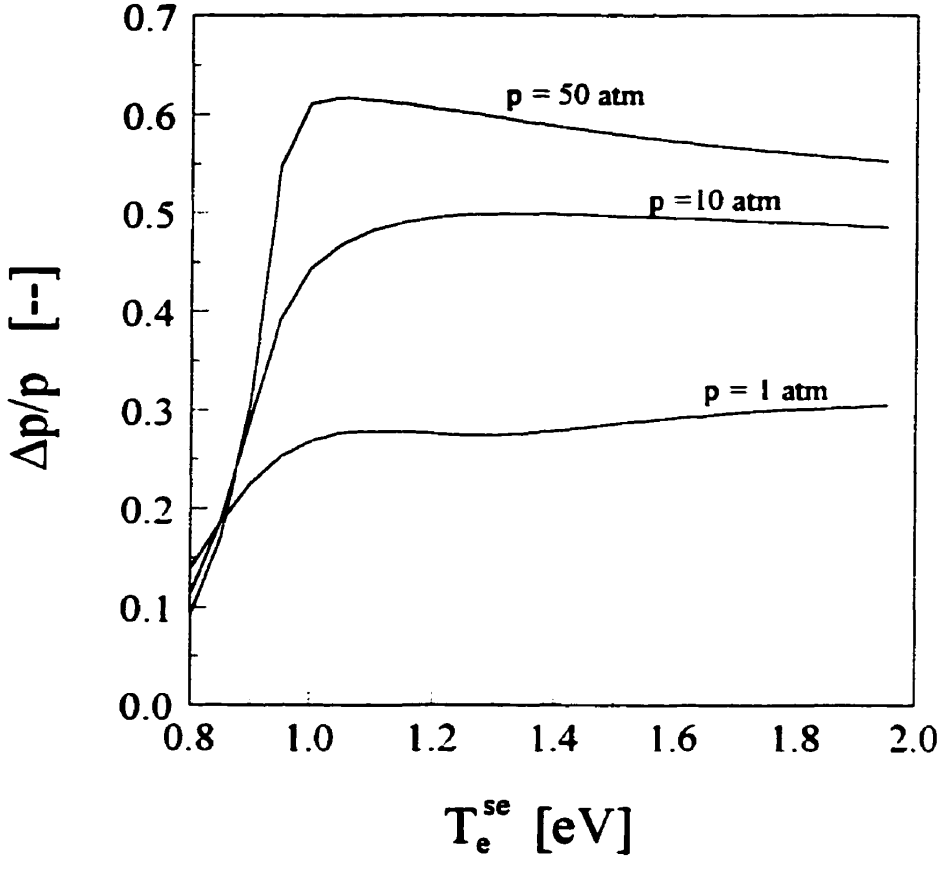

FIGURE 5.2.5. Pressure correction for a two-temperature Cu plasma as a function of T_e^{se} and p.

Unfortunately, for the conditions (p, T_e^{sc}) inducing a pressure correction $\Delta p/p$ larger than ~0.65 (metallic plasma pressures larger than ~75 atm), the calculation of the two-temperature plasma composition became impossible due to important numerical instabilities. The source of these instabilities is not known. The large gap between the electron and heavy particle temperatures might be the cause since these instabilities are not observed under LTE conditions (unique temperature). Fortunately, this limitation occurs at a pressure where criterion 4.4.2b is violated for T_e^{sc}=1.0 eV and therefore, the maximum pressure for a self-sustaining operation (p_{max}) can at least be estimated for one case with Cu. This problem is not observed with Fe and Ti since the self-sustaining pressure ranges are well below 75 atm as it will be seen later in section 5.3.

5.2.4. Current Transfer to the Cathode

The total current density in the cathode sheath j_{tot} is plotted in figure 5.2.6 as a function of the cathode spot metallic plasma pressure p and electron temperature T_e^{sc} at the cathode sheath edge. The current transport in the cathode sheath is mainly due to the ion (j_{ion}) and emitted electron currents ($j_{T\text{-}F}$): the relatively important voltage drop in the cathode sheath makes the back-diffusing plasma electron current (j_{bdc}) negligible.

The total current density is ~10^8 A m^{-2} for p=1 atm (n_e^{sc}=6x10^{23} m^{-3}, T_e^{sc}=1.0eV) and increases with the metallic plasma pressure. This value of ~10^8 A m^{-2} for j_{tot} corresponds to the maximum current density that can be obtained for an atmospheric pressure arc burning on a boiling cathode when the process of pressure build up in the cathode region is not considered. This is the so-called 'limit' of the thermionic arc cathode model discussed in section 2.3.4.

For the minimum metallic plasma pressure necessary for a self-sustaining arc obtained earlier in section 5.2.2 (p_{min}~19 atm for T_e^{sc}=1 eV, figure 5.2.1), a minimum total current density of ~3.5x10^9 A m^{-2} (T_e^{sc}=1 eV) is observed. This value agrees well with the rough estimate of the minimum current density per spot reported in section 2.3.3 for a clean Cu cathode exposed to an atmospheric pressure argon arc (~5x10^9 A m^{-2}).

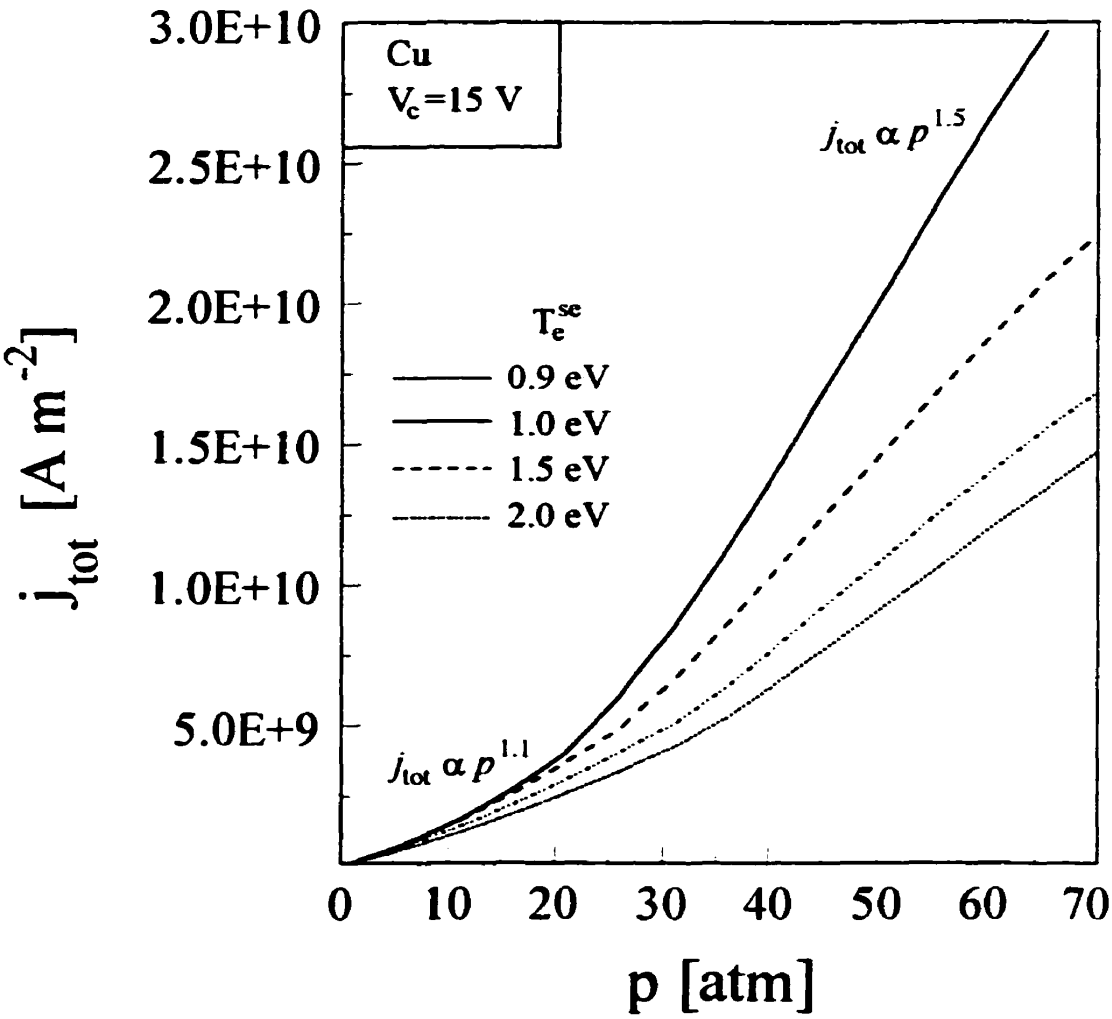

FIGURE 5.2.6. Total spot current density as a function of p for V_c=15 V and $0.9 < T_e^{se} < 2.0$ eV.

The model predicts a maximum current density for any value of the pressure at $T_e^{se} \sim 1.0$ eV attributable to the peak in the electron density (and ion density) of a Cu plasma at this temperature (figure 5.2.3). Indeed, the high ion densities have a fivefold enhancing effect on the total current density: 1) A high ion density means a high ion current density. 2) A high density of charged particles is associated with a high metallic plasma pressure and therefore, to a high cathode surface temperature which favors electron emission since both parameters are related to each other via a vapor pressure curve. 3) A high density of ions present in the cathode region establishes large surface electric fields at the cathode

surface which induces an important reduction of the cathode material work function ($\Delta\phi$=1.2 eV for E_s=10^9 V m^{-1}). 4) For surface electric fields larger than 10^9 V m^{-1}, field emission across the potential barrier at the metal surface becomes considerable leading to thermo-field emission of electrons (see figure 2.2.2). 5) A high density of slowly moving ions in the cathode region further enhances the emission process by forming high transition probability states for the electrons outside the metal surface (section 2.2.3). Since the current density is strongly coupled with the surface temperature, electric field strength and ion density, the choice of the proper equation to describe the electron emission processes under such conditions is again of primary importance.

The rate at which the total current density j_{tot} increases with the metallic plasma pressure shows a change in slope when the current transport in the cathode sheath changes from an ion-dominated, low current density mode ($j_{tot} \propto p^{1.1}$) to an emitted electron-dominated, high current density mode ($j_{tot} \propto p^{1.5}$) as it can be seen with figures 5.2.7 and 5.2.8. These figures show the fraction of the total current density carried respectively by the ions (j_{ion}/j_{tot}, figure 5.2.7) and thermo-field electrons ($j_{T\text{-}F}/j_{tot}$, figure 5.2.8). In comparison, the current density of back-diffusing plasma electrons normalized to the total current density (j_{bde}/j_{tot}) always stays below 1% for the whole pressure and electron temperature ranges.

Obviously, the transition from an ion-dominated to an emitted electron-dominated current transport mode occurs at the metallic plasma pressure p for which $j_{ion}/j_{T\text{-}F}$ =1, which pressure corresponds to the minimum pressure allowing a self-sustaining arc attachment for a given electron temperature (validation of criterion 4.4.2a). At low metallic plasma pressures (non-self-sustaining case), the flux of vaporized atoms is important in comparison to the flux of emitted electrons (see figure 5.2.2) and thus, the flux of cathode material ions accelerated back to the cathode after ionization in the plasma is quite large with respect to the thermo-field electron current. As the metallic plasma pressure increases, the emission conditions at the cathode surface become favorable for

strong thermo-field emission (high E_s, T_s, and n_i), and the electron emission current becomes dominant.

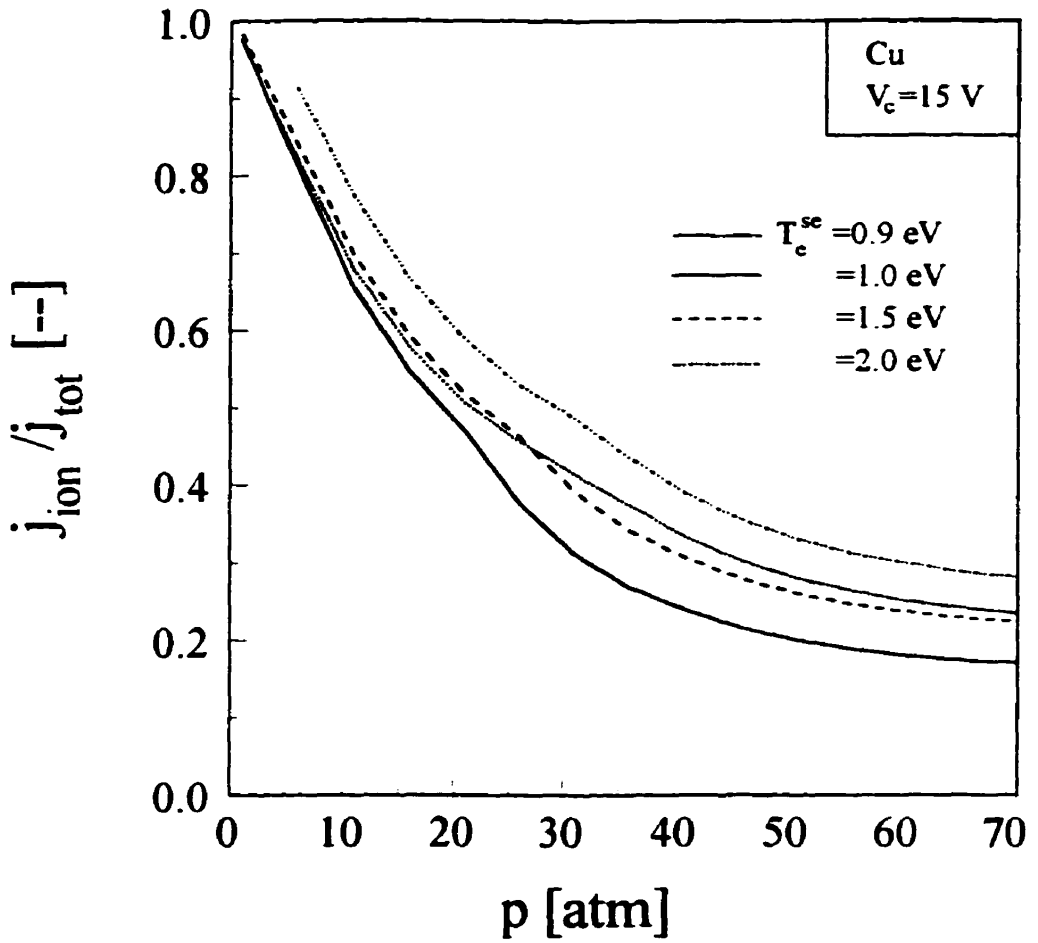

FIGURE 5.2.7. Fraction j_{ion}/j_{tot} of the total spot current density carried by the ions as a function of p for V_c=15 V and 0.9< T_e^{se} <2.0 eV.

The change of slope can now be interpreted from a theoretical standpoint. For low pressures (low current densities), the ion current is dominant and increases with the metallic plasma pressure approximately as $j_i \propto p^{1.1}$ since $j_i \propto n_i^{se} \cdot T_s^{1/2} \approx p \cdot p^{0.1}$ (equation (4.2.6)). For higher pressures, the thermo-field electron current is dominant and increases with the metallic plasma pressure approximately like $j_{T-F} \propto p^{1.5}$. Indeed, for T_s~3500-4000 K, $j_{T-F} \propto E_s^3$, and since $E_s \propto n_i^{1/2} \propto p^{1/2}$ by equations (4.2.18) and (4.6.5), $j_{T-F} \propto p^{1.5}$.

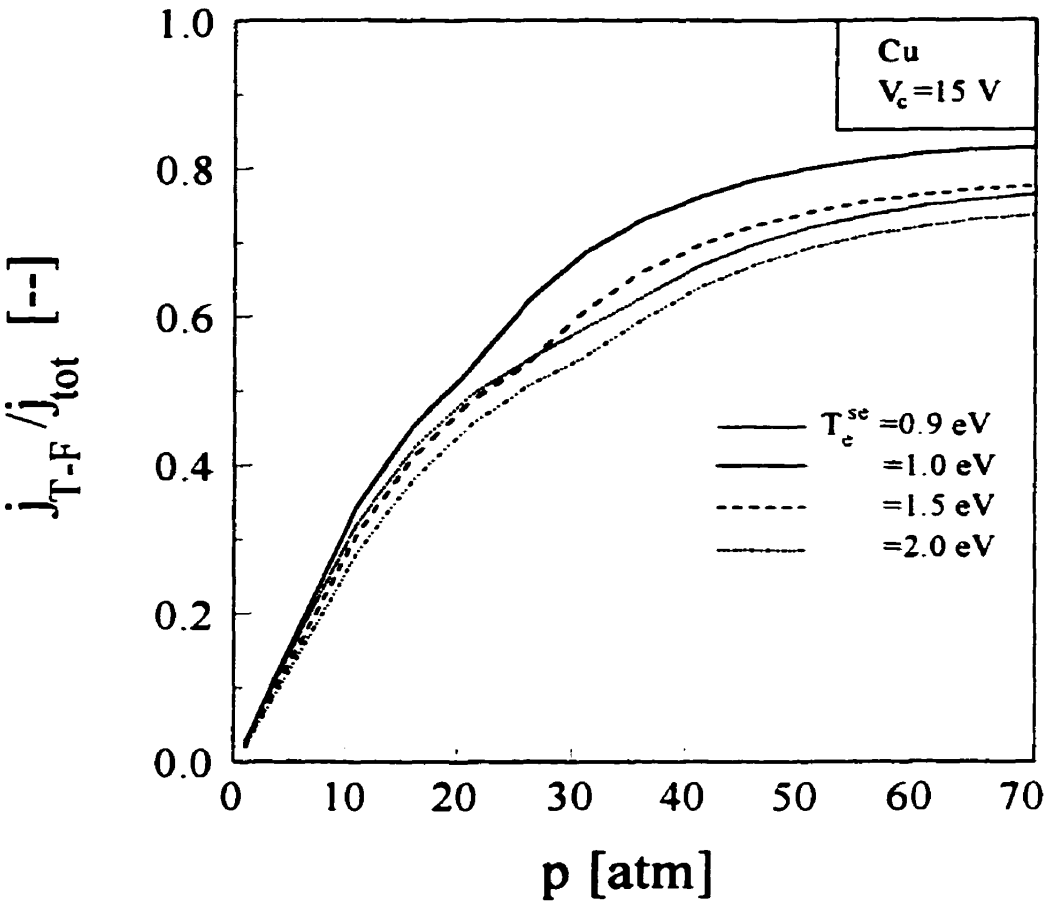

FIGURE 5.2.8. Fraction $j_{T\text{-}F}/j_{tot}$ of the total spot current density carried by the emitted electrons as a function of p for V_c=15 V and 0.9< T_e^{se} <2.0 eV.

5.2.5. Electron Emission Conditions

Figure 5.2.9 shows the evolution of the electron emission conditions at the cathode surface as a function of the metallic plasma pressure and electron temperature. The higher is the plasma pressure the higher is the surface temperature since the equilibrium vapor pressure curve is an increasing function of the temperature. It is shown that for a self-sustaining operation of the arc spot ($p>p_{min}$), the cathode surface temperature under the spot T_s is higher than ~3500 K which is ~660 K higher than the normal boiling of copper (2836 K). The surface electric field strength E_s increases from ~10^8 V m^{-1} for p=1 atm to ~2x10^9 V m^{-1} for p=70 atm explaining the strong increase of the thermo-field emission current density observed. The surface electric field strength is shown to depend on the electron temperature and reaches its maximum values for T_e^{se}=1 eV where the electron

density peaks for any value of the pressure. Indeed, the higher is the electron density at the cathode sheath edge, the higher is the degree of compression of the cathode sheath (thickness x_c, figure 5.2.10), and therefore the higher is the resulting surface electric field strength. The compression of the cathode sheath is theoretically studied in section 5.2.6.

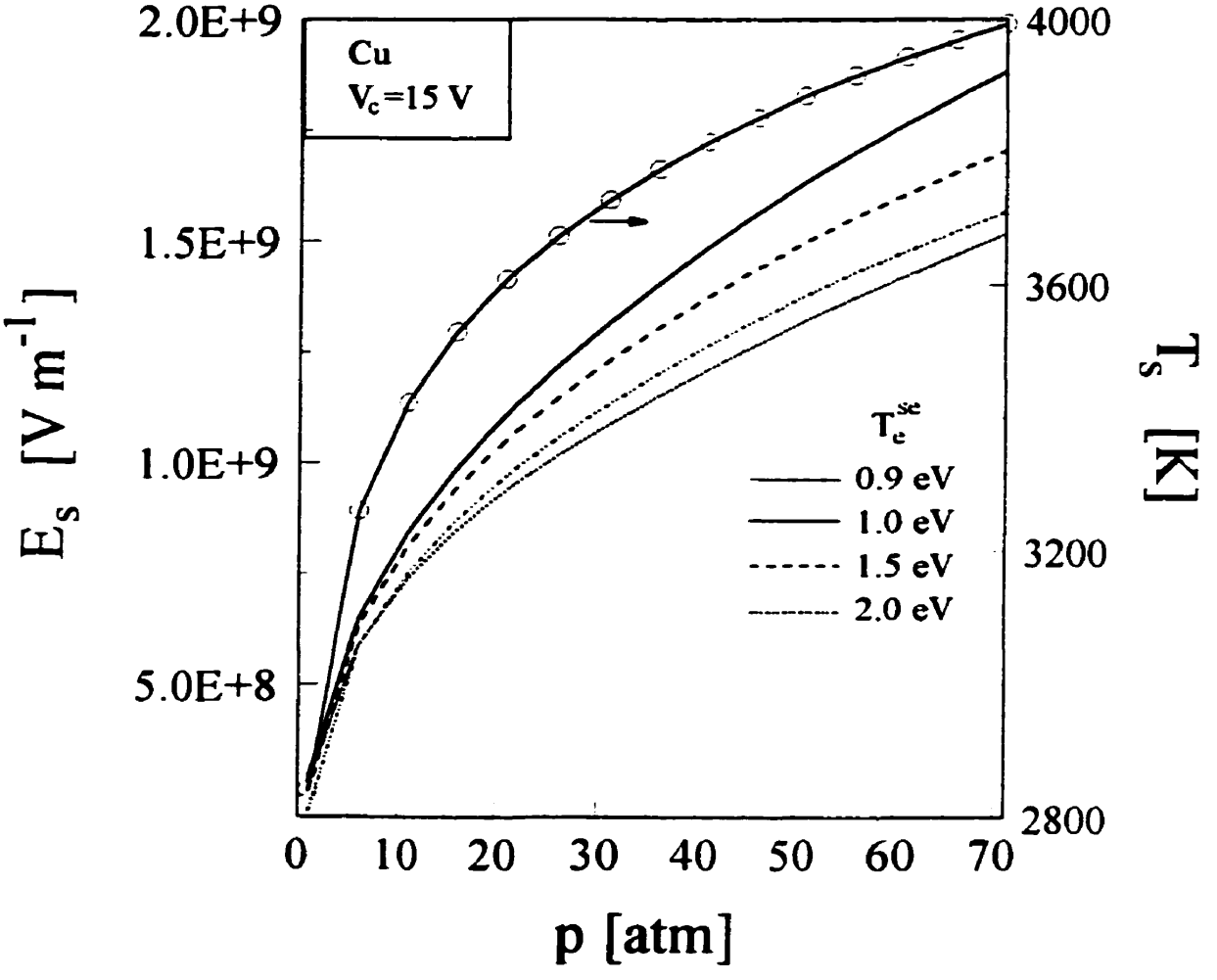

FIGURE 5.2.9. Surface electric field strength E_s and cathode surface temperature under the spot T_s as a function of p for V_c=15 V. E_s is plotted for 0.9< T_e^{se} <2.0 eV. T_s is independent of T_e^{se}.

As we have seen in section 2.2.3, the electron emission current is further enhanced due to the presence of a high density of charges in the cathode region. Table 5.2.1 reports the values taken by the enhancement factor β as a function of the total current density

(plasma pressure) and for T_e^{se}=1.0 eV. Remember that β is defined as the ratio of the thermo-field emission current calculated while taking into account the presence of ions (equation (2.2.6)) to the thermo-field electron emission current calculated in the absence of ions (equation (2.2.5)). β is shown to be around 2 for the conditions expected to prevail within the cathode spots on a Cu cathode.

TABLE 5.2.1. Ion-enhancement factor β of the thermo-field emission current $j_{T\text{-}F}$ as a function of the conditions prevailing within the cathode spots.

j_{tot} [x10^9 A m^{-2}]	p [atm]	T_s [K]	n_i^{se} [x10^{24} m^{-3}]	β [--]
1	7.4	3316	3.44	1.73
5	23.6	3648	9.24	1.88
10	34.2	3759	12.8	2.15
30	65	3964	22.3	1.75

The enhancement factor β is shown to increase slightly with the current density j_{tot} up to around β~2.15 for j_{tot}~10^{10} A m^{-2} and starts to decrease for higher current densities. Remember that the factor β is an increasing function of the ion density n_i^{se} and a decreasing function of the surface temperature of the emitter T_s (see Table 2.2.1). For low current densities, the increase of the ion density with the current density has a more important effect on β than the surface temperature. For high current densities, the reverse phenomenon is observed: β decreases due to the dominant effect of the increasing surface temperature. As it was reported in Table 2.2.1 the presence of doubly charged ions would considerably enhance the value of β. However, for a metallic Cu plasma having an electron temperature of 1 to 2 eV, the density of Cu^{--} ions is weak and these ions do not have any observable effects on β.

The compression of the cathode sheath which results in an increase of the surface electric field strengths when the electron density increases is shown in figure 5.2.10. The

cathode sheath thickness x_c is obtained from the double integration of Poisson's equation (4.2.16) over the distance to the cathode surface (x) until a potential $V=V_c$ is reached. This figure shows the evolution of the cathode sheath thickness x_c as a function of the metallic plasma pressure and electron temperature at cathode sheath edge (both effects combined indicate the effect of the electron density). Indeed, the higher is the pressure and the closer is the electron temperature to 1 eV, the higher is the electron density. Actually, for pressures higher than 5 atm, the cathode sheath thickness is shown to be inversely proportional to the pressure; i.e. $x_c \propto p^{-1}$. For the conditions allowing a self-sustaining operation of the cathode spots (p >19 atm), the cathode sheath thickness is less than 0.03 μm. Such a small thickness indicates why the cathode sheath region of this type of arc is almost impossible to study experimentally.

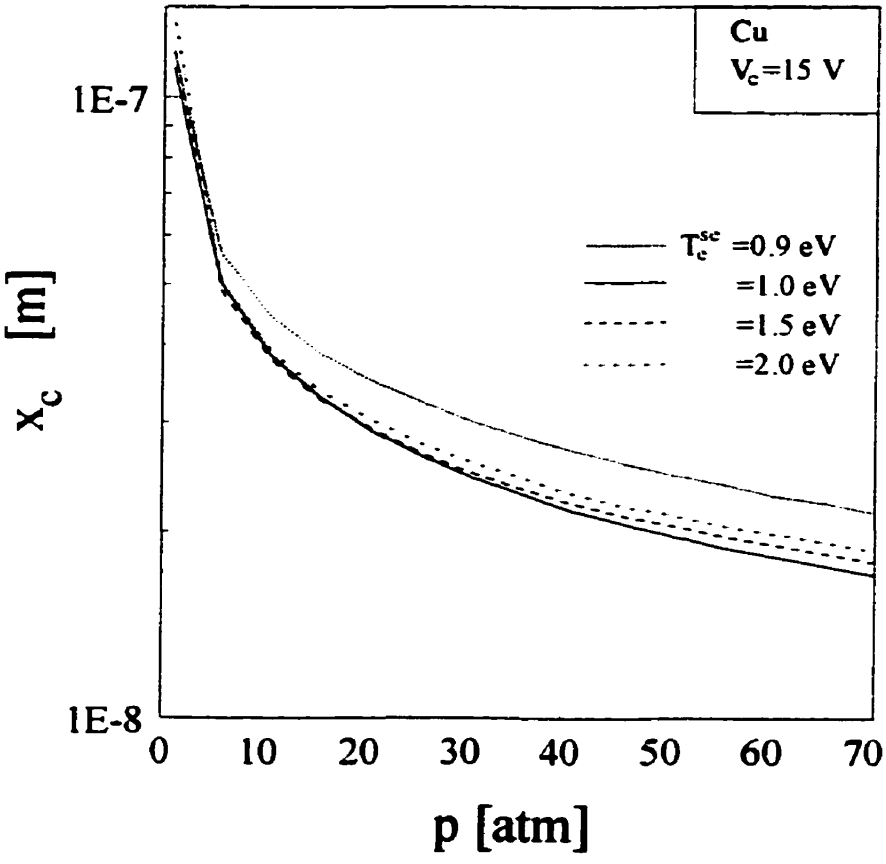

FIGURE 5.2.10. Cathode sheath thickness x_c as a function of p for V_c=15 V and $0.9< T_e^{sc} <2.0$ eV.

5.2.6. Internal Structure of the Cathode Sheath

The establishment of high surface electric fields at the cathode surface is closely related to the electrical phenomena involved inside the cathode sheath. The internal structure of the cathode sheath is presented in figure 5.2.11 for a particular self-sustaining situation where p=35 atm and T_e^{se}=1 eV. The distributions of local potential V and particle number densities (n_{ion}, n_e, n_{bde} and $n_{T\text{-}F}$ vs x) are plotted as a function of the distance in the cathode sheath. This distance was normalized by the Debye length λ_D in order to give a feeling of the distances involved with respect to the characteristic length for the electrostatic interactions. The total current density corresponding to this situation is $j_{tot}=10^{10}$ A m^{-2}, typical of such discharges. Such a high metallic plasma pressure in the cathode region is responsible for an electron density at the cathode sheath edge $n_e^{se}=1.3\text{x}10^{25}$ m^{-3}, and a cathode sheath thickness of only $2.2\text{x}10^{-8}$ m, which corresponds to ~22 times the Debye length evaluated at the cathode sheath edge conditions ($\lambda_D=1.02\text{x}10^{-9}$ m).

The total density of ions (Cu^+ and Cu^{++}) close to the cathode surface is reduced to ~20 % of its value at the cathode sheath edge while this number is less than 10^{-5}% for the back-diffusing plasma electrons. Due to the strong thermo-field emission of electrons at the cathode surface, the electron density stops decreasing at a distance x/λ_D ~5 from the cathode and starts increasing for lower distances to reach ~0.8% of n_e^{se} at the cathode surface. The ions and thermo-field emitted electrons are being accelerated in the cathode sheath by the favorable potential gradient. As a result, their respective densities decrease as their velocities increase in order to conserve the individual current densities. It is interesting to note that, even though the ion density is much higher than the electron density in the close vicinity of the cathode surface, the ion current is lower than the emitted electron current (see figures 5.2.7 and 5.2.8). This is attributable to the much higher velocities assumed by the emitted electrons (~$5\text{x}10^5$ m s^{-1} for the emitted electrons in comparison to ~$7\text{x}10^3$ m s^{-1} to the Cu^+ ions impinging on the cathode).

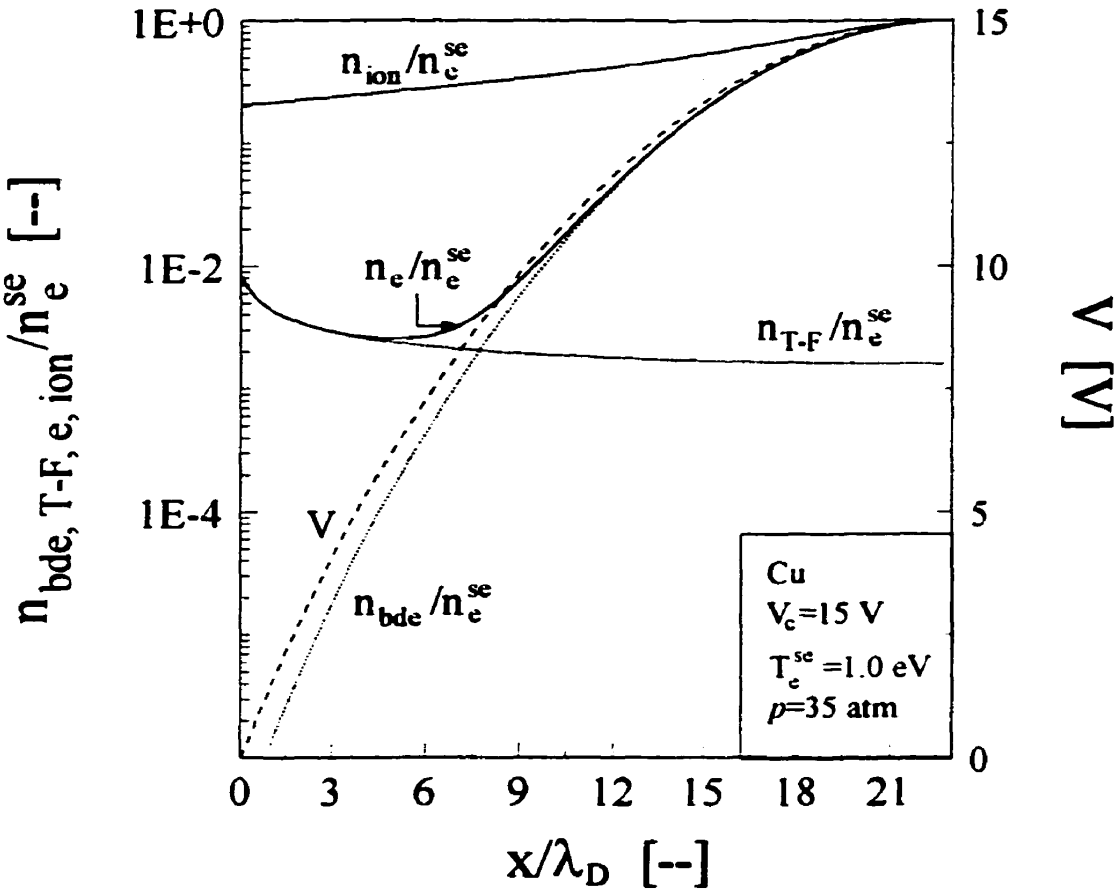

FIGURE 5.2.11. Distribution of the particle number densities and voltage in the cathode sheath as a function of the distance from the cathode surface for V_c=15 V, T_e^{se}=1.0 eV and p=35 atm. λ_D~1.02x10^{-9} m and the corresponding total current density is j_{tot}=10^{10} A m^{-2}.

The voltage distribution in the cathode sheath shows a sharp decrease as one goes towards the cathode surface producing large surface electric field strengths as reported in figure 5.2.9. Due to the formation of a net positive space charge in the cathode sheath ($n_{sc} = n_{ion} - n_{T-F} - n_{bde}$), the local electric field $E(x)$ is not constant throughout. Actually, it increases from zero at the cathode sheath edge (Mackeown's assumption, equation (4.2.17b)) and takes its largest value at the cathode surface (E_s). The formation of this net positive space charge in the cathode sheath is shown in figure 5.2.12. At the cathode sheath edge the plasma is still electrically neutral and therefore, the space charge vanishes. As one goes towards the cathode, the ions being attracted and the plasma electrons

repelled, a space charge starts to form and reaches its maximum density at a distance of around $13\lambda_D$ from the cathode surface. Closer to the cathode, the thermo-field electrons emitted from the surface attenuate the space charge.

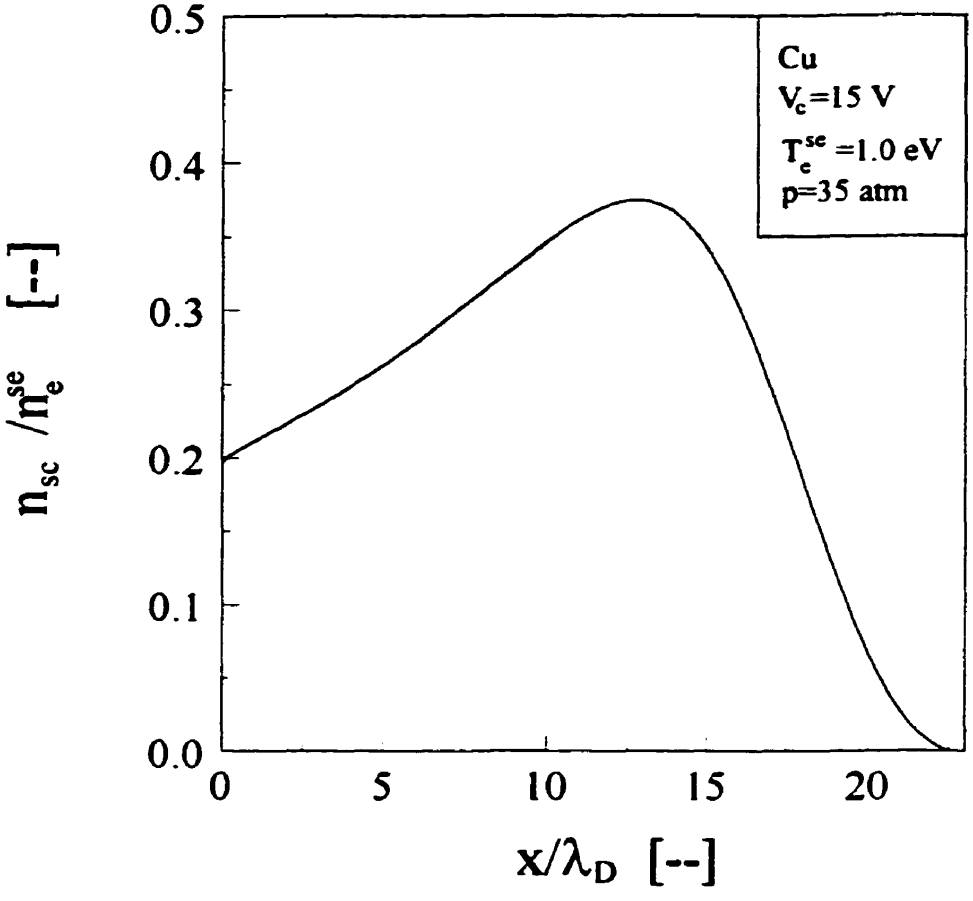

FIGURE 5.2.12. Space charge formation in the cathode sheath for V_c=15 V, T_e^{se}=1.0 eV and p=35 atm. λ_D~1.02x10^{-9} m and the corresponding total current density is j_{tot}=10^{10} A m^{-2}.

From this simple analysis it becomes clear that the strong thermo-field emission of electrons from the surface of clean metal cathodes is due to the formation of an important space charge, which is itself due to the presence of a high density of charged particles (ions and electrons) in the cathode region. For the case of non-refractory cathodes, the plasma ions formed by ionization of the ambient gas atoms would not be in a sufficient number to form the space charge necessary for strong electron emission (criterion 4.4.2a, $j_{T\text{-}F} > j_{ion}$);

the ionization of the metallic vapors coming from the cathode erosion and the pressure build up are necessary. Indeed the space charge density n_{sc} is shown to increase with the metallic plasma pressure in the cathode region as it can be seen with figure 5.2.13 which shows the evolution of the space charge density as a function of the local potential in the cathode sheath, and for two values of the pressure. The local potential V is used rather than the distance to the cathode surface x in order to have the same scale for the two conditions investigated.

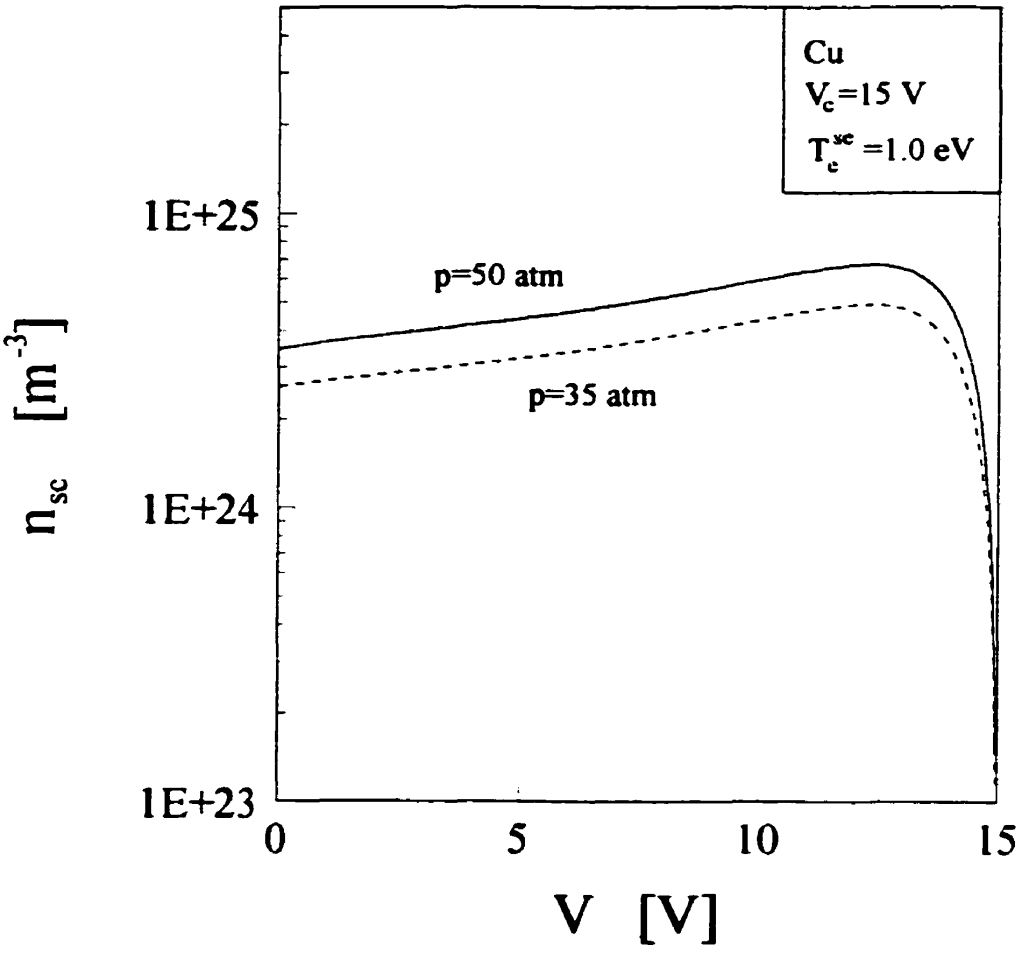

FIGURE 5.2.13. Space charge n_{sc} as a function of the local potential in the cathode sheath $V(x)$ for V_c=15 V, T_e^{sc}=1.0 eV and for two values of p (35 and 50 atm).

Figure 5.2.13 can now be used to understand from a theoretical standpoint the concept of compression of the cathode sheath with the increasing electron density

introduced in section 5.2.5. The cathode sheath thickness x_c is determined by integration of the Poisson's equation from the cathode surface where V=0 and x=0 to V=V_c and x=x_c. The right hand side of the Poisson's equation is proportional to the net space charge density n_{sc} and therefore, the higher is n_{sc} the shorter is the integration distance x_c before getting V=V_c.

5.2.7. Heat Transfer to the Cathode

The knowledge of the incoming heat flux to the cathode, and how this flux is dissipated is of fundamental importance for understanding the erosion phenomena. Figure 5.2.14 shows the calculated total incoming heat flux from the cathode spot plasma to the surface under the spot q_{in} as a function of the metallic plasma pressure p, and electron temperature T_e^{sc}. As for the current transfer from the plasma to the cathode, the impinging ions are responsible for almost all the incoming heat flux from the plasma since the back-diffusing plasma electron current is low for this cathode sheath voltage drop (<1 %). The incoming heat flux peaks again at an electron temperature of ~1 eV as is the case for the current density.

The incoming heat flux is shown to increase with the metallic plasma pressure and a gradual change of slope is also observed when the current transfer mode changes from the ion-dominated to the emitted electron-dominated mode. However, rather than having an increase in slope as observed with the total current density j_{tot}, we observe a decreasing trend: in terms of current transfer, the strong emission of thermo-field electrons helps increasing the total current density to the cathode while in terms of heat transfer, electron emission induces an heat loss from the cathode. Indeed, for the range of surface temperatures and electric field strengths expected, which values are respectively higher than 3500 K and lower than $2\text{x}10^9$ V m^{-1} (see figure 5.2.9), the Nottingham potential ε_N is greater than zero (see figure 4.3.1) and therefore, the electron emission always results in a cooling effect for the cathode. This phenomenon has an important practical consequence as it will be discussed later in section 5.5.

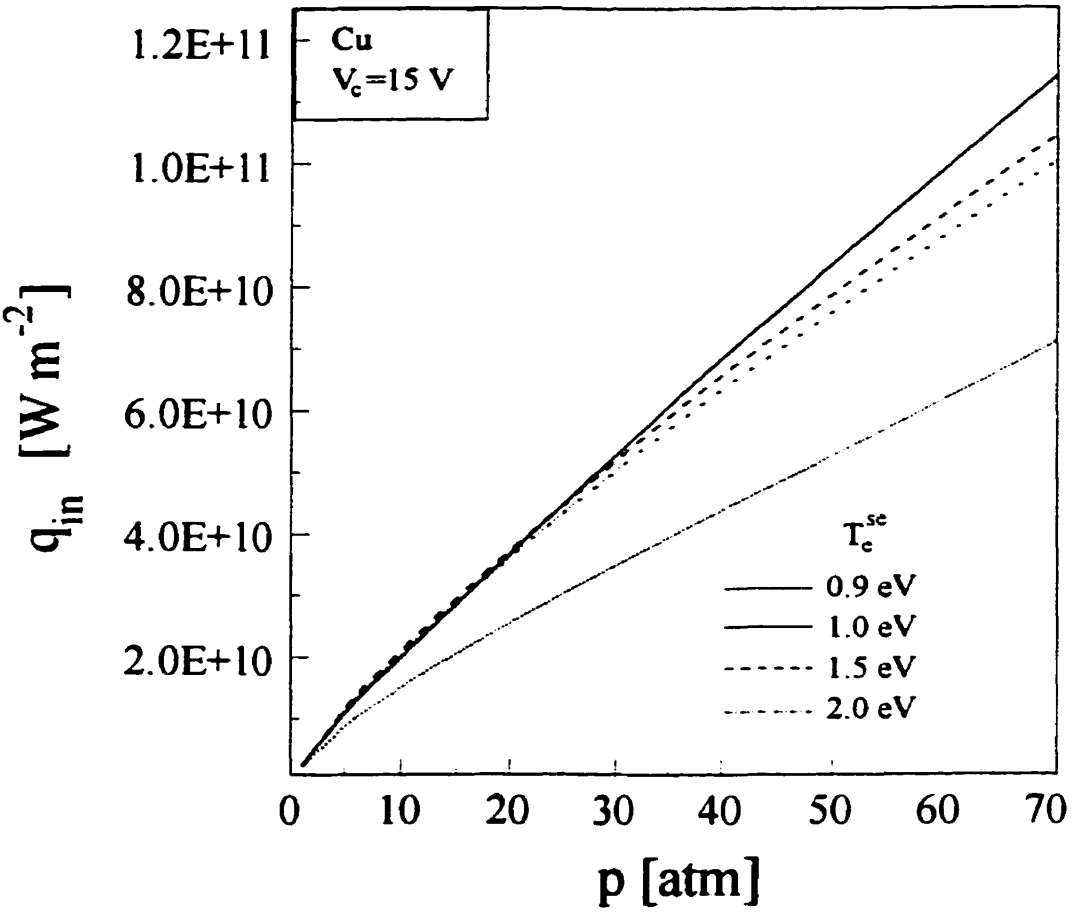

FIGURE 5.2.14. Total incoming heat flux to the cathode spot surface q_{in} as a function of p for V_c=15 V and 0.9< T_e^{se} <2.0 eV.

An incoming heat flux larger than 3×10^{10} W m^{-2} is evaluated for the self-sustaining operation of the arc spots on Cu (p>19 atm). This incoming heat flux is dissipated by conduction into the cathode q_{cond}, latent heat of vaporization q_{vap}, and electron emission cooling q_{not} as it can be seen with figure 5.2.15. For low pressures (low current densities), the main heat loss is by conduction into the cathode bulk while Nottingham cooling becomes dominant at high pressures (high current densities) due to the favorable electron emission conditions (figure 5.2.9). The fraction q_{vap}/q_{in} of the incoming heat flux lost by cathode material vaporization only slightly increases with the metallic plasma pressure due to the slow increase of Γ_{vap} with p (equation (2.3.1)). On the other hand, the fractions q_{cond}/q_{in} and q_{not}/q_{in} are shown to vary strongly with the pressure and electron temperature due to their dependency on their respective current densities, which are themselves

strongly dependent on these two parameters. The effects of the electron temperature are more pronounced at elevated current densities (high pressures). Important variations of the electron emission current density result from small variations of the surface electric field strength ($j_{tot} \propto E_s^3$), themselves being induced by the variations of the electron density ($E_s \propto n_e^{1/2}$) with the electron temperature. It is not surprising to observe that for the conditions allowing the maximum electron density for a given pressure, i.e. T_e^{se}=1.0 eV, the electron emission cooling is the highest. Indeed, as it was discussed in section 5.2.6, the higher is the electron density n_e^{se}, the higher is the surface electric field strength E_s and therefore, the higher is the electron emission current density.

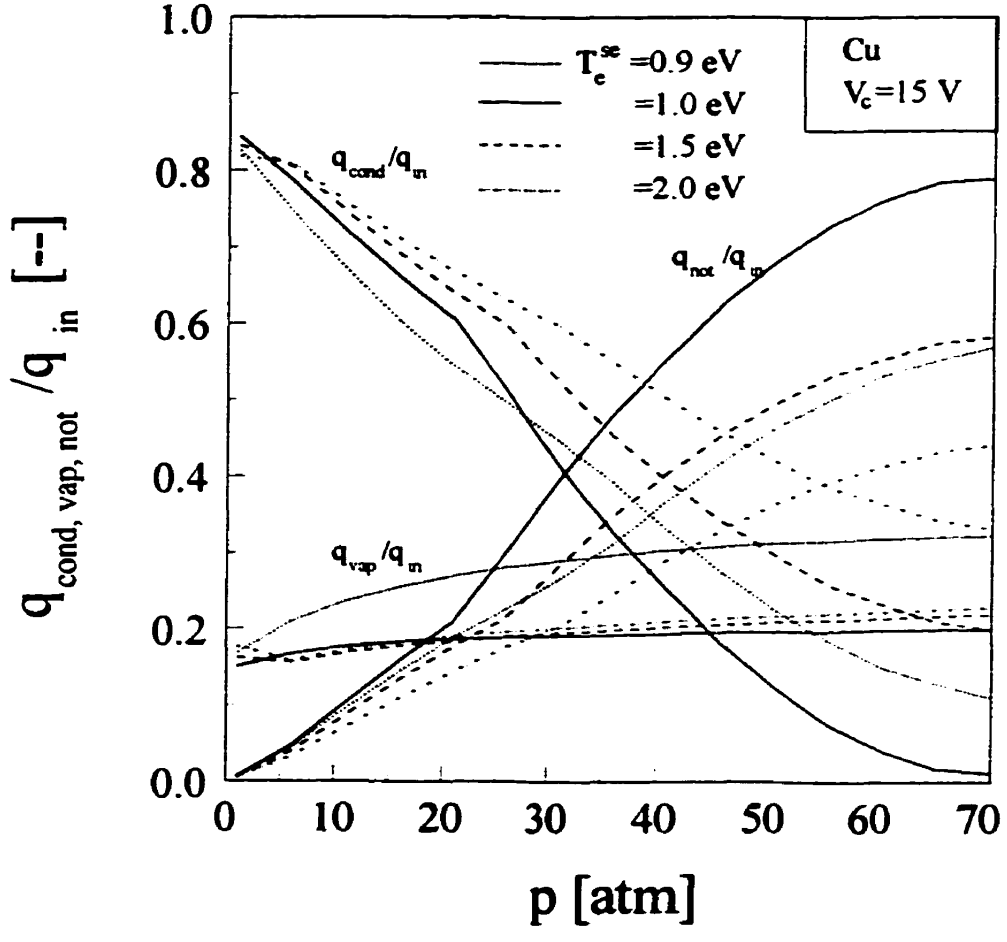

FIGURE 5.2.15. Distribution of the different heat losses from the cathode spot surface as a function of p for V_c=15 V and 0.9< T_e^{se} <2.0 eV.

Figure 5.2.16 shows the heat losses by conduction only (q_{cond}) as a function of the metallic plasma pressure and electron temperature. Criterion (4.4.2b) states that for a self-sustaining operation of the arc discharge, $q_{cond} > 0$. Figure 5.2.16 shows this criterion is validated for metallic vapor pressures below ~67 atm when T_e^{sc}=1 eV, and somewhat higher values for T_e^{sc} different than 1.0 eV. Unfortunately, the model did not allow the calculation of the exact pressure p above which criterion (4.4.2b) fails for T_e^{sc} different than 1.0 eV due to the problems mentioned in section 5.2.3. However, one can see than the evolution of p_{max} with T_e^{sc} follows the same trend as p_{min}; both p_{min} and p_{max} take their lowest values at T_e^{sc}=1.0 eV. On the other hand, some reasons discussed later in section 6.3.3 allow us to think that the cathode spot plasma on a Cu cathode is operating at T_e^{sc}=1.0 eV, which temperature is at which the charged particle densities and total current density peak.

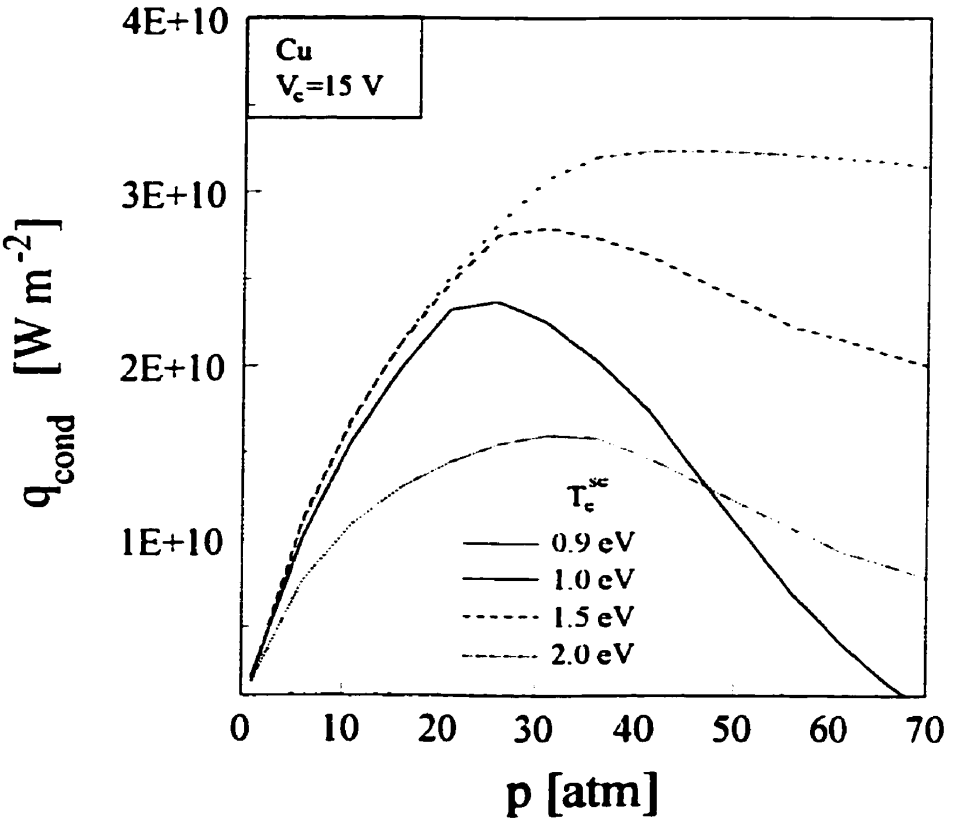

FIGURE 5.2.16. Heat flux lost by conduction q_{cond} as a function of p for V_c=15 V and 0.9< T_e^{sc} <2.0 eV.

A metallic vapor pressure p_{max}=67 atm for T_e^{sc}=1.0 eV allows a maximum current density at the cathode surface j_{tot}~3x10^{10} A m^{-2} (see figure 5.2.6). Considering the minimum value estimated in section 5.2.4 for p=p_{min}, the range ~3.5x10^{9}-3x10^{10} A m^{-2} is obtained from the present model for the range of total current densities per spot needed for a self-sustaining operation on a Cu cathode. Such a range of total current densities corresponds to a range of current per spot I_s of 0.5 to 10 A (see figure 2.3.3) when crater diameters of around 5 to 15 μm are considered (see figure 3.3.1), and when the assumption that the arc current is flowing through the crater surface area only is made. Such currents per spot agree well with those estimated for vacuum arc on Cu (Siemroth *et al* 1995 reported values of around 2-20 A).

5.2.8. Erosion by Vaporization

Knowing the flux of vaporized atoms necessary to maintain a self-sustaining arc spot, one can estimate the erosion rate due to vaporization. According to equation (4.5.1), the erosion rate by vaporization $E_{r,vap}^{max}$ is proportional to the metallic plasma pressure p and inversely proportional to the total current density j_{tot}. For self-sustaining operations of the arc spot (p>19 atm), $j_{tot} \propto p^{1.5}$ and therefore $E_{r,vap}^{max}$ decreases as p increases like $1/p^{0.5}$ as can be seen in figure 5.2.17. When no redeposition of ions nor neutrals is considered, the erosion rate is fairly high. When some ions bombarding the cathode surface condense upon impact, the erosion rate by vaporization is reduced and stands between the limits given by relation (4.5.2). The range of experimentally measured vacuum erosion rates for copper cathodes (65-115 μg C^{-1}, Farall 1980) is also indicated in Figure 5.2.17. These measurements stand between the limits imposed by relation 4.5.2) for 1.0<T_e^{sc}<2.0 eV.

Two observations are important to make here: 1) The present model developed for a high pressure arc on a non-refractory cathode allows to predict relatively well the vacuum arc erosion rates. This shows again the similitude between the vacuum arc cathode spots and the atmospheric arc cathode spot (this seems to be true for Cu). 2) It is interesting to note that the measured vacuum erosion rates, which correspond to overall

erosion including microdroplets ejection, in fact fall within the limits evaluated considering only cathode material vaporization and ion condensation. Such a behavior correlates with small ratio of conductive heat flux to vaporizing heat flux for copper as the current density is increased (figure 5.2.15 for pressures at or above 45 atm). This indicates that a very small volume, if any, should be present in the copper cathode spot at high current densities (point to be discussed in Chapter 7). The high thermal conductivity and the high vapor pressure of copper are mainly responsible for this behavior.

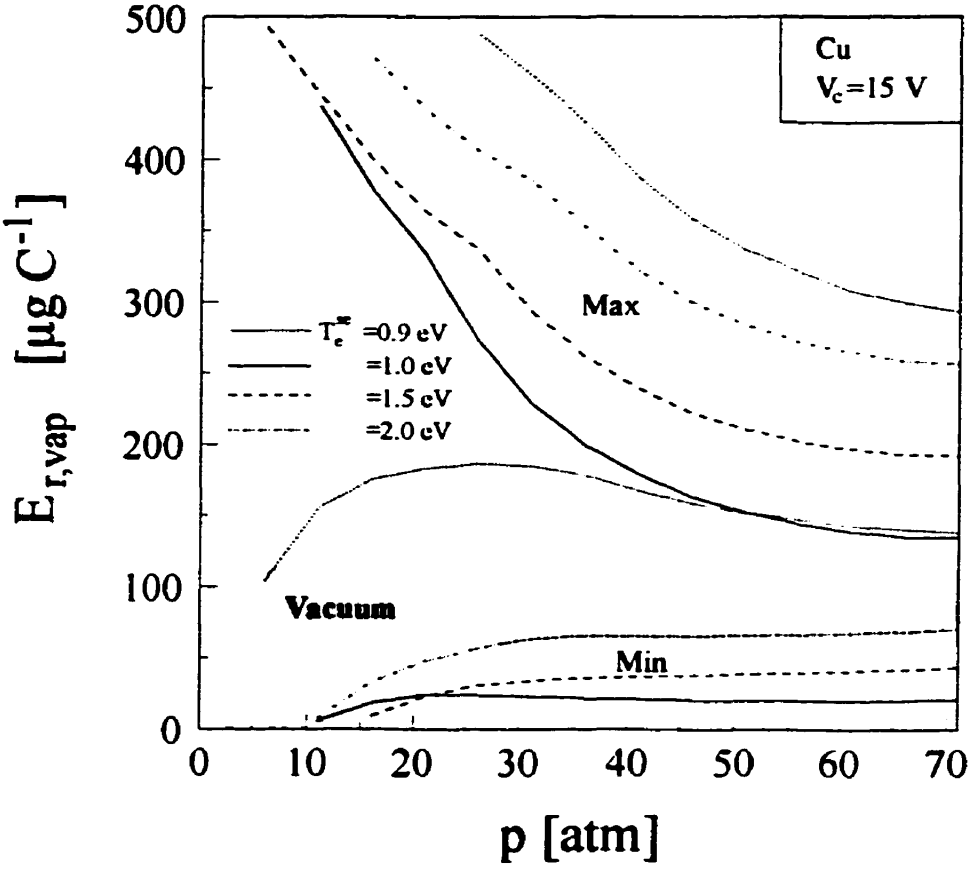

FIGURE 5.2.17. Calculated erosion rate by vaporization ($E_{r,vap}^{max}$) and erosion rate by vaporization considering ion redeposition ($E_{r,vap}^{min}$) for a clean Cu cathode as a function of p for V_c=15 V and $0.9 < T_e^{sat} < 2.0$ eV. The measured vacuum erosion rate for Cu (~ 65-115 μg C^{-1}) is represented by the shaded area.

According to Figure 5.2.17 the model predicts a minimum erosion rate of approximately 20 $\mu g\ C^{-1}$ if all the ions recondense on the cathode surface. This scenario is however not likely to occur explaining why such low erosion rate values are not observed under vacuum conditions. However, such a low value for the erosion rate would be possible if part of the neutral atoms present in the cathode region condense. Indeed, at higher ambient gas pressures, the cathode spot plasma is confined within an hemisphere of a much lower radius than under vacuum conditions and redeposition of neutrals occurs (Meunier 1990).

Erosion rate values reported by Szente *et al* (1992) for an atmospheric pressure argon arc interacting with a non-refractory copper cathode show, like under vacuum conditions, a rather large variation of ~4 to 50 $\mu g\ C^{-1}$. It is shown that the erosion rate is strongly dependent on the conditions prevailing in the chamber (e.g. type of gas and gas flow rate) and the velocity at which the arc moves (when forced to do so); the lowest values of erosion being observed for low gas flow rates, high arc velocities, and as a general rule, for gas compositions and surface conditions that promote arc ignition and arc mobility. High values of 25-50 $\mu g\ C^{-1}$ close to those of the vacuum situation are observed when the arc is almost stationary. Thus, these observations suggest that when a gas is present in the chamber and external means are used to move the arc, the erosion rate is also function of the properties outside the cathode spots. Such surface properties would affect strongly the mechanism of new spot ignition. The present model cannot take into account these effects.

5.3. Model's Predictions with Fe and Ti Cathodes

As it was discussed in section 2.3.2, copper and tungsten when used as high pressure arc cathodes represent two extreme cases: for copper, we have seen that a strong vaporization of the cathode is necessary for establishing the self-sustaining arc conditions while for tungsten, this seems not necessary since only a weak vaporization is observed (generally below 0.1 $\mu g\ C^{-1}$). According to figure 2.3.1, an intermediary behavior should be observed with metallic elements such as iron (Fe) and titanium (Ti).

Table 5.3.1 shows the model's predictions of the self-sustaining arc spot conditions for Cu, Fe and Ti cathodes. The cathode sheath voltage drops of Fe and Ti are not known. However, the properties of these materials let suggest that their cathode sheath voltage drops fall in between the large value of V_c=15 V for Cu and the lower value of V_c=8 V for W. Therefore, V_c=10 and 15 V were chosen for the calculations. All the results reported in Table 5.3.1 were obtained with T_e^{sc}=1 eV which is the approximate electron temperature at which the electron densities of Cu, Fe and Ti plasmas peak (the three elements having similar first ionization potentials). Like for a Cu cathode, the minimum pressure for self-sustaining operation (p_{min}) was shown to be determined by criterion 4.4.2a while the maximum pressure (p_{max}), determined by criterion 4.4.2b for both Fe and Ti cathodes.

TABLE 5.3.1. Model's predictions of the self-sustaining operating conditions for the arc spots on Cu, Fe and Ti cathodes

Material	T_v [K]	V_c [V]	p_{min} [atm]	j_{tot} (p_{min}) [A m^{-2}]	p_{max} [atm]	j_{tot} (p_{max}) [A m^{-2}]	T_s [K]	$j_{ion}/j_{T\text{-}F}$ (p_{max}) [--]
Cu	2836	15	19	3.5×10^{9}	67	3×10^{10}	>3600	0.25
Fe	3135	15	8.5	2.3×10^{9}	36	2.2×10^{10}	>3780	0.22
Ti	3562	15	~1	~3.1×10^{8}	8	5.9×10^{9}	>3560	0.24
Fe	3135	10	12.5	3.1×10^{9}	37	1.6×10^{10}	>3900	0.33
Ti	3562	10	1.25	2.78×10^{8}	6.5	3.5×10^{9}	>3560	0.38

Results show an interesting behavior that could be expected after analysis of figure 2.3.1: the more refractory is the cathode material the lower is the metallic plasma pressure needed for a self-sustaining operation of the arc spots. The highest pressure range is observed with Cu (19-67 atm) which has the lowest boiling temperature of the three materials, followed by Fe (8-37 atm) with the intermediary boiling temperature, and finally by Ti (1-8 atm) with the highest boiling temperature. This can be seen clearly with figure 5.3.1 where the range of metallic plasma pressures needed for a self-sustaining operation of the arc spots is plotted against the cathode material boiling temperature. The range of

metallic vapor pressures corresponding to the estimated range of surface temperatures for W (T_s=3700-4600 K, Benilov and Marotta 1995) is also plotted in figure 5.3.1.

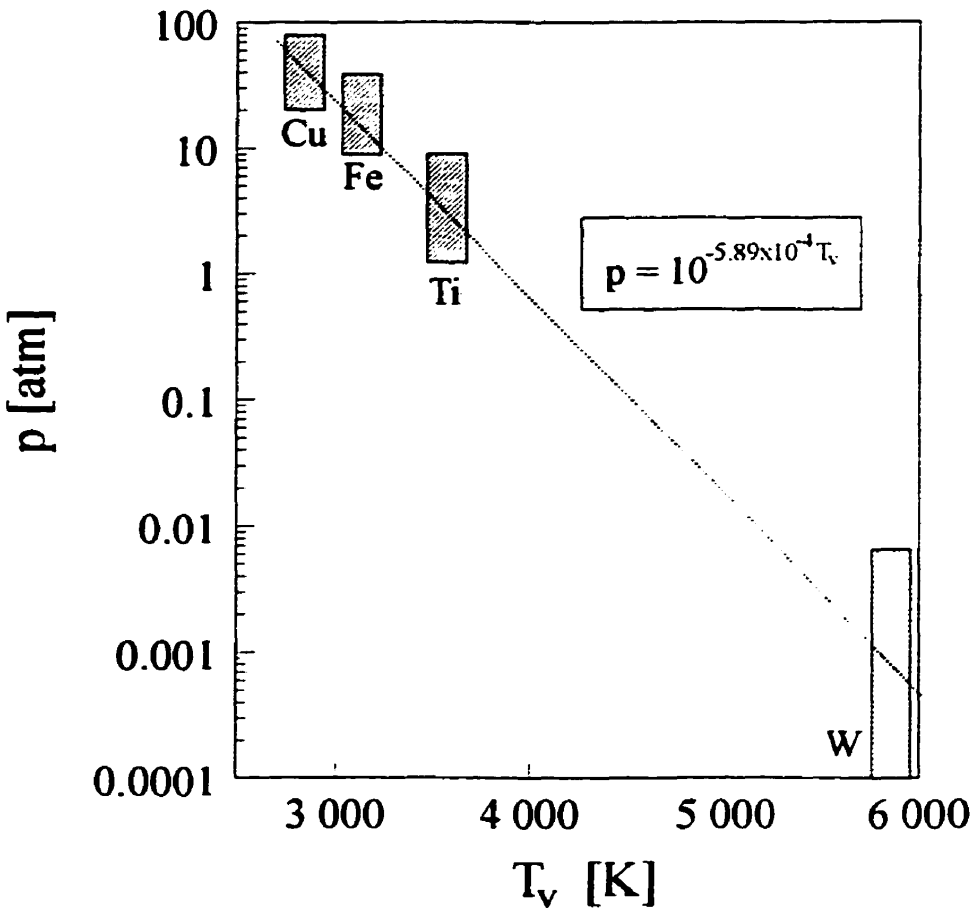

FIGURE 5.3.1. Range of metallic plasma pressure needed for a self-sustaining operation of the arc spots as a function of the cathode material's boiling temperature T_v.

The results presented in figure 5.3.1 allow to draw an important conclusion: It becomes clear from the analysis that led to figure 5.3.1 that refractory and non-refractory cathodes of high pressure arc systems differ only in the way they achieve the necessary conditions for a self-sustaining operation of the arc. Indeed, it is shown with figure 5.3.1 that the two extreme situations are actually representing the two limits of a unique description; the self-sustaining operation of an arc discharge on a refractory (hot) cathode (e.g. W) is achieved without the need of vaporization of the cathode surface while on a

non-refractory (cold) cathode (e.g. Cu), a strong vaporization resulting in a pressure build up in the cathode region is necessary. We can now understand why an arc over a W cathode which has a normal boiling of 5828 K does not require a high vapor pressure of cathode material to be self-sustaining.

The current density per spot also decreases as the material becomes more refractory. The mean current density on a Cu cathode is $\sim 1.7 \times 10^{10}$ A m^{-2} while it is around $\sim 10^{8}$ A m^{-2} for W. Note also that the operating temperatures for all the cathode materials considered are higher than ~3500 K, and that the ratios $j_{ion}/j_{T\text{-}F}$ are all approximately the same (for $p=p_{max}$ for instance). Finally, it is interesting to make a link between the theoretically estimated total current densities and the experimentally determined erosion rates since both parameters are thought to be closely related to each other (relation (4.5.1)). The erosion rates of clean Cu and Ti cathodes obtained after arcing under similar conditions are respectively, E_r^{Cu}=13.5 μg C^{-1} and E_r^{Ti}=1.6 μg C^{-1} (Kwak 1994), giving rise to a ratio of ~10 for their erosion rates. The ratio of their respective average current densities is also of ~10 (Table 5.3.1) showing again the intimate relationship between erosion rate and current density.

5.4. Validity of the Collisionless Cathode Sheath Assumption

The collisionless cathode sheath assumption was made in the development of the physical model in order to considerably simplify the problem. In such a situation, no collisions involving ionization nor momentum exchange occur allowing the current densities to be conserved in the cathode sheath. In order to validate such an assumption, the characteristic lengths for ionization (λ^{i}) and momentum exchange (λ^{M}) must be compared to the thickness of the cathode sheath x_c. As suggested by equation (4.1.1), an important number of such characteristic lengths must be estimated. However, we limit ourselves here to the estimation of two characteristic lengths that we think are the most important. These are respectively the characteristic lengths for single-impact ionization of

a neutral atom by a beam electron, λ^{t}_{e-o}, and for momentum exchange between a beam electron and a neutral atom, λ^{M}_{e-o}.

The beam electrons exit the cathode sheath with a mean kinetic energy of the order of the cathode sheath voltage drop eV_c. For the present case, this corresponds to 15 eV. At this incident electron energy, the single-impact ionization cross section with a neutral Cu atom is σ^{i}_{e-Cu}=3.19x10^{-20} m^2 (Freund *et al* 1990). For the conditions reported in figure 5.2.11 for instance (p=35 atm and T_e^{∞} =1 eV), the density of neutral atoms is 5.4x10^{25} m^{-3} and therefore, $\lambda^{t}_{e-Cu} = 1/n_o\sigma^{i}_{e-Cu}$=5.85x10^{-7}. Such a value is ~27 times the cathode sheath thickness evaluated under the same conditions (x_c=2.2x10^{-8} m). Therefore, the ionizing collisions occur much farther in the presheath and this, for the whole range of pressures investigated in this study.

According to the experimental measurements of Trajmar *et al* (1977), the momentum exchange cross section for an electron having an energy of 15 eV and colliding with a Cu atom is $\sigma^{M}_{e\ Cu}$=58x10^{-20} m^2, which value is considerably higher than $\sigma^{i}_{e\ Cu}$. Therefore, much smaller characteristic lengths for this interaction are expected as it can be seen with figure 5.4.1 which shows the evolution of the ratio $x_c / \lambda^{M}_{e\ Cu}$ as a function of the metallic plasma pressure for T_e^{∞}=1.0 eV. The results show that the assumption of a collisionless cathode sheath is easily validated at atmospheric pressure but, becomes less accurate as the metallic plasma pressure (density) increases. Up to a pressure of around 55 atm, the ratio x_c / λ^{M}_{e-Cu} is still lower than unity. This observation lets suggest that, above such a high pressure, a transition from a collisionless cathode sheath to a collision-dominated cathode sheath should occur (Benilov 1997).

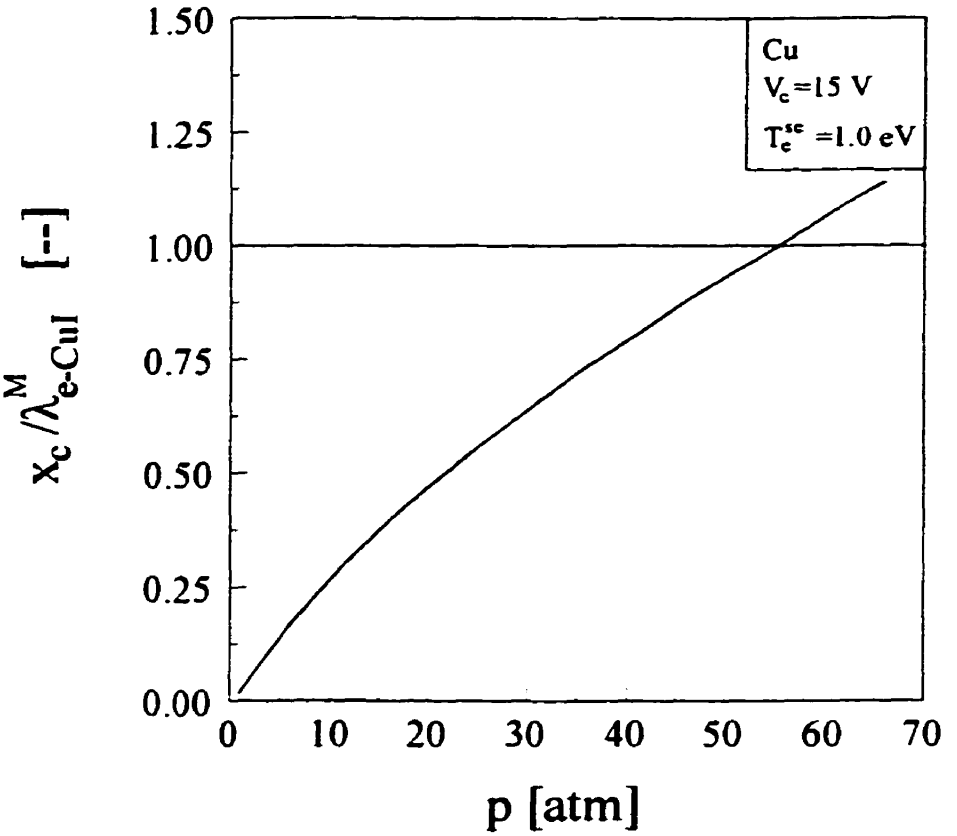

FIGURE 5.4.1. Evolution of the ratio $x_c / \lambda^M_{e\text{-}CuI}$ as a function of p for V_c=15 and T_e^{sc}=1.0 eV.

5.5. Influence of the Cathode Sheath Voltage Drop

For all the results presented in section 5.2 for a Cu cathode, the cathode sheath voltage drop was set to the best experimental estimate known (V_c=15 V). The simple analysis of section 5.2.1 showed that a value for V_c significantly different than 15 V is not likely. A sensitivity study of the model's predictions using slightly different values for V_c has been carried out and the results have shown that:

i) The higher is the metallic plasma pressure the higher are the effects of a slight variation of V_c on the estimate of the total current density as shown on figure 5.5.1. This is due to the fact that as the pressure increases, the total current density becomes proportional to E_s^3, where E_s significantly varies with V_c according to relation (4.2.18). For V_c

varying by the large amount of ±3 V, the corresponding variations of j_{tot} are around ±20% for p=65 atm.

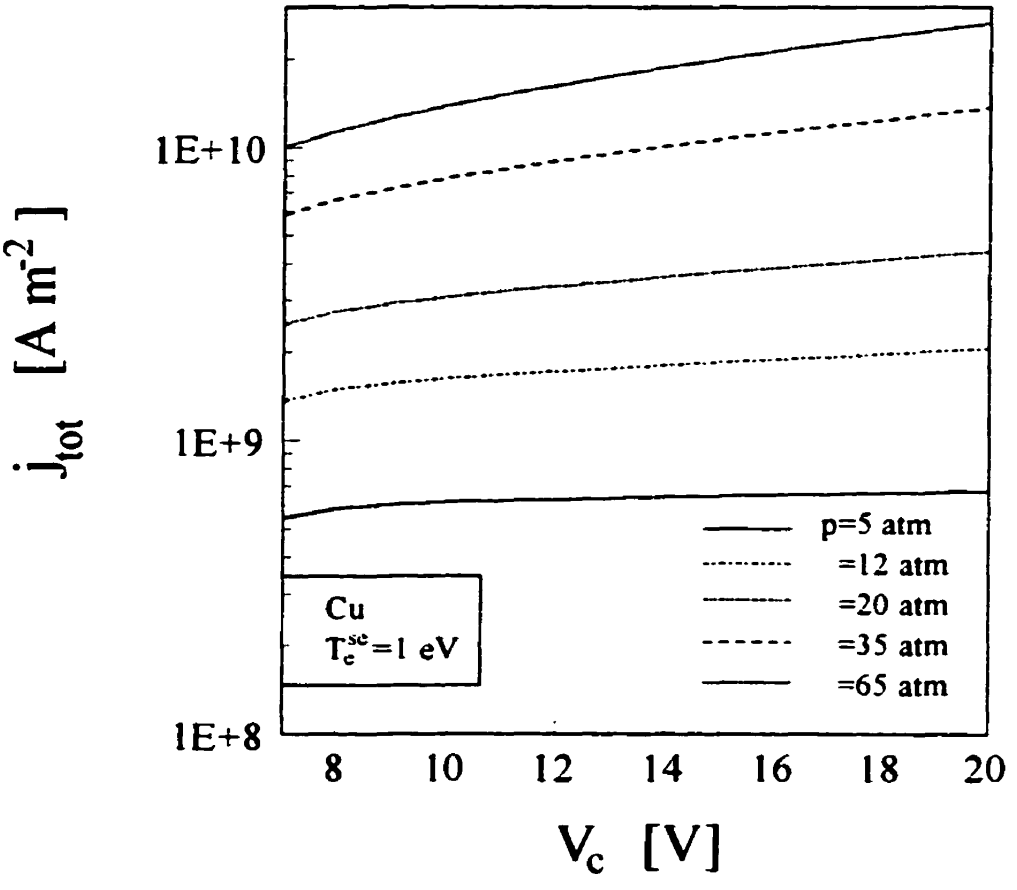

FIGURE 5.5.1. Total current density j_{tot} as a function of V_c and p for T_e^{sc}=1 eV.

ii) The higher is the cathode sheath voltage drop, the lower is the minimum metallic plasma pressure necessary for a self-sustaining operation (p_{min}) as shown on figure 5.5.2. For V_c varying of ±1V, p_{min} varies of ±1 atm. For V_c varying by an important amount of ±3V, p_{min} varies by around ±4 atm only.

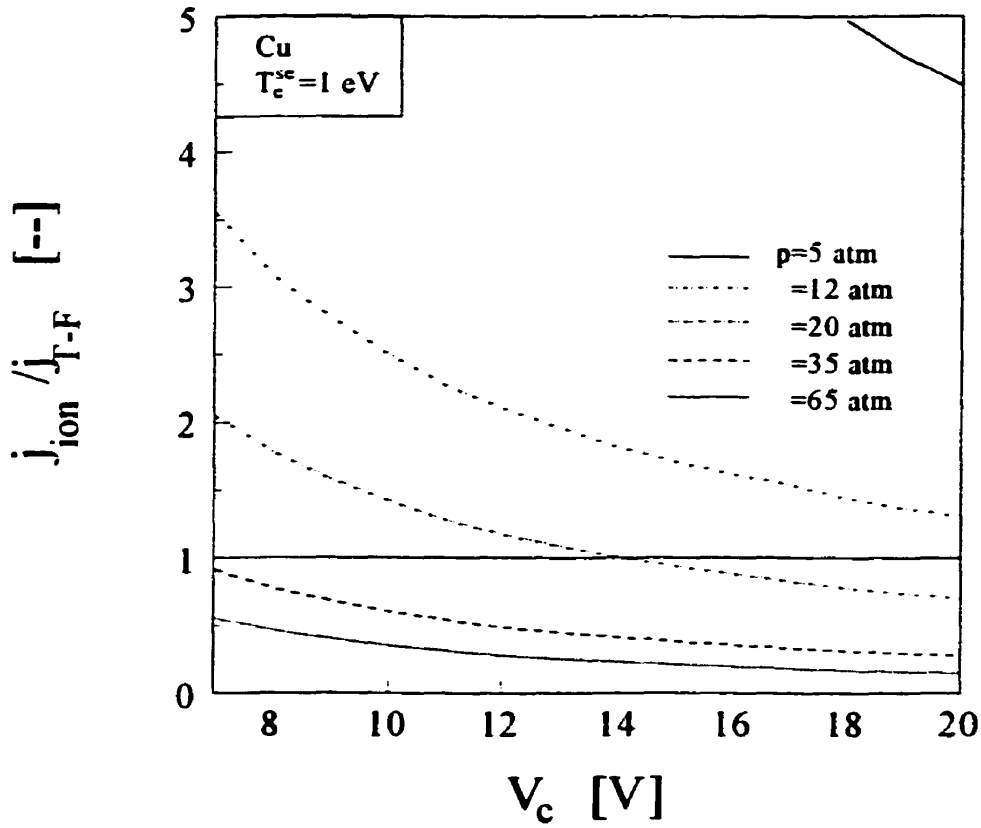

FIGURE 5.5.2. Ratio $j_{ion}/j_{T\text{-}F}$ (criterion 4.4.2a) as a function of V_c and p for T_e^{sc}=1 eV.

5.6. Discussion and Conclusions

The results presented in this chapter have shown that the self-sustaining attachment of high pressure arcs on non-refractory cathodes such as Cu, Fe and Ti is possible only if a significant vaporization of the cathode surface occurs. The current transfer to the cathode in such a case is mainly assumed by ion-enhanced thermo-field electron emission from the surface. This mechanism however requires the establishment of large electric fields at the cathode surface by the space charge formed by the ions. Since the plasma formed in the ambient gas covering the cathode surface cannot furnish enough ions, the supplementary ions are generated by ionization of the metallic vapors coming from the cathode erosion. These ions are efficient in bombarding the cathode and allow maintaining high surface temperatures and therefore, high vapor pressures of cathode material (p>19 atm for Cu) in the cathode region causing the strong erosion rates observed. The strong erosion rates of

non-refractory cathodes exposed to high pressure arcs must then be seen as a *necessary condition* for the self-sustaining attachment of the arc rather than a simple *consequence* of the important heat load coming from the arc that cannot be dissipated by conduction into the cathode bulk. This observation suggests that a minimum erosion is necessary for the operation of electric arcs on non-refractory cathodes. Therefore, forcing the arc to move or increasing the cooling rate of the cathode, though proved to be efficient in reducing the erosion rate, cannot totally prevent it.

An existence domain for the cathode spots on a Cu cathode was found for current densities ranging from ~3.5×10^9 to ~3×10^{10} A m^{-2} when T_e^{sc}=1.0 eV. For current densities higher than 10^{10} A m^{-2}, the ratio of the ion to emitted electron current $j_{ion}/j_{T\text{-}F}$ remains essentially constant as the current density increases and ranges from ~0.25 to 0.40. Surprisingly, such fractions correlate well with those encountered for the self-sustaining operation regime of high pressure argon arcs on refractory W cathodes, but under totally different spot conditions (we are thinking especially in terms of the metallic pressure). Such a behavior is very interesting and was also observed with non-refractory Fe and Ti cathodes. With such an approach to the definition of the self-sustaining operating conditions, no special distinction is made between refractory and non-refractory cathodes: only the sufficient production of ions by a beam of electrons emitted from the cathode is concerned. A simple rough analysis of the ionization processes in the ionization zone told us why the ratio $j_{ion}/j_{T\text{-}F}$ must be lower than unity but, a detailed analysis is needed to explain why this ratio would preferably range from 0.25 to 0.4.

It was shown that the validation of criterion (4.4.2a) allows to estimate the minimum metallic plasma pressure p_{min} for a self-sustaining operation of the arc attachment while criterion (4.4.2b), the maximum pressure p_{max}. It is important to note that the range of pressures predicted this way is rather large since both criteria are not too restrictive. As discussed in the previous paragraph, the actual ratio $j_{ion}/j_{T\text{-}F}$ is lower than unity giving rise to a value for p_{min} larger than the one estimated with $j_{ion}/j_{T\text{-}F}$=1 (see figure 5.2.1). On the other hand, the value estimated for p_{max} is certainly too high since this pressure was

determined by setting q_{cond}=0. Indeed, since liquid volumes are formed, q_{cond}>0 and therefore, the actual value taken by p_{max} is lower than the one estimated using q_{cond}=0 as it can be seen with figure 5.2.16.

An analysis of the heat transfer to the cathode surface under the spot has shown that as the total current density per spot increases, the fraction of the incoming heat that is lost by conduction into the cathode bulk decreases. Indeed, the heat losses by electron emission and cathode material vaporization are shown to increase with the total current density suggesting that the ratio of the liquid mass formed to the vapor mass formed decreases as the current density increases. This behavior is interesting; It suggests that one could enhance the production of vapor and reduce the production of liquid volumes (conduction losses) by increasing the local plasma pressure in the arc spots by means of confinement. This is of interest in applications such as arc-ion plating (AIP) or electrongun arc welding (Raja *et al* 1997) where the internal confinement of the cathode spots would enhance the cathode material vaporization and reduce the formation of liquid droplets. Results obtained recently by Kandah (1997) showed that the application of a magnetic field in the close vicinity of the cathode surface resulted in a considerable reduction of the microdroplets production (liquid volumes) and an increase of deposition rate (vapor production). Further investigations are needed to determine if the internal cathode spot confinement by such magnetic means is responsible for this behavior. A priori, this seems a plausible explanation.

The model's predictions for the erosion rate of a Cu cathode are in fairly good agreement with the experimental measurements obtained under vacuum conditions where the redeposition of neutrals can be neglected. At high chamber pressures the effects of the conditions external to the cathode spots (gas nature, flow rate, magnetic field ...) can no longer be ignored and therefore, the present model could not predict the erosion rate accurately. In fact, any attempt to theoretically determine the erosion rate of copper cathodes exposed to a high pressure arc will have to account for: 1) The redeposition of neutrals on the cathode surface. For now, the accommodation coefficients of copper at

elevated temperatures are not known (point also raised in section 4.3.1). 2) The coalescence of the cathode spots at elevated pressures. In such a situation, vaporization of the cathode surface occurs not only from under the isolated cathode spots, but also from the surface located between the spots since high temperatures are maintained there (Szente 1989). Furthermore, the pattern formed by the group of cathode spots affects the erosion rate. For instance, the cathode spots line up along the external magnetic field lines (Drouet 1985) and lower erosion rates result from this. The nature of the ambient gas also affects the dynamics of the cathode spots and therefore, their mean distances and residence times at given locations (Szente 1989, Jüttner 1997).

The application of the model to other metallic elements (Fe and Ti) showing intermediary boiling temperatures respective to Cu and W has shown the progressive transition from a regime necessitating a pressure build up in the cathode region for a self-sustaining operation of the arc spots (e.g. Cu) to a regime not necessitating it (e.g. W). Indeed, as we saw with figure 5.3.1, the average metallic plasma pressure needed for a self-sustaining operation decays exponentially with the boiling temperature of the cathode material. Figure 5.3.1 could actually be used to predict the range of metallic plasma pressures needed for a self-sustaining operation on other intermediary metallic elements. Since the cathode erosion phenomenon is mainly due to material vaporization which is itself related to the vapor pressure, the erosion rate also correlates with the boiling temperature of the cathode material.

A well-known method of reducing the cathode erosion rates is to favor the existence of highly electron emissive sites on the cathode surface that do not necessitate the presence of a high density of ions to operate. Such high emission sites can be dielectric impurities embedded at the cathode surface as we believe it is the case for an arc burning in $Ar+N_2$ or Ar+CO and on a non-refractory Cu cathode for instance. In such a situation, dielectric inclusions are thought to form at the cathode surface by reaction of the plasma gas with the cathode material. However, though highly electron emissive, such dielectric inclusions are eventually being destroyed by the action of the arc according to the scenario

presented in section 3.4. Therefore, the erosion rate is momentary reduced when the arc is attached to such dielectric inclusions but, increases again after the inclusions have been destroyed and the cathode spots formed. In order to maintain a low erosion rate, dielectric inclusions must constantly being formed, and the arc constantly moved to avoid long lasting cathode spots. This is probably why the combination of rotating the arc and making it burn in reactive main plasma gases is successful in reducing the cathode erosion rates (Szente 1989).

On the other hand, in some applications of the thermal arc plasma technology, the plasma gas must stay inert or the contaminant gas added to the main plasma gas does not react with the cathode surface to form inclusions favorable for electron emission. In both situations then, no erosion rates below the minimum value characteristic of the cathode material can be achieved. Voluntary addition of contaminants to the cathode has its limits too since the embedded contaminants diffuse out the cathode surface during the arc operation due to the important temperature gradients in the cathode. It is known that the low-erosion qualities of thoriated-tungsten cathodes when used as arc cathodes degrade with aging of the cathode due to the bulk diffusion and evaporation of the thorium atoms from the surface (Zhou *et al* 1996). The same phenomenon is observed with silver-metal-oxide cathodes (AgMeO cathodes) such as AgCdO or $AgSnO_2$ which are known for their erosion-resistant qualities when used as contact materials, but which suffer also of thermal degradation (Sun *et al* 1994).

We believe that the search for a solution to the cathode erosion problems must now be oriented towards multi-layer cathodes where a different mode of arc attachment might be observed. Such a multi-layer cathode could be made of a strongly adherent coating of a refractory insulator or semiconductor deposited on a base metallic cathode for instance.

CHAPTER 6

ELECTRON EMISSION FROM THE CATHODE: A COMPARATIVE STUDY

6.1. Introduction

As discussed in section 2.2, the accurate calculation of the current of electrons emitted from the cathode surface is of primary importance in modeling of the arc-cathode interactions. In this chapter, we compare the predictions of the cathode sheath model described in Chapter 4 for both the refractory and non-refractory arc cathode situations using three different equations for the thermo-field (T-F) electron emission current density. These equations are respectively: 1) the field-enhanced thermionic emission equation (j_{T-F}^{FEE}, equation (2.2.4)), 2) the Murphy and Good equation (j_{T-F}^{MG}, equation (2.2.5)), and 3) the Murphy and Good equation enhanced by the presence of a high density of slowly moving ions in the cathode region (j_{T-F}^{MG+I}, equation (2.2.6)). The goals of this comparative study are: 1) define the domain of applicability of each equation by considering the MG+I equation (j_{T-F}^{MG+I}) as the most accurate, and 2) quantify the consequences of using a less accurate formulation for the emitted electron current on the model's predictions.

For both arc-cathode interaction systems considered in this comparative study, the values of the ion-enhancement factor β used were extrapolated from the data presented in Table 2.2.1 for a macroscopic surface electric field strength of 10^9 V m^{-1} (the data of Gayet *et al* 1996 are limited to T_s<3 500 K and to E_s=10^9 V m^{-1}). It was also assumed as a first approximation that the values of β reported in Table 2.2.1. are independent of the

nature of the ions incident on the cathode (Ar^+ on W cathode for the refractory case and Cu^- on Cu cathode for the non-refractory case) and on the nature of the cathode material.

6.2. Refractory W Arc Cathode

For this modeling case, the field-enhanced thermionic emission equation (2.2.4) is the equation used to describe the electron emission current (e.g. Zhou and Heberlein 1994, Rethfeld *et al* 1996, Lowke *et al* 1992, and references therein). To our knowledge, no study relating the use of the formalism of Murphy and Good (equation (2.2.5) has been reported in the literature for this particular arc-cathode system justifying then the present work.

To perform this analysis, the physical model developed in Chapter 4 had to be slightly modified in order to realize the calculations under the usual assumptions of the thermionic arc cathode model. Both models are essentially the same except for the nature of plasma gas present in the cathode region; for refractory cathodes no excess pressure is observed in the cathode region and therefore, the plasma gas there is the same as the ambient gas filling the chamber. The cathode erosion rate is low and the effects of the metallic ions on the properties of the cathode sheath are assumed negligible. The plasma pressure p cannot be related to the cathode surface temperature T_s via a vapor-pressure curve and therefore, this temperature has to be calculated by coupling the cathode sheath model to a heat transfer model in the cathode bulk. For this study however, T_s is taken as an independent parameter and is set equal to a specific value taken from experimental measurements. A pure Ar plasma operating at a pressure p was considered.

For high pressure argon arcs on tungsten cathodes and for the typical range of electron temperatures reported in the literature, the ion density in the cathode region becomes higher than $n_i \sim 10^{24}$ m^{-3} only for ambient pressures exceeding 10 atm. Therefore, the ion-enhancement effects are negligible for lower pressures. At atmospheric pressure then, only the surface electric field strength E_s, the surface temperature T_s and the cathode material work function ϕ play a role in the determination of the emitted electron current

density (the predictions of the emitted electron current using the MG and the MG+I equations are therefore the same). The effects of these three parameters alone on the ratio $j_{T-F}^{MG} / j_{T-F}^{FEE}$ are first studied in the next two sections (sections 6.2.1 and 6.2.2), while the effects associated with a high density of ions (gas pressure and electron temperature combined) on both ratios $j_{T-F}^{MG} / j_{T-F}^{FEE}$ and $j_{T-F}^{MG-I} / j_{T-F}^{FEE}$ are studied in section 6.2.3.

6.2.1. Influence of Temperature and Surface Electric Field Strength

Figure 6.2.1. shows the isocontours of the ratio $j_{T-F}^{MG} / j_{T-F}^{FEE}$=constant in the surface temperature-electric field strength plane for ϕ=4.5 eV. Systems with predominantly thermionic emission (T_s is high and E_s low) correspond to the bottom-right part of figure 6.2.1, whereas field-emitting systems (T_s is low and E_s high) correspond to the top-left part.

As expected with figure 2.2.2, low-temperature--low-electric field values generate extremely small current densities and poorly defined $j_{T-F}^{MG} / j_{T-F}^{FEE}$ ratios as shown in figure 6.2.1. An overview of figure 6.2.1 shows that the perfect agreement of the field-enhanced thermionic equation (j_{T-F}^{FEE}) and the Murphy and Good equation (j_{T-F}^{MG}) is the exception rather than the rule for the range of electric field strengths and cathode surface temperatures investigated. It was predictable that the best agreement between the two equations would be achieved within the 'thermionic emission' region. As one goes towards the 'field emission' region, the discrepancy between the two equations grows quickly and the ratio $j_{T-F}^{MG} / j_{T-F}^{FEE}$ tends towards infinity.

The typical range of cathode surface temperatures and electric field strengths reported in the literature for the diffuse attachment of an atmospheric pressure argon arc on a tungsten cathode is indicated by the region labeled W in figure 6.2.1 (inspired from Zhou and Heberlein 1994, Rethfeld *et al* 1996 and Lowke *et al* 1992). One can see that the use of the field-enhanced thermionic equation (j_{T-F}^{FEE}) rather than the more accurate

formulation of Murphy and Good (j_{T-F}^{MG}) leads to an underestimation of the actual emitted electron current densities by 20-30%.

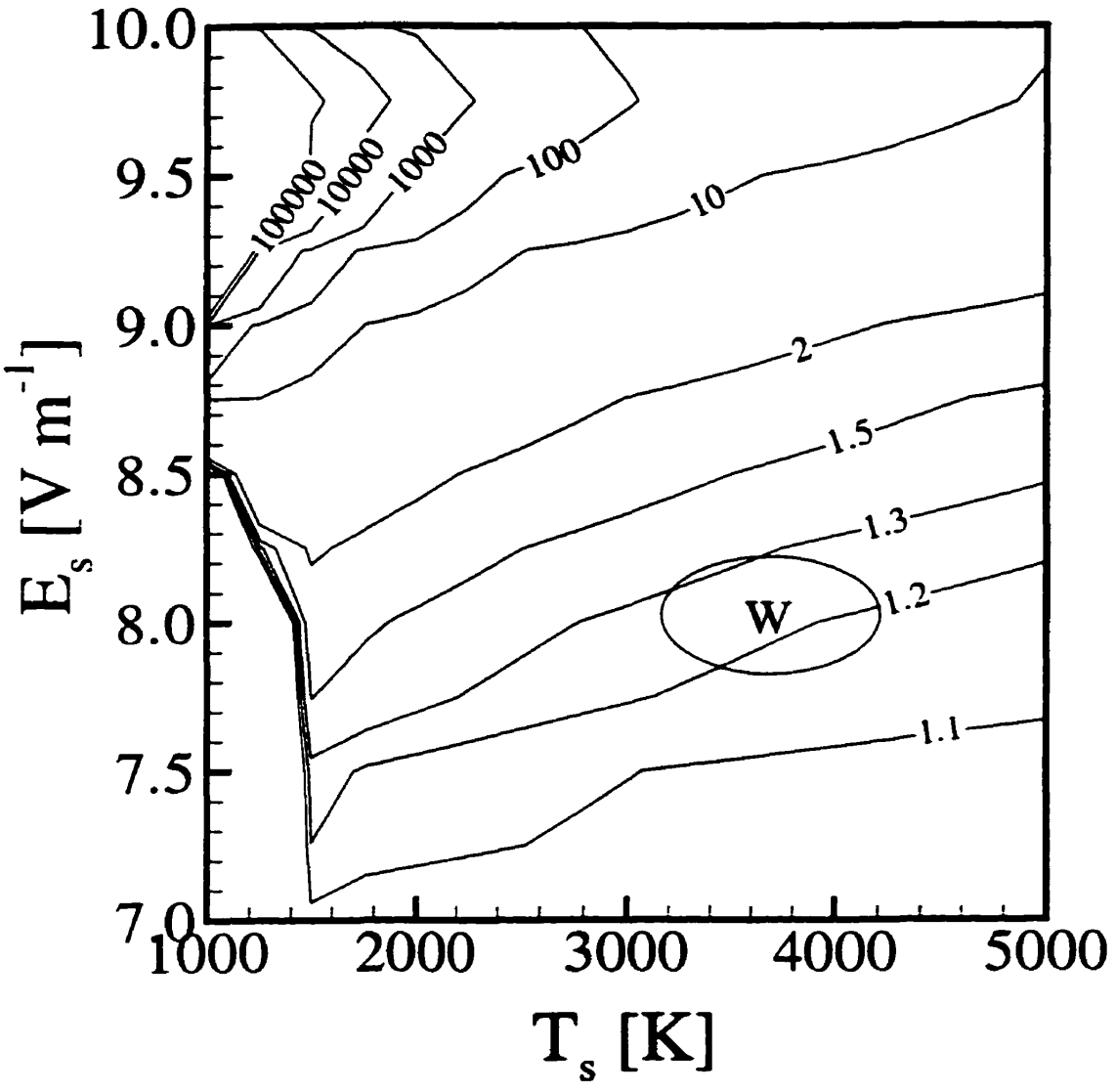

FIGURE 6.2.1. Isocontours $j_{T-F}^{MG} / j_{T-F}^{FEE}$ = constant in the T_s-E_s (logarithmic scale) plane for ϕ=4.5 eV. Typical conditions encountered at the cathode surface of an atmospheric pressure argon arc on a W cathode are delimited.

6.2.2. Influence of Work Function

Calculations similar to those presented in figure 6.2.1 were performed for work functions of 2, 3, 4 and 5 eV and for the same range of cathode surface temperatures and surface electric field strengths. The results showed a negligible influence of ϕ on the ratio

$j_{T-F}^{MG} / j_{T-F}^{FEE}$ for the range of temperatures and electric field strengths corresponding to $j_{T-F}^{MG} / j_{T-F}^{FEE} < 2.0$ in figure 6.2.1. The dependence on ϕ becomes significant only for the range of temperatures and electric field strengths for which $j_{T-F}^{MG} / j_{T-F}^{FEE} > 2.0$ in figure 6.2.1. Such conditions are however not expected to prevail at the cathode surface of atmospheric pressure argon arcs on tungsten cathodes.

6.2.3. Influence of Ambient Gas Pressure and Electron Temperature

When the ion-enhancement effects cannot be neglected ($n_i > 10^{24}$ m^{-3} or $p > 10$ atm), a simple parametric study of the influence of the different parameters affecting the electron emission current density can no longer be made since the number of independent parameters is now five rather than three (see equation (2.2.6)). One has to fix the parameters that are the best known and allow the remaining parameters to vary for the parametric study. By specifying the cathode surface temperature T_s, the cathode sheath voltage drop V_c and the work function ϕ, the cathode sheath model developed in section 4 allows the self-consistent calculation of all the parameters pertinent to the cathode spot, especially the electron emission current density. The two remaining independent parameters are the ambient gas pressure p and the electron temperature at the cathode sheath edge T_e^{se} which, once combined, are representative of the ion density.

The cathode sheath voltage drop and the cathode surface temperature were set equal to the estimated values of V_c=8 V (Zhou and Heberlein 1994 and references therein) and $T_s = T_h^{se}$=3750 K (Zhou *et al* 1996, Zhou and Heberlein 1996), respectively for a 200 A atmospheric pressure argon arc. This surface temperature corresponds to the lowest value reported by Benilov and Marotta (1995) (they reported 3700 to 4600 K) and therefore, the departures in the ratios $j_{T-F}^{MG} / j_{T-F}^{FEE}$ and $j_{T-F}^{MG-I} / j_{T-F}^{FEE}$ reported in this study will be the highest since β decreases at the surface temperature increases (see Table 2.2.1). The ambient gas (argon) pressure p was allowed to vary from 1 to 50 atm (0.1-5 MPa), and the electron temperature at cathode sheath edge T_e^{se} from 1 to 2 eV (11 600 - 23 200 K) in order to represent a wide range of conditions (typically 1.25-1.75 eV (14 500 - 20 300

K), Zhou and Heberlein 1994, Rethfeld *et al* 1996). It is important to note here that the cathode surface temperature is obviously not constant over the pressure range considered. This temperature is expected to increase slightly with the ambient gas pressure due to the increasing ion bombardment.

Figure 6.2.2 shows the cathode sheath model's predictions of the ratios $j_{T-F}^{MG} / j_{T-F}^{FEE}$ and $j_{T-F}^{MG+I} / j_{T-F}^{FEE}$ for a tungsten cathode exposed to a high pressure argon arc under the conditions previously specified. A bird eye view of figure 6.2.2 shows that the use of the FEE equation induces an underestimation of the electron emission current when compared to the predictions made using the MG and MG+I equations. This underestimation is shown to increase with the ambient pressure p, and thus with the ambient gas ion density n_i. The underestimation shows a non-monotonic behavior with the electron temperature which peaks, for high pressures, at an electron temperature T_e^{sc}~1.5 eV (17 400 K). This electron temperature corresponds to the temperature where the ion density peaks for a pure high pressure Ar plasma with T_h^{sc}=3 750 K.

The underestimation of the electron emission current density is around 20-30% for p=1 atm as demonstrated in section 6.2.1 and reaches respectively ~200% with the MG equation (ratio $j_{T-F}^{MG} / j_{T-F}^{FEE}$) and peaks at ~500% for T_e^{sc}=1.5 eV (17 400 K) and p=50 atm (5 MPa) with the MG+I equation (ratio $j_{T-F}^{MG+I} / j_{T-F}^{FEE}$). These deviations in the model's predictions are shown to increase more slowly for the ratio $j_{T-F}^{MG} / j_{T-F}^{FEE}$ since this ratio is less dependent on the ion density (no ion-enhancement effects). The calculated surface electric field strengths are ~10^8 V m^{-1} for p=1 atm and ~10^9 V m^{-1} for p=50 atm (5 MPa). The deviation of ~50% shown on figure 6.2.3 for $j_{T-F}^{MG+I} / j_{T-F}^{FEE}$ at a pressure p=1 atm (0.1 MPa) is overestimated since the values for the ion enhancement factor β were taken for E_s=10^9 V m^{-1}. Similar calculations carried out for T_s>4000 K have shown that the ion-enhancement effects become negligible for such high temperatures; the favorable effect of an increase of the ion density associated with a higher ion temperature (T_h=T_s) on β does

not compensate for the unfavorable effect associated with a higher cathode surface temperature (remember that β increases with n_i, but decreases with T_s).

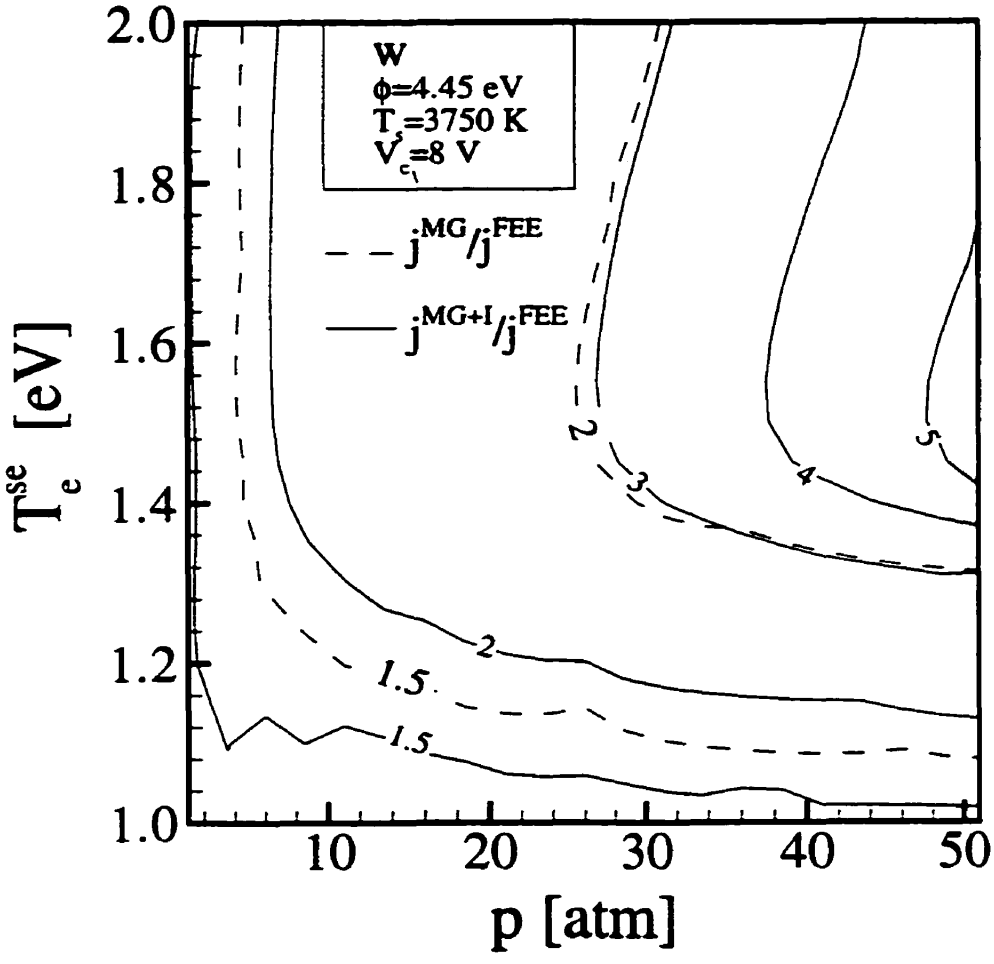

FIGURE 6.2.2. Model's predictions in the p-T_e^{se} plane of the ratios $j_{T-F}^{MG} / j_{T-F}^{FEE}$ (long dashes) and $j_{T-F}^{MG-I} / j_{T-F}^{FEE}$ (continuous line) for a high pressure arc on a refractory W cathode with T_s=3 750 K, V_c=8 V and ϕ=4.5 eV.

6.3. Non-Refractory Cu Arc Cathode

The high density of ions thought to be present in the cathode region of high pressure arcs on non-refractory cathodes induces high surface electric field strengths and

high cathode surface temperatures. Hence, the Murphy and Good equation for thermo-field emission (equation (2.2.5)) was commonly used over the years to describe the electron emission current (e.g. Lee 1959 and Ecker 1973). In some particular cases however, the field-enhanced thermionic equation (equation (2.2.4)) was used, even though the spot conditions investigated were such that thermo-field emission of electrons prevailed (e.g. Bolotov *et al* 1995 and Benilov 1993).

For this comparative study, the cathode sheath voltage drop V_c, the cathode material work function ϕ and the electron temperature at cathode sheath edge T_e^{sc} were fixed for the calculations. The metallic plasma pressure p was the only independent parameter since, in this case, the heavy species temperature $T_h^{sc}=T_s$ is related to this pressure via a vapor pressure curve (section 4.1). The cathode sheath voltage drop was set equal to 15 V as in Chapter 5 (with Cu) while the electron temperature at cathode sheath edge was set equal to 1 eV (11 600 K). This value for T_e^{sc} corresponds to the electron temperature where the ion density is maximum for a pure copper plasma (section 6.2.2). The results are presented as a function of the calculated total current density j_{tot} rather than the metallic plasma pressure for convenience.

6.3.1. Ion Effects on Current Density Distribution

Figure 6.3.1 shows the model's predictions of the ratio $j_{T\text{-}F}/j_{tot}$ for a copper cathode obtained using the three different equations for the electron emission current density as a function of the total current density j_{tot} with V_c=15 V.

One can see a general trend of $j_{T\text{-}F} / j_{tot}$ increasing with j_{tot} which is the same for the three equations used for the electron emission current density. However, the actual values taken by the ratio $j_{T\text{-}F}/j_{tot}$ depend significantly on the choice of the equation. The field-enhanced thermionic emission equation (FEE) shows the lowest value for the ratio $j_{T\text{-}F}/j_{tot}$ for any value of j_{tot} while the ion-enhanced Murphy and Good equation (MG+I) shows the highest. For a total current density $j_{tot}=10^{10}$ A m^{-2}, the ratio $j_{T\text{-}F}/j_{tot}$ predicted by

the FEE, the MG and the MG+I equations are respectively ~0.45, ~0.62 and ~0.71, giving rise to cathodic electron current densities of 4.5×10^9, 6.2×10^9 and 7.1×10^9 A m^{-2}.

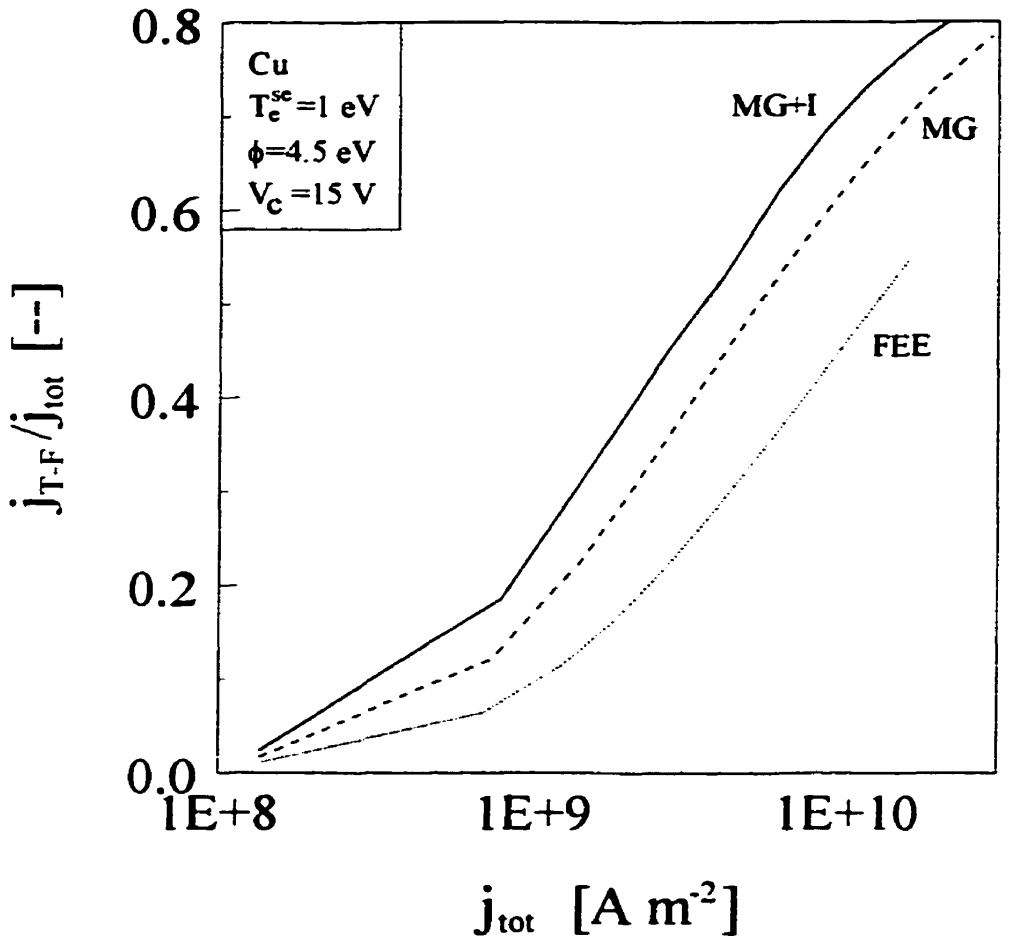

FIGURE 6 3 1 Model's predictions of the ratios $j_{T\,F}^{FEE} / j_{tot}$, $j_{T\,F}^{MG} / j_{tot}$ and $j_{T\,F}^{MG+I} / j_{tot}$ for a high pressure arc on a non-refractory Cu cathode as a function of j_{tot} with V_c=15 V, T_e^{se}=1 eV (11 600 K) and ϕ=4.5 eV.

The deviations in the three model's predictions are shown to increase with the total current density j_{tot}. The higher the total current density the higher is the metallic plasma pressure in the cathode spot plasma, so the higher are the amplification effects induced by the ions present in the cathode region. This can be better understood with the help of figure 2.2.1. The presence of ions only induce a reduction of the material work function via the increased electric field strength for the FEE equation (Schottky effect) while it has

respectively a double and triple effect on the MG and MG+I equations. For the MG equation, the thermionic emission component of the T-F emission is enhanced by the reduction of the work function, but the field emission component is also enhanced due to the increase of the electron tunneling probability across the Schottky barrier with the increase of the macroscopic electric field strength associated with higher ion densities. For the MG+I equation, the electron emission current is further increased by the action of the ions on the actual potential 'experienced' by the electrons outside the metal surface. This discussion is also valid for the refractory W arc cathode case studied in section 6.2.

6.3.2. Ion Effects on Spot Conditions

Figure 6.3.2 and 6.3.3 show respectively the metallic plasma pressure p and cathode surface temperature under the spot T_s needed to account for a specific range of total current densities as predicted by the cathode sheath model using the three different equations for the electron emission current density. For low pressures (~1 atm (0.1 MPa)) the three equations predict the same values for p and T_s since both the ion density (n_i~10^{23} m^{-3}) and surface electric field strength (~10^8 V m^{-1}, see figure 6.3.4) are low. As the total current density increases, deviations in the model's predictions for the three equations of the electron emission current density start to appear due to the increasing effect of the ions on the emission conditions; the metallic plasma pressure (ion density) needed to account for a given current density increases with this current density. For a total current density of 10^{10} A m^{-2}, the predicted metallic plasma pressures are respectively ~70, ~45 and ~35 atm (0.7, 0.45 and 0.35 MPa) for the FEE, MG and MG+I equations. The same decreasing trend is observed for the cathode surface temperatures under the spot which are respectively ~3990, ~3885 and 3765 K for the FEE, MG and MG+I equations and for the same current density. Even higher deviations are expected for total current densities higher than 10^{10} A m^{-2}.

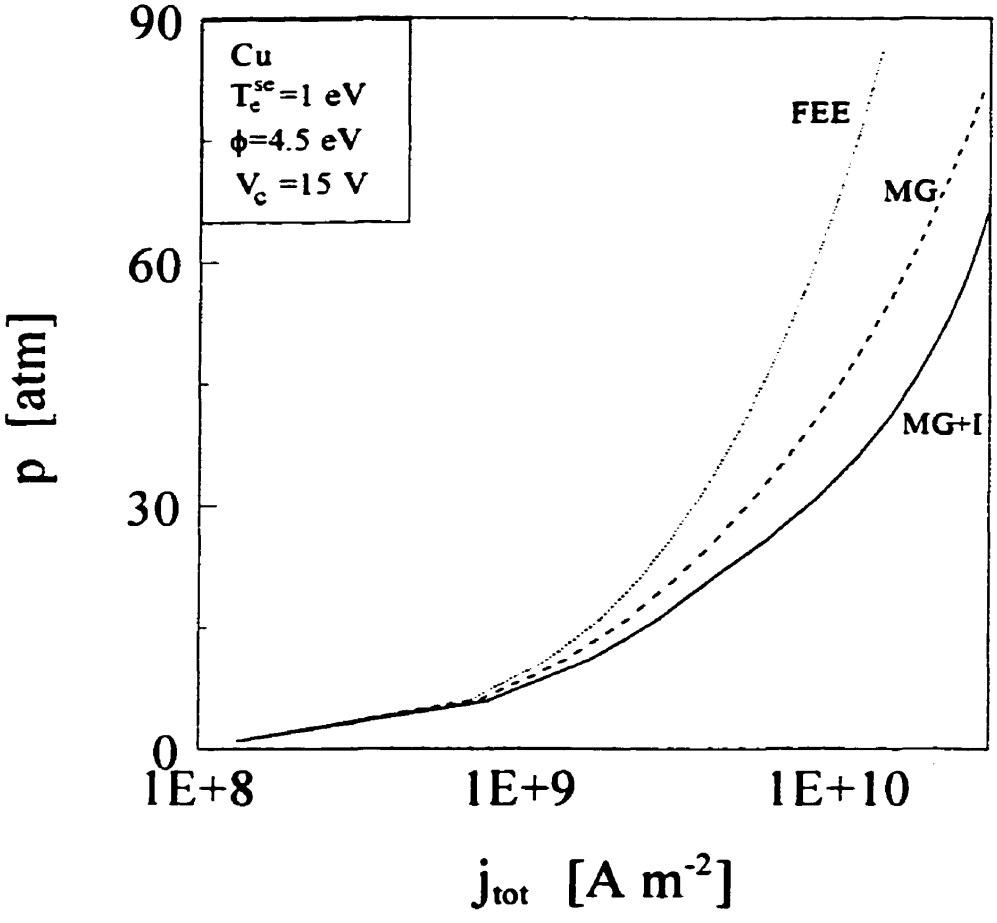

FIGURE 6.3.2. Model's predictions of the metallic plasma pressure within the cathode spot p for a high pressure arc on a non-refractory Cu cathode as a function of j_{tot} with V_c=15 V, T_e^{se}=1 eV (11 600 K) and ϕ=4.5 eV.

Figure 6.3.4 shows the values of the surface electric field strength E_s calculated using the MG+I equation as a function of the total current density j_{tot} for V_c=15 V. One can see that the surface electric field strengths range from 2×10^8 to 2×10^9 V m^{-1} for the range of total current densities expected for this system. Since the ion-enhancement factor β depends weakly on E_s for $E_s \sim 10^9$ V m^{-1} and since the calculated values for E_s are close to 10^9 V m^{-1}, the assumption made for the ion enhancement factor β is validated posteriori (β ~constant for $E_s \sim 10^9$ V m^{-1}).

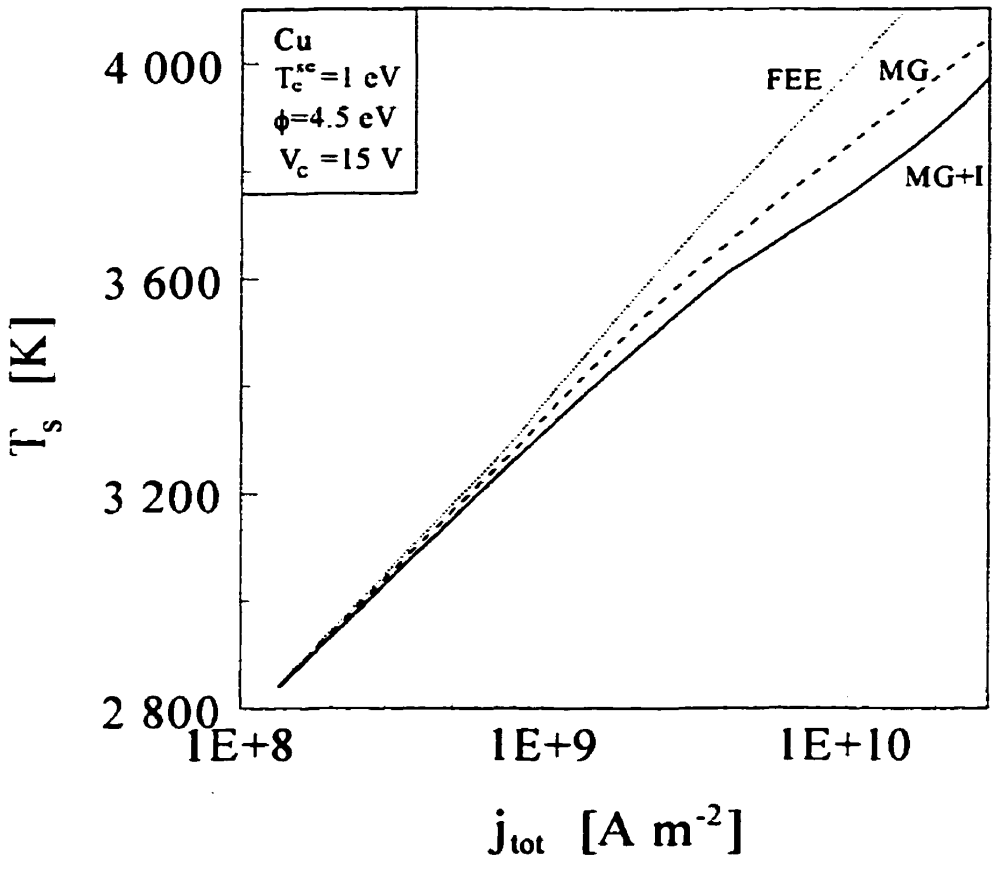

FIGURE 6.3.3. Model's predictions of the cathode surface temperature under the spot T_s for a high pressure arc on a non-refractory Cu cathode as a function of j_{tot} with V_c=15 V, T_c^{sc}=1 eV (11 600 K) and ϕ=4.5 eV.

It is important to note here that, as demonstrated recently by Josso (1997), the method used to calculate β which is based on a 1-dimensional (1-D) treatment of the electron potential at the cathode surface is accurate for E_s lower than 10^9 V m^{-1}, but becomes less accurate as the macroscopic surface electric field becomes much larger than this value. Indeed, a comparison with a 3-D treatment of the electron potential for a much higher macroscopic electric field strength (E_s = 4x10^9 V m^{-1}) has shown that the 1-D treatment underestimates the value of β by a factor of ~3 (Josso 1997). This observation and the results presented in figure 6.3.4 for a Cu cathode suggest that the cathode spot conditions can be relatively well-predicted up to a current density of around 5x10^{10} A m^{-2}, which happens to be the upper limit for the self-sustaining operation of the arc spots

reported in Chapter 5. The coincidence is fortunate here, but for other non-refractory cathode materials where self-sustaining operating current densities might be much higher than those predicted for Cu, one would have to implement the 3-D treatment developed by Josso (1997). Such 3-dimensional treatment for the electron emission current is however considerably more complicated. Indeed, for higher values of the macroscopic electric field strength, the radial dependency of the transmission probability for an electron to cross the barrier formed by the ions in the close vicinity of the cathode comes into play (Josso 1997).

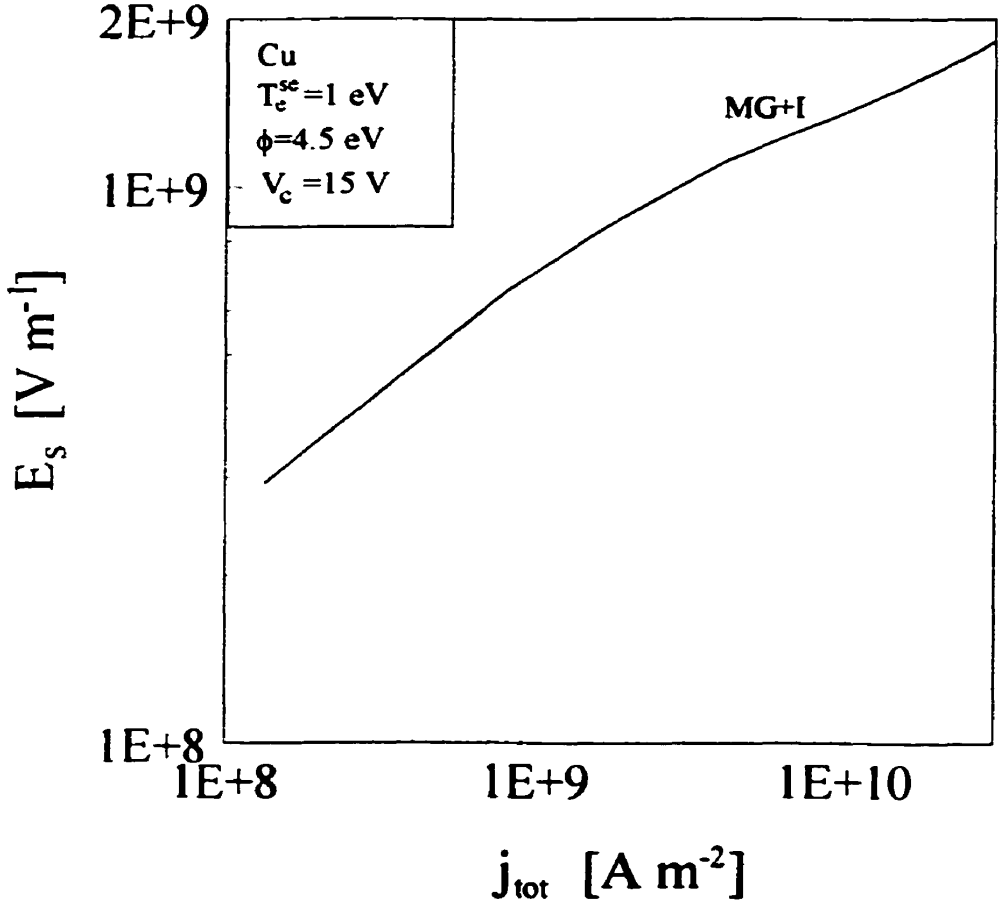

FIGURE 6.3.4. Model's predictions of the surface electric field strength E_s for a high pressure arc on a non-refractory Cu cathode as a function of j_{tot} with V_c=15 V, T_e^{se}=1 eV (11 600 K) and ϕ=4.5 eV.

One can use the information reported in figure 2.3.1 and Table 5.3.1 to identify cathode materials that could possibly need a 3-D treatment for the calculation of the emitted electron current density. Results reported in Table 5.3.1 have shown that the highest total arc spot current densities are observed for the cathode materials showing the highest ratio $e\Gamma_{vap}/j_{RD}$ (figure 2.3.1). Therefore, metallic elements showing ratios $e\Gamma_{vap}/j_{RD}$ higher than Cu can possibly show higher arc spot current densities. Ag and Mg are certainly two candidates. Indeed, Tioursi and Haug (1997) estimated a total current density $j_{tot}=8\text{x}10^{10}$ A m^{-2} for Ag.

6.3.3. Comparison with other Studies

It is now interesting to compare the results obtained in this comparative study to the results obtained by two other models developed for vacuum arc cathode spots which use a similar approach for the cathode sheath. Again, the similitude in the behaviors of both vacuum arc cathode spots and high pressure arc spots on Cu cathodes allows this comparison. These are respectively the models of Benilov (1993) and Klein *et al* (1994). However, these models are not based on the validation of criteria such as those defined by equations (4.4.2a) and (4.4.2b) for a self-sustaining operation of the arc spots. Therefore, the calculations performed using the present model were carried out for the conditions reported in Benilov (1993) and Klein *et al* (1994) for comparison only and this, without validating the criteria for self-sustaining operation. In the three cases, the cathode sheath voltage drop was V_c=15 V. The results of the comparison are presented in Table 6.3.1.

Results presented in Table 6.3.1 clearly show two important points: 1) the use of the less accurate field-enhanced thermionic equation (FEE) and Murphy and Good equation (MG) leads to an underestimation of the electron emission current density which in turn makes the ion current density overestimated for a given total current density. To compensate for the underestimation of the electron emission current, the cathode surface temperatures must be higher that the ones estimated using the MG+I equation in order to account for a given total current density (~300 K for the FEE equation and ~100 K for the

MG equation). 2) The agreement between the three models is fairly good in terms of prediction of the fractions of the current carried by the two major species (ions and emitted electrons) when the same formulation for the electron emission current density is used.

Note here that Benilov (1993) determined the cathode spot operating conditions assuming that the mode of operation of the cathode spot is the one allowing the maximum heat flux to the cathode surface (for stability reasons). As we have seen in section 6.2.4, these conditions providing the maximum heat flux are those for which the ion density (current density) is the largest too. Therefore, the maximum heat flux is also observed for an electron temperature T_e^{sc}=1.0 eV (11 600 K) which explains the agreement with the two other model's predictions obtained by setting explicitly T_e^{sc}=1.0 eV.

TABLE 6.3.1. Comparison between the results obtained with the present model to the results of Benilov (1993) and Klein *et al* (1994) for the current transfer to the surface under a Cu cathode spot.

Author	Electron emission model	j_{tot} (A m^{-2})	T_s (K)	$j_{ion}/j_{T\text{-}F}$ (--)
Present model	MG+I equation	$3.7\text{x}10^{10}$	3 980	0.16
Present model	MG equation	$3.7\text{x}10^{10}$	4 080	0.235
Klein *et al*'s model[1]	MG equation	$3.7\text{x}10^{10}$	---	~ 0.24
Present model[2]	FEE equation	$3.7\text{x}10^{10}$	~ 4 290	~ 0.42
Benilov's model	FEE equation	$3.7\text{x}10^{10}$	4 320	0.43

[1]: also with T_e^{sc}= 1 eV (11 600 K)
[2]: data extrapolated from figures 6.3.1 and 6.3.3.

6.4. Summary

The following important comments can be made from the comparative study on the electron emission equations:

Refractory W Arc Cathodes

i) The field-enhanced thermionic equation (2.2.4) commonly used to calculate the emitted electron current density in high pressure arc systems with refractory cathodes tends to underestimate the actual emitted electron current density. This underestimation is around 20-30% at atmospheric pressure and grows quickly as the ambient gas pressure increases to reach ~500% for p=50 atm (5 Mpa), T_e^*=1.5 eV (17 400 K) and T_s= 3 750 K. However, this underestimation of ~500% corresponds to the highest value possible since an increase of the cathode surface temperature leads to a reduction of β. For T>4000 K, the ion-enhancement effects become negligible.

ii) One does not have to take into account the enhancement effects due to the presence of ions in the cathode region (β factor) for an atmospheric pressure argon plasma since the ion density is too low to show significant effects. At atmospheric pressure, the use of the MG equation (2.2.5) rather than the FEE equation (2.2.4) is sufficient.

iii) The underestimation of the FEE equation (2.2.4) with respect to the MG equation (2.2.5) does not depend on the cathode material work function for the range of surface temperatures and electric field strengths expected for such systems at atmospheric pressure.

Non-Refractory Cu Arc Cathodes

i) The use of the Murphy and Good formalism (equation (2.2.5)) to calculate the electron emission current tends to underestimate this current for high current densities at the cathode surface (j_{tot} >10^9 A m^{-2}). The consequences of that phenomenon are the overestimation of the ion current fraction $j_{ion}/j_{T\text{-}F}$, the cathode

surface temperature under the spot T_s, and the metallic plasma pressure within the spot p to compensate for the lack of electron emission.

ii) The 1-D treatment of the electron emission processes and ion-surface surface interactions used to calculate the current transfer in the cathode region of non-refractory cathodes is limited to total current densities j_{tot} below ~5×10^{10} A m^{-2} for Cu. A 3-D treatment is required to determine the cathode spot parameters accounting for higher current densities. Fortunately, this limit happens to correspond to the maximum current density for a self-sustaining arc spot operation on a Cu cathode. However, metallic elements having vapor pressures higher than Cu could possibly need a 3-D treatment (e.g. Ag and Mg on figure 2.3.1).

iii) An important point has been raised when comparing the predictions of the present model to the predictions of Benilov's model (Benilov 1993): Is the cathode spot operating under the conditions favoring the optimum current density? The optimum current density would provide the lowest voltage drop in the cathode region and therefore, the lowest operating voltage for the whole arc system. This concept of lowest possible voltage drop as a stability criterion for the arc was commonly used in arc physics over the years (e.g. Zhou and Heberlein 1994 and references therein).

CHAPTER 7

LIQUID VOLUME FORMATION

7.1. Introduction

Up to now in this thesis, only the cathode material consumption due to its vaporization has been considered. As we have seen in Chapter 5, a strong vaporization is necessary for non-refractory cathodes in order to achieve the conditions allowing a self-sustaining arc attachment. Indeed, an important fraction of the heat flux brought to the cathode surface by the high pressure metallic plasma is used for vaporization but, an important amount is also dissipated by Nottingham cooling and conduction losses into the cathode bulk. Figure 5.2.16 showed that the conduction heat losses for a self-sustaining situation depend strongly on the metallic vapor pressure, and take values ranging from 0 to over 10^{10} W m^{-2}. The first objective of this chapter is to answer the question whether such high heat fluxes are sufficient to form liquid volumes in the μs time scale as is observed experimentally. Once formed, such liquid volumes may represent another source of cathode erosion if ejection of liquid metal from the molten bath occurs. Therefore, as a secondary objective, an estimation of the maximum erosion rate that can be caused by liquid volume ejection is made as a function of the conditions prevailing at the arc attachment point. In order to achieve these objectives, a transient heat transfer model for the cathode region under the arc attachment is developed and applied to a non-refractory Cu cathode using the conditions obtained in Chapter 5 while analyzing the cathode region.

7.2. Description of the Heat Transfer Model

The heat transfer to the cathode surface located underneath the arc attachment point is described in the transient regime with a 2-dimensional, axisymmetric *r-z* geometry (figure 7.2.1). The arc delivers a heat flux q_{cond} at the attachment point which describes a

circle having a radius r_s (cathode spot radius). The values of q_{cond} and j_{tot} are taken from the results reported in Chapter 5 for a pure copper cathode. No flow of liquid metal neither inside the liquid bath nor by expulsion from the crater is considered here since it would require a numerical model taking into account the deformation of the calculation domain with time. Therefore, the thermo-convection and viscous dissipation terms do not appear in the energy equation and no momentum equation is solved.

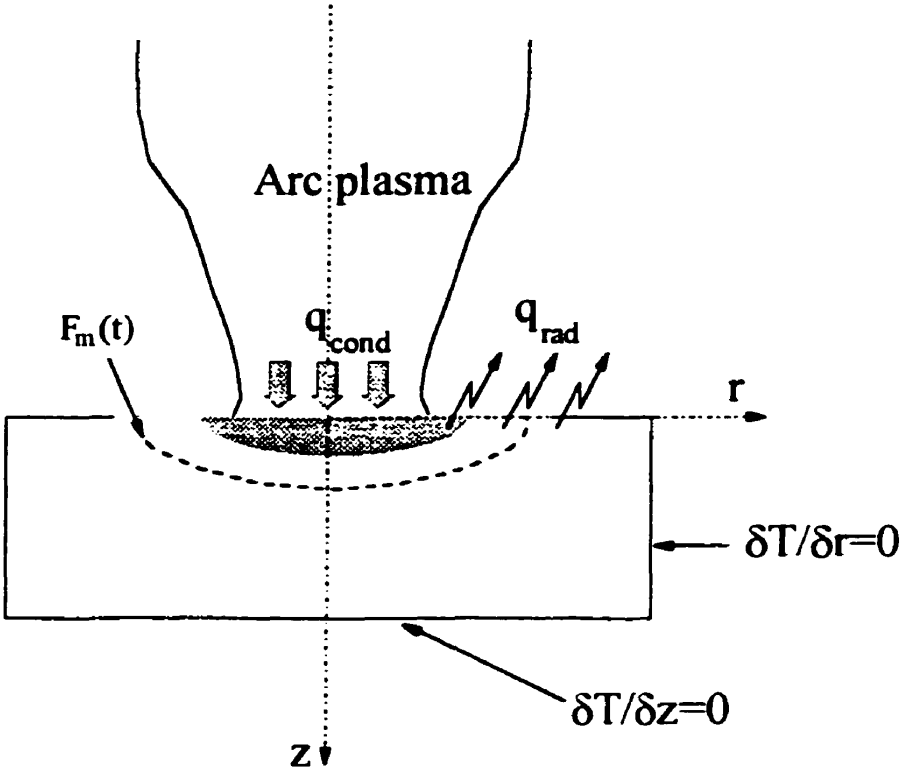

FIGURE 7.2.1. Geometry used for the heat transfer model. F_m=location of the moving boundary $T=T_m$.

The density of the cathode material ρ is assumed constant; no expansion of the cathode volume is considered. The heat capacity C_p and the thermal conductivity λ of the cathode material are considered as temperature-dependent properties. The solid-liquid and liquid-vapor phase changes are taken into account. The heat flux brought by the arc is dissipated by heat conduction into the cathode bulk and by radiative exchange with the surrounding at the cathode surface. Neumann conditions expressing the boundary

conditions in terms of heat fluxes are used elsewhere. The establishment of a heat flux q_{cond} at the cathode surface lets suppose that this surface is already boiling since the cathode region is composed of the metallic vapors coming from the erosion of the cathode. It is therefore assumed for simulation purposes that at time t=0, the cathode spot plasma is established and burning on an infinitely thin boiling surface layer of thickness δ, where δ is much thinner than the radial (Δr) and axial (Δz) spatial steps used for the resolution of the heat transfer equations. Using this assumption, one can assume that the cathode surface is initially cold and its temperature equal to the initial temperature of the cathode bulk. This assumption makes sense when we compare the dimensions of the cathode sheath to the dimensions of the cathode itself; 10^{-8}-10^{-7} m in comparison to spot radii of ~10^{-5} m.

7.2.1. Mathematical Formulation

Considering the assumptions made, the energy equation in the solid and liquid phases takes the general form:

$$\rho C_p \frac{\partial T}{\partial t} = \nabla \cdot \lambda \nabla T + S \qquad (7.2.1)$$

where S is a volumetric source term for heat generation/dissipation such as Joule heating. The link between the solid and liquid phases is made by tracking the moving boundary defined by the isotherm T=T_m located at F_m at time t. A box analysis allows to obtain the following equation for the heat balance around the moving boundary $F_m(t)$:

$$\rho L_m \frac{dF_m}{dt} = -\left[\lambda \frac{\partial T}{\partial \xi}\right]_2^1 \qquad (7.2.2)$$

where L_m is the latent heat for melting, and ξ the spatial coordinate in the direction normal to the interface defined by $F_m(t)$. The liquid-vapor phase change is associated with a deformation of the liquid free-surface exposed to the arc. Since the fluid-dynamic aspects

of the problem are not considered, the calculations will stop before the cathode surface temperature will reach its boiling point.

7.2.2. Solution Method

Difficulties arise in the numerical resolution of equations (7.2.1) and (7.2.2) using a finite-difference scheme for the discretization because the location of the melting boundary, $F_m(t)$, falls in between two grid points most of the time. In such a situation, the grid used for the numerical solution of the equations must be constantly redefined.

One way of avoiding such a problem is to use the enthalpy method (Hunter and Kuttler 1989) for the simultaneous solution of equations (7.2.1) and (7.2.2). In this method, a continuous function H for the enthalpy of the material is defined for the whole temperature range. By solving the energy equation in its enthalpy form, the enthalpy is first obtained, and the temperature back-calculated afterwards. Knowing the local enthalpy, one knows the local phase present without having to track the moving boundary using equation (7.2.2). The continuous enthalpy function H is defined by assuming that the phase changes occur in a small temperature interval Δ around the phase change temperatures (solid-liquid and/or liquid-vapor). In doing so, the following equation is obtained for H:

$$H(T) = \begin{cases} \rho \int_{T'=0}^{T} C_p(T')dT' & \text{for } T \le T_m - \Delta/2 \\ H_{T_m - \Delta/2} + \rho(T - T_m + \Delta/2)\dfrac{L_m}{\Delta} & \text{for } T_m - \Delta/2 < T \le T_m + \Delta/2 \\ H_{T_m - \Delta/2} + \rho \int_{T'=T_m-\Delta/2}^{T} C_p(T')dT' & \text{for } T_m + \Delta/2 < T \le T_v - \Delta/2 \\ H_{T_v - \Delta/2} + \rho(T - T_v + \Delta/2)\dfrac{L_v}{\Delta} & \text{for } T_v - \Delta/2 < T \le T_v + \Delta/2 \end{cases} \quad (7.2.3)$$

where L_m and L_v are respectively, the latent heat for melting and vaporization. Such a definition of a continuous enthalpy function H allows to obtain an unique enthalpy for a given temperature T since the enthalpy variations at the phase changes are not

discontinuous. The evolution of the enthalpy function H for copper is plotted on figure 7.2.2 to help understanding this concept.

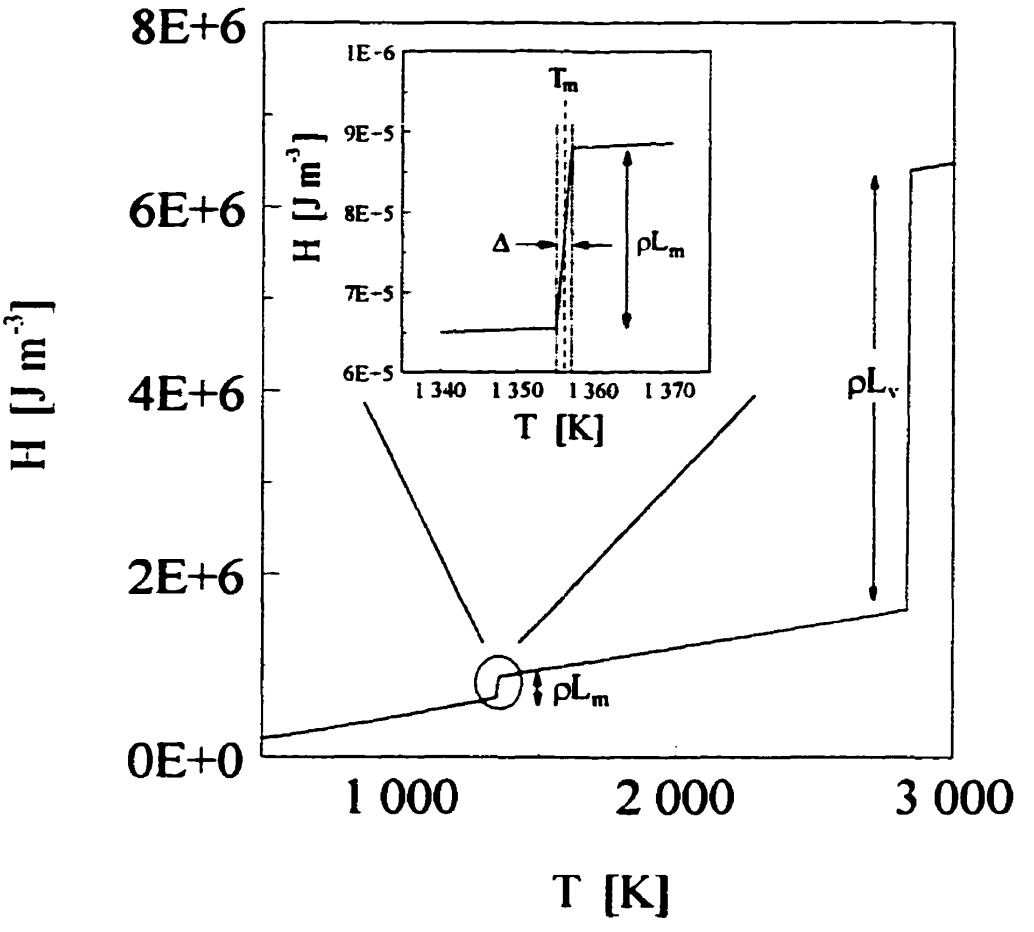

FIGURE 7.2.2. Evolution of the continuous enthalpy function H of copper. Insert: Evolution of H around $T=T_m$ (T_m=1356 K, T_v=2836 K, Δ=1 K, L_m=23.38 J kg^{-1} and L_v=536.4 J kg^{-1}).

In its enthalpy form, the energy equation (7.2.1) reads:

$$\frac{\partial H}{\partial t} = \lambda_w \nabla^2 \theta + S \tag{7.2.4}$$

where the Kirrchoff's transform:

$$\theta(T) = \frac{1}{\lambda_w} \int_{T_w}^{T} \lambda(T')dT' \qquad (7.2.5)$$

is used to eliminate the unwieldy term ∇T in equation (7.2.1), and to avoid the problem encountered with the discontinuities of the thermal conductivity λ occurring at the phase changes. λ_w is the thermal conductivity evaluated at a reference temperature T_w. The Kirrchoff's transform for copper is plotted in figure 7.2.3.

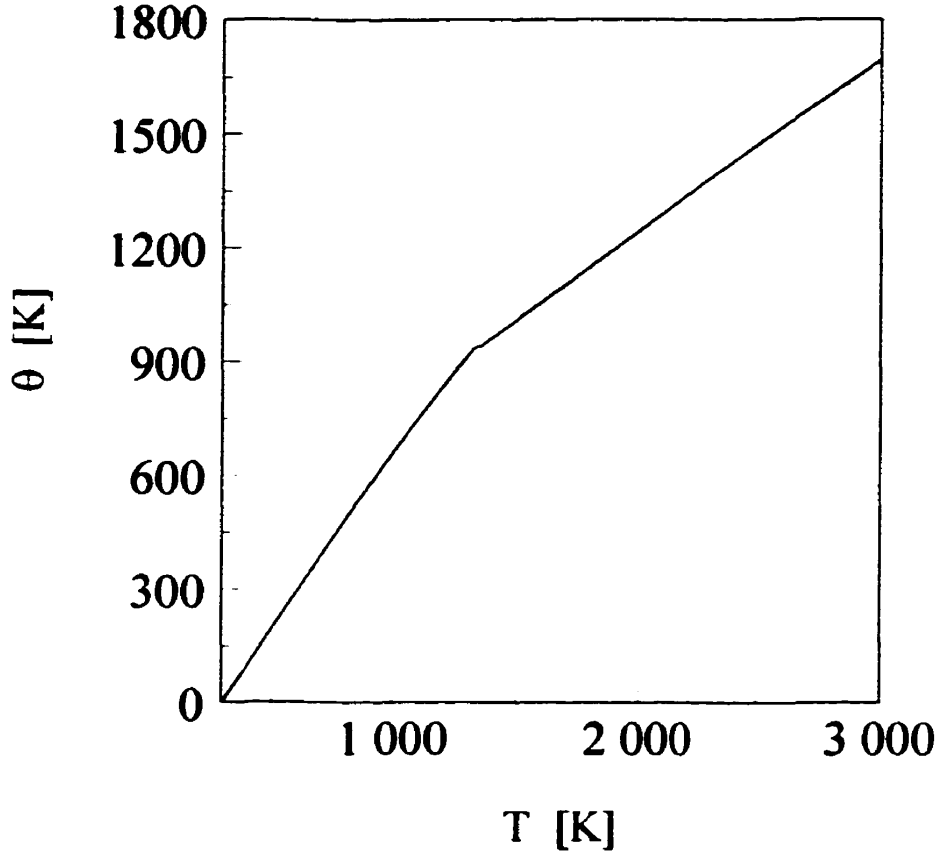

FIGURE 7.2.3. Kirrchoff's transform of copper calculated with T_w=300 K.

A source term taking into account the Joule dissipation in the cathode bulk ($S = j_{tot}^2 / \sigma_e$) was initially considered but, preliminary calculations have shown that this term is negligible for current densities below 10^{11} A m^{-2} (which value is higher than the maximum current density predicted by the model, see figure 5.2.6). This source term was

therefore neglected for this study (assumption also verified by Kharin 1992 and Marotta and Sharakovsky 1996) which considerably simplifies the problem since the equations for the potential distribution in the cathode do not have to be solved simultaneously.

7.2.3. Discretization Scheme and Grid Definition

Equation (7.2.4) without the source term is written in axisymmetric *r-z* coordinates as:

$$\frac{\partial H}{\partial t} = \lambda_w \left[\frac{1}{r} \frac{\partial}{\partial r} \left(r \frac{\partial \theta}{\partial r} \right) + \frac{\partial^2 \theta}{\partial z^2} \right] \tag{7.2.6}$$

Using a finite difference scheme for the discretization with constant axial and radial spatial steps, respectively Δz and Δr, and a time step Δt, one can discretize equation (7.2.6) as:

$$\frac{H_{i,j}^{k+1} - H_{i,j}^{k}}{\Delta t} = \lambda_w \left[\frac{\theta_{i+1,j}^{k} - 2\theta_{i,j}^{k} + \theta_{i-1,j}^{k}}{\Delta r^2} + \frac{1}{r_i} \frac{\theta_{i+1,j}^{k} - \theta_{i,j}^{k}}{\Delta r} + \frac{\theta_{i,j+1}^{k} - 2\theta_{i,j}^{k} + \theta_{i,j-1}^{k}}{\Delta z^2} \right] \tag{7.2.7}$$

where i, j and k are the indices indicating respectively the radial, axial and temporal coordinates.

The temporal evolution of the temperature distribution over the calculation domain is obtained using an explicit scheme for the parameter t. At time $t = t^{k+1}$, the new enthalpies $H_{i,j}^{k+1}$ are calculated using equation (7.2.7) over the entire grid using the $\theta_{i,j}^{k}$ and $H_{i,j}^{k}$ values obtained from the previous time $t = t^{k}$. Knowing the new enthalpies, the new temperatures $T_{i,j}^{k+1}$ are calculated over the entire domain. The corresponding Kirrchoff's transforms $\theta_{i,j}^{k+1}$ are calculated at every time t using a fit of equation (7.2.5) since a unique value of θ exists for a temperature T.

The origin of the coordinate system, $(r, z) = (0,0)$ and $(i, j) = (1,1)$, corresponds to the intersection point made by the centerline of the arc column at $r = 0$ with the cathode surface at $z = 0$ (see figure 7.2.1). A grid point (i, j) is therefore located at $r_i = (i-1)\Delta r$ and $z_j = (j-1)\Delta z$ on a rectangular grid.

7.2.4. Boundary and Initial Conditions

Neumann boundary conditions were used to define all the boundaries. The physical boundary conditions and their corresponding discretized expressions are:

Under the spot ($r<r_s$):

$$q_{cond} = -k\frac{\partial T}{\partial z} \text{ or } q_{cond} = -k_{i,1}\frac{T_{i,2} - T_{i,1}}{\Delta z} \tag{7.2.8a}$$

Outside the spot, at the surface ($r>r_s$):

$$-k\frac{\partial T}{\partial z} = \sigma\varepsilon(T_s^4 - T_\infty^4) \text{ or } -k_{i,1}\frac{T_{i,2} - T_{i,1}}{\Delta z} = \sigma\varepsilon(T_{i,1}^4 - T_\infty^4) \tag{7.2.8b}$$

At $r=R$ (no flux condition):

$$-k\frac{\partial T}{\partial r} = 0 \text{ or } T_{maxi-1,j} = T_{maxi,j} \tag{7.2.8c}$$

At $z=Z$ (no flux condition):

$$-k\frac{\partial T}{\partial z} = 0 \text{ or } T_{i,maxj-1} = T_{i,maxj} \tag{7.2.8d}$$

where *maxi* and *maxj* are the number of grid points in the r and z directions, respectively. The boundary conditions (7.2.8c) and (7.2.8d) are only good approximations of the actual conditions if the calculation domain dimensions are such that $Z >> r_s$ and $R >> r_s$.

The time $t = 0$ is defined as the time after which the cathode spot as been initiated and established. According to the assumptions made in Chapter 4, the cathode spot properties do not change in time after t=0 until extinction and therefore, the current density j_{tot} and heat flux q_{cond} to the surface do not change neither. Another assumption has to be made in order to define the initial conditions within the cathode: It is assumed that at time t=0, the volume of cathode material that has been vaporized or liquefied vanishes and therefore, that the cathode spot plasma is initially burning on an infinitely thin liquid surface layer. At time t=0, a constant heat flux q_{cond} coming from the arc is applied to a surface πr_s^2 of the cathode, where r_s depends on the total current j_{tot} and the current per spot I_s like $r_s^2 = I_s / j_{tot}$.

7.3. Results

7.3.1. Simulation Conditions

The results reported in this section were obtained using as simulation conditions those determined for a Cu cathode exposed to a high pressure arc at T_e^{sc}=1.0 eV (Chapter 5) and are presented in figure 7.3.1 (letters A through E). The heat losses by conduction q_{cond} were taken from figure 5.2.16 while the radii of the arc attachment point r_s were calculated assuming a current per spot I_s and using the current density values plotted in figure 5.2.6. Case A represents the situation where p=p_{min}, case B the situation where the heat flux peaks for this electron temperature, case C the situation where j_{tot}=10^{10} A m^{-2} (~average current density over the whole self-sustaining pressures range), while cases D and E represent the situations where q_{cond}=10^{10} W m^{-2} and 5x10^9 W m^{-2}, respectively. The initial cathode temperature T_{ini} is allowed to range from 300 to 1000 K in order to represent situations of arc spot ignition on a cold surface and on a moderately hot surface. The last situation would correspond to new spot ignition in between several other burning spots maintaining a relatively high cathode surface temperature under the macrospot area. The choice of T_e^{sc}=1.0 eV is not arbitrary. As discussed in sections 6.3.3 and 6.4, such a value for the electron temperature is thought to be highly probable. The current carried per spot I_s is taken equal to characteristic values of 5 or 10 A. Unless specified, the grid

dimensions are i=61 by j=61, R=Z=100 μm and Δt=4 ns. Grid independence was achieved for this grid dimensions.

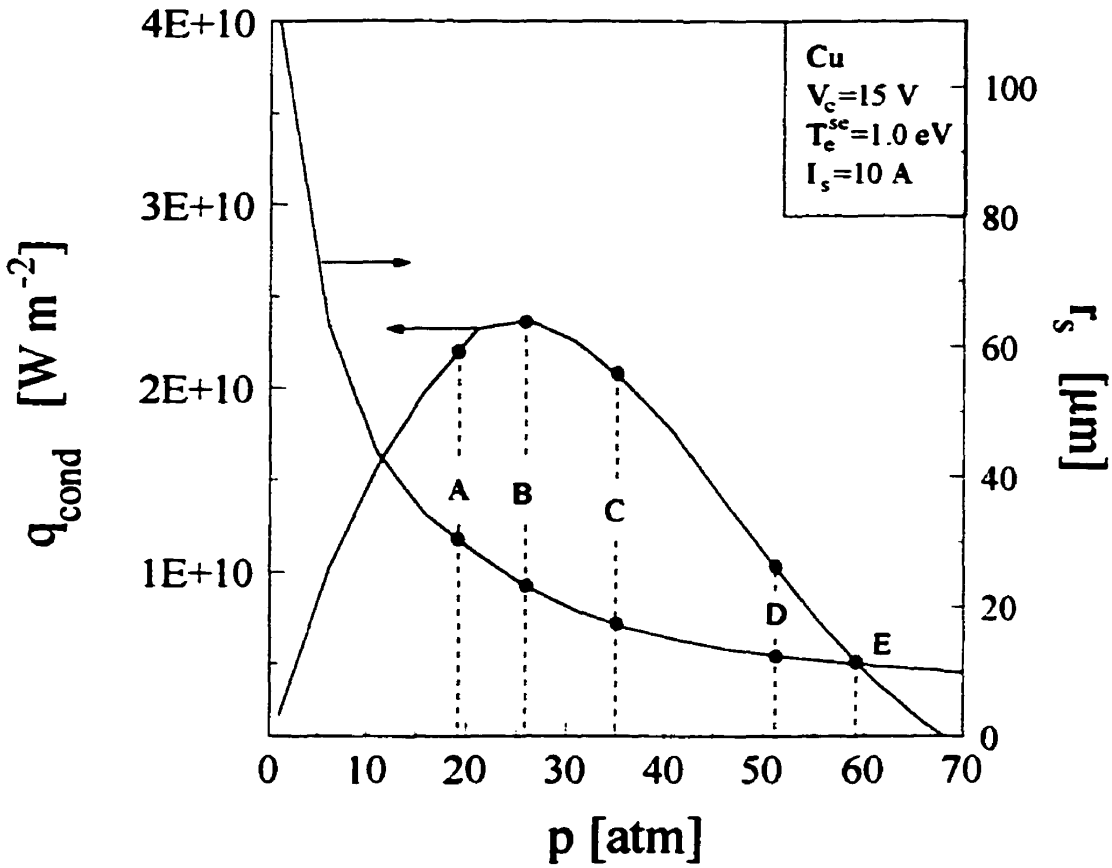

FIGURE 7.3.1. Evolution of q_{cond} and r_s as a function of p. Points linked by letters A through E correspond to the simulation conditions.

7.3.2. Time Scale for Liquid Volume Formation

One important question to answer in this study is whether the heat losses by conduction q_{cond} predicted by the model are large enough to justify the liquid volume formation observed experimentally. Figure 7.3.2 presents the minimum time t_{min} needed to form a liquid volume at the cathode surface (control volume located at r=0 and z=0) for the conditions corresponding to cases A through E of figure 7.3.1 and as a function of the initial cathode temperature T_{ini} and for I_s=10 A.

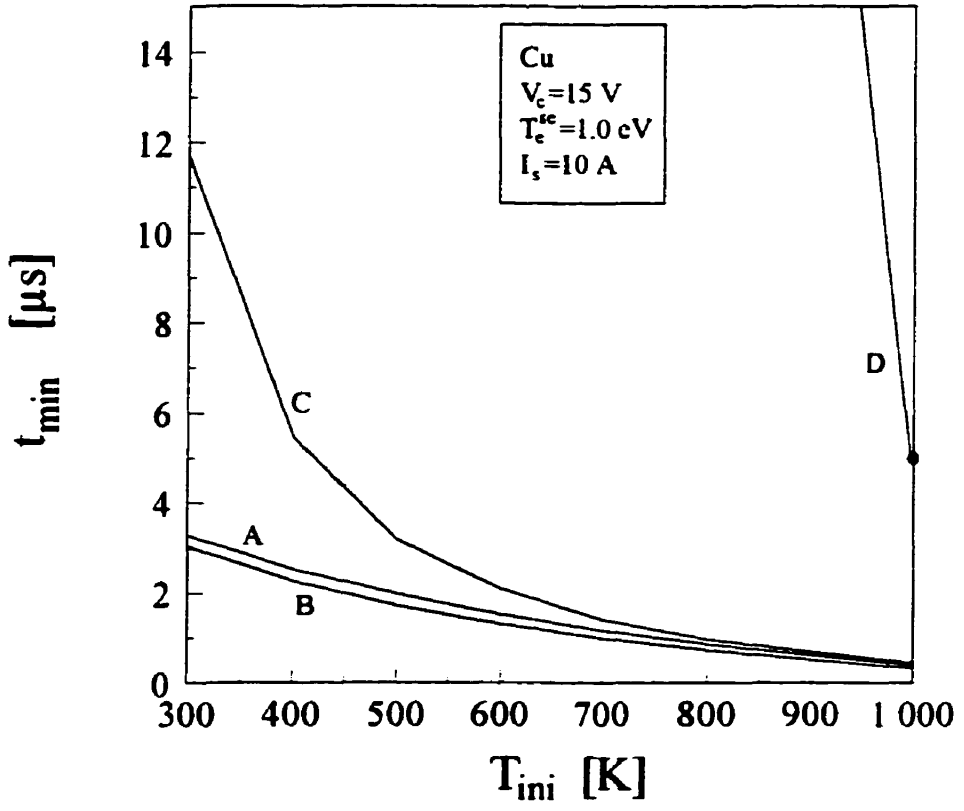

FIGURE 7.3.2. Minimum time t_{min} needed to form a liquid volume underneath the arc attachment point on the cathode as a function of T_{ini} for cases A through E presented in figure 7.3.1.

Four important observations can be made from the analysis of figure 7.3.2.

1) For the conditions corresponding to cases A through C, liquid volumes are formed quickly underneath the arc attachment point. Typical time scales are less than 10 μs for these cases, and somewhat larger time scales are observed for case D (probably >>10 μs for T_{ini}<900 K). For all the values of T_{ini} investigated, it was impossible to see any liquid volume formation for case E. Figure 5.2.16 lets suggest that such time scales are even lower for electron temperatures above T_e^{sc}=1.0 eV since the values taken by q_{cond} for T_e^{sc}>1.0 eV are higher than those at T_e^{sc}=1.0 eV.

2) The higher is the initial cathode temperature T_{ini}, the lower is the time needed to form a liquid volume. This result was easily predictable. However, it shows an important

feature; When the cathode spots are closely grouped under a macrospot, high temperatures are maintained in between them at the cathode surface and therefore, liquid volume formation is this situation is highly probable. This concept of high initial cathode temperatures favoring the formation of liquid volumes and possibly liquid droplet ejection was investigated experimentally by Nürnberg *et al* (1981) who observed an increase of the erosion rates with an increase of the cathode temperature. In this case, the cathode temperature was voluntary maintained high by external means.

3) As the metallic plasma pressure increases, and therefore as the total current density increases (see figure 5.2.6), the conditions leading to liquid volume formation become less favorable. This can clearly be seen by analyzing the evolution of t_{min} from case A through D for instance. This observation was discussed in another context in Chapter 5. At high metallic vapor pressures, the Nottingham cooling losses associated with the strong thermo-field emission of electrons become more important than the heat losses by conduction.

4) A detailed analysis of cases A and C reveals an interesting feature. The conditions associated with case A are $q_{cond}=2.2\text{x}10^{10}$ W m^{-2} and $j_{tot}=3.5\text{x}10^{9}$ A m^{-2} while those associated with case C are $q_{cond}=2.1\text{x}10^{10}$ W m^{-2} and $j_{tot}=10^{10}$ A m^{-2}. For a given heat flux (both values are essentially the same), the time scale for liquid volume formation increases as the current density increases. The higher is the current density, the lower is the arc attachment radius r_s on the cathode surface for a given current I_s, and therefore, the higher are the temperature gradients close to the surface. Thus, the higher is the heat dissipation from the volume underneath the arc attachment towards the colder regions of the cathode.

7.3.3. Maximum Erosion by Liquid Volume Ejection

Three situations will enhance the cathode erosion due to liquid volume formation and ejection. 1) When the residence time of the arc foot at a given location on the cathode is long in comparison with the time scale necessary for the onset of thermo-capillary

convection within the liquid bath, liquid metal is displaced and damages are made to the cathode (Kharin 1992). Indeed, violent displacement of liquid metal outside the crater and possibly emission of droplets may occur thus causing erosion. 2) When a high ion pressure is maintained on the liquid metal bath as it is the case for non-refractory cathodes, liquid ejection under the form of microdroplets may occur upon the pressure release associated with the cathode spot extinction (Gray and Pharney 1974). 3) When an intense Joule heating occurs due to the important constriction of the current carrying channel at the arc attachment point, a localized liquid volume is formed rapidly underneath the cathode surface and the resulting overheating may cause micro-explosions (He and Haug 1997). As it was discussed in section 2.3.7, this situation occurs when a new cathode spot is ignited from an initially cold surface (in such a case field emission of electrons initiates the discharge) and therefore, the liquid volume formation here is not due to the action of the plasma ions bombarding the cathode surface. It is not likely that such micro-explosions leading to erosion by liquid ejection will be important for long lasting discharges where high surface temperatures are maintained and where the surface electric fields due to the space charge are thought to be sufficient for new spot ignition (He and Haug 1997).

The heat transfer model developed in section 7.2 is now used to estimate the masses of liquid formed and the maximum erosion rates due to liquid ejection, $E_{r,liq}^{max}$, under typical conditions. $E_{r,liq}^{max}$ is calculated assuming that all the liquid volume formed is ejected from the cathode surface. Such a situation is not likely to occur but, the calculation of $E_{r,liq}^{max}$ (and $E_{r,vap}^{max}$, Chapter 5) allows to determine the maximum limit for the cathode erosion rate. The conditions corresponding to situation B on figure 7.3.1 were used and the influence of the time t, current per spot I_s and initial temperature of the cathode T_{ini} on these two parameters was investigated.

Figure 7.3.3. presents the evolution of the liquid mass formed as a function of time for two values of I_s, respectively 5 and 10 A, and T_{ini} ranging from 300 to 700 K. The apparent instabilities are due to the way the volumes are numerically evaluated; the mass

within a given control volume must be completely melted before being considered a liquid volume. One can observe a general trend followed by all the curves presented: the first liquid volume appears at a time t_{min} which is function of I_s and T_{ini}, and the mass of liquid formed increases with time with a parabolic dependency. This last behavior is consistent with a system that will eventually reach a steady state. Again, the higher is T_{ini} the larger is the liquid volume formed at a time t. A higher current per spot means a larger arc attachment radius r_s, and therefore, a higher formation of liquid.

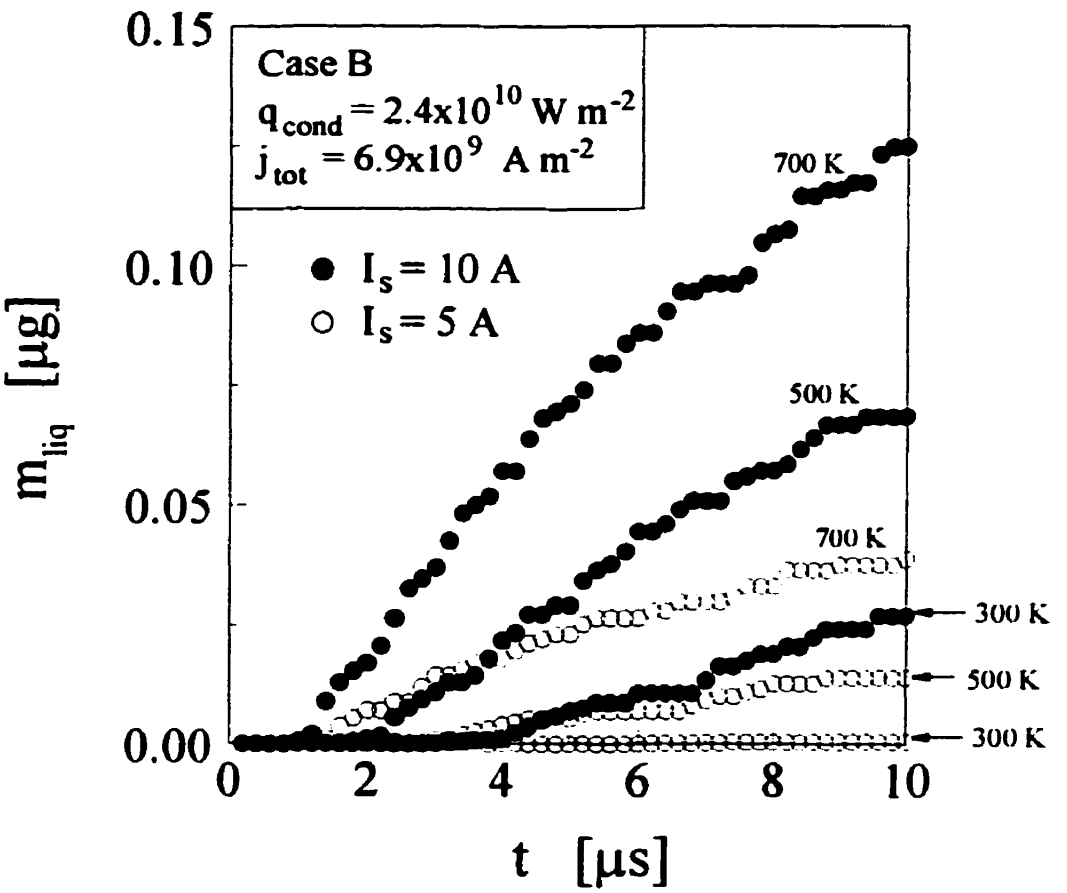

FIGURE 7.3.3. Temporal evolution of the liquid mass formed underneath the arc attachment for the self-sustaining conditions corresponding to case B.

The process of liquid volume formation can be better seen with figure 7.3.4 which shows the temporal evolution of the temperature distribution within the cathode region located underneath the arc attachment point for the conditions corresponding to case B with I_s=10 A and for two initial cathode temperatures: 1) T_{ini}=500 K and 2) T_{ini}=700 K.

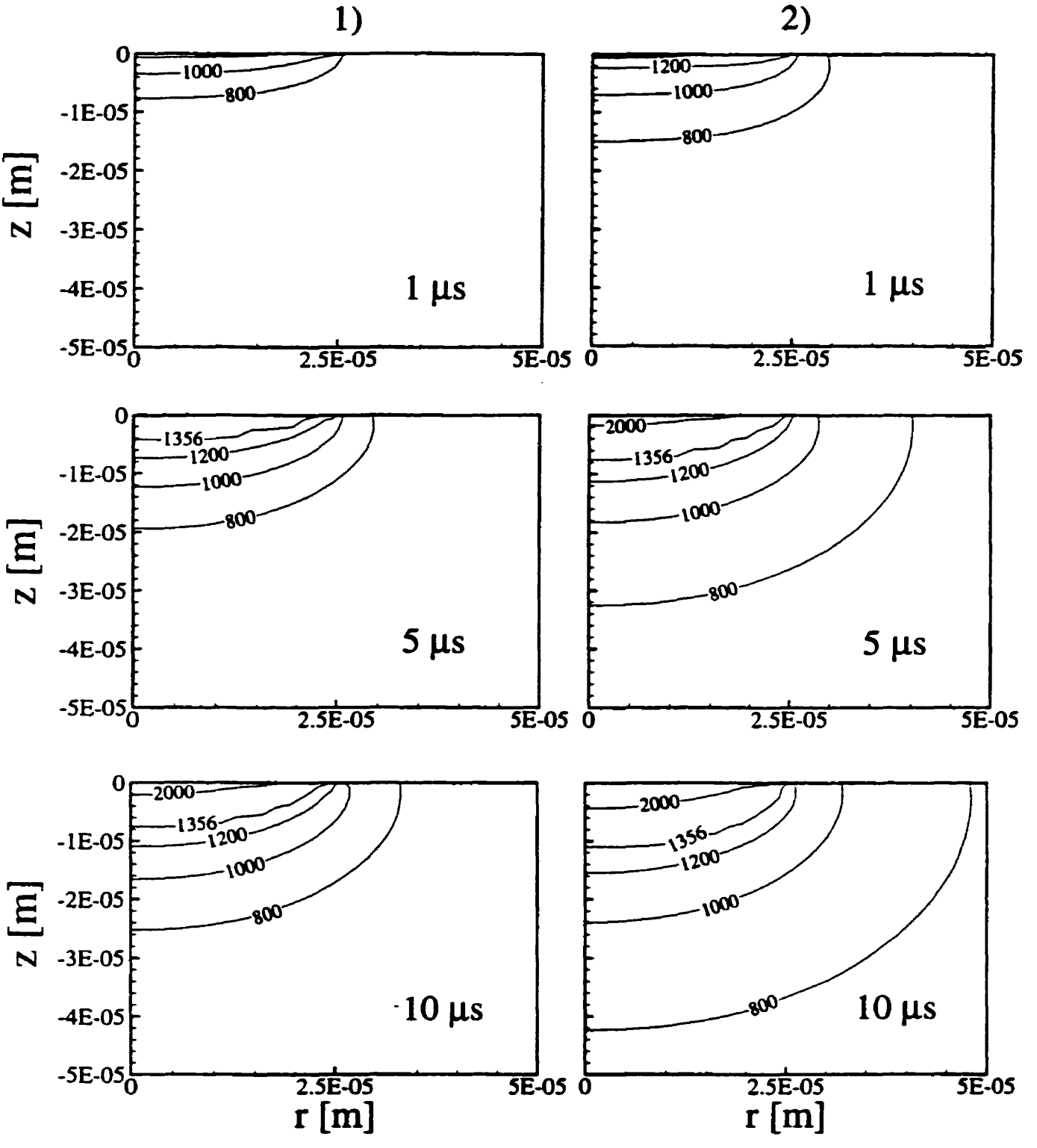

FIGURE 7.3.4. Temporal evolution of the temperature distribution within the cathode for the conditions corresponding to case B with 1) T_{ini}=500 K and 2) T_{ini}=700 K.

One can follow the process of liquid volume formation by looking at the movement of the melting point isotherm $T=T_m=1356$ K with time. Again, as it can be seen by comparing situations 1) and 2) in figure 7.3.4, the higher is initially the cathode temperature the faster is the liquid volume formation process.

The maximum rate at which liquid mass can be ejected from the cathode region located underneath the arc attachment is shown in figure 7.3.5 as a function of time, current per spot, and initial cathode temperature. This maximum erosion rate by liquid ejection $E_{r,liq}^{max}$ is defined as the liquid mass formed during a time t when a current I_s is flowing through the arc attachment point on the cathode. Defined in such a way, $E_{r,liq}^{max}$ can be compared to $E_{r,vap}^{max}$.

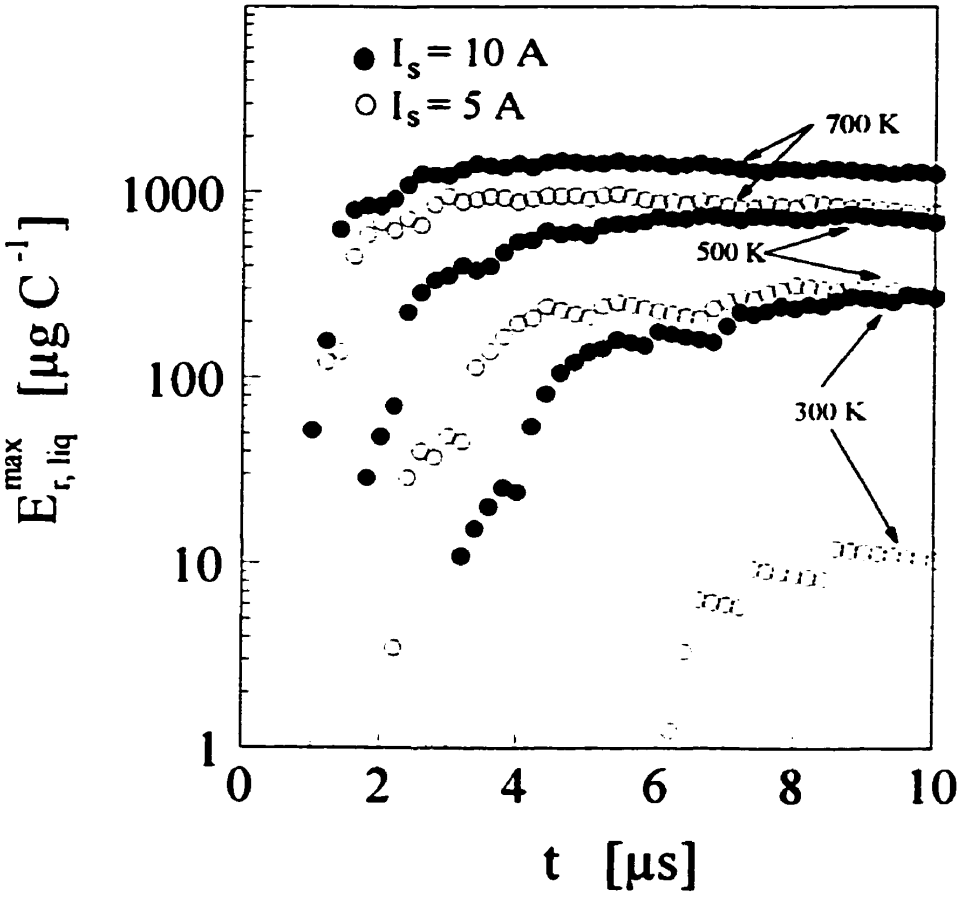

FIGURE 7.3.5. Temporal evolution of the maximum erosion rate by liquid volume ejection $E_{r,liq}^{max}$ for the self-sustaining conditions corresponding to case B.

$E_{r,liq}^{max}$ is shown to increase rapidly as the first liquid volume is formed, and to reach its maximum value within a few microseconds. Once this value is reached, $E_{r,liq}^{max}$ starts to decrease slowly. For the conditions reported in figure 7.3.5, $E_{r,liq}^{max}$ ranges from around 10 to nearly 2000 μg C^{-1}. Such values are high. However, only a limited fraction of the liquid mass formed actually leaves the cathode and causes erosion. As discussed by Gray and Pharney (1974), the liquid ejection induced by the pressure release upon spot extinction is less than 1% of this entire liquid volume formed underneath the arc attachment region.

7.4. Discussion and Conclusions

The self-sustaining operating conditions allowing for the production of liquid volumes in the μs time scale at the arc attachment on a Cu cathode are those corresponding to the lowest metallic vapor pressures. For high metallic vapor pressures, the Nottingham cooling heat losses become dominant over the conduction heat losses (see figure 5.2.15). As discussed in Chapter 5, one may possibly reduce the liquid volume formation by confining the cathode spots to enhance the local pressures.

The results presented in figures 7.3.3 to 7.3.5 clearly show that the maximum erosion rates by liquid volume ejection $E_{r,liq}^{max}$ depend strongly on the initial cathode temperature and the current carried per spot. These also show that this parameter can reach considerably high values. The higher are the current per spot I_s and initial cathode temperature T_s, the higher is $E_{r,liq}^{max}$. We have seen with figure 5.2.17 that the maximum erosion rates by vaporization $E_{r,vap}^{max}$ for a Cu cathode with T_e^{sc}=1.0 eV range from 100 to 300 μg C^{-1}, while those associated with liquid volume ejection $E_{r,liq}^{max}$ range from 10 to values above 2000 μg C^{-1} when T_{ini} is larger than 700 K. Such high values are well above the erosion rates values observed experimentally (4-50 μg C^{-1}) since neither the redeposition of neutrals and ions on the surface nor the limited ejection of liquid have been considered. Indeed, considering all the sources of erosion, one can write a general expression for the erosion rate of the cathode of a high pressure arc that reads:

$$E_r = (1-\chi_{vap})E_{r,vap}^{max} + (1-\chi_{liq})E_{r,liq}^{max} \qquad (7.4.1)$$

where χ_{vap} and χ_{liq} represent respectively, the fractions of the vapors being formed that are condensing back on the cathode surface (ions and neutrals; redeposition effect) and the fraction of the liquid mass formed that stays on the surface. The calculation of the coefficients χ_{vap} and χ_{liq} requires the knowledge of the accommodation coefficients for metallic vapors on their own solid or liquid phases, and the development of a fluid-dynamics model of the liquid volume displacement from the liquid bath.

In order to reduce the formation of liquid volumes that may eventually cause liquid droplet ejection, two scenarios are conceivable. First, enhance the cathode spot internal confinement as discussed earlier in Chapter 5 to favor the existence of high current density cathode spots (cathode spots with high metallic vapor pressures). Such a solution would however increase the production of metallic vapors. Secondly, favor the alignment of the cathode spots forming the macrospots in order to lower the heat flux to the surface maintained by several cathode spots closely grouped. As reported by Drouet (1995) and Szente (1989), an alignment of the cathode spots along the magnetic field lines occurs naturally when the arc column is driven into rotation by an external magnetic field. The higher is the magnetic field intensity, the better is the alignment of the cathode spots and the lower is the erosion rate.

Finally, we may note that the above discussion and the range of measured erosion rates stated do not include the very low erosion rate values measured by Szente *et al* (1992) on CO and N_2 contaminated copper ($E_r \geq 0.4\,\mu g\ C^{-1}$ for ~0.3%vol. contamination). Such low values reflect the rapid arc jumping action on highly emissive sites formed by dielectric layers at the surface (mode 1 type of spots, see Chapter 2). In order to take these phenomena into account, an arc initiation probability distribution should be established (Schmoll and Hartmann 1997) and the time dependent evolution of the cathode spot plasma and surface temperature are needed.

PART 3: CONCLUSIONS

GENERAL CONCLUSIONS

In this study, the attachment of a high pressure electric arc on an electron emitting non-refractory (cold) cathode was theoretically investigated. A model for the cathode region was developed considering the possibility of a pressure build up on the cathode surface, Bohm's approach for the cathode sheath formation, and the ion-enhanced thermo-field emission from the cathode surface. The definition of the conditions prevailing in the cathode region and allowing a self-sustaining attachment of the arc on the cathode was made by validating two simple criteria based on particle and energy balance considerations.

The most important result obtained from the model is that, in order to have a self-sustaining attachment of an electric arc on a non-refractory cathode, an important vaporization of the cathode surface leading to a pressure build up in the cathode region is necessary. It was shown that a minimum metallic vapor pressure of around 19 atm is necessary for copper. According to this scenario, the strong erosion rates observed on such type of cathode must not be seen as a consequence of the strong heat input from the arc that cannot be dissipated by conduction into the cathode bulk; the strong vaporization of the cathode is a *necessary condition* for the establishment of a self-sustaining arc attachment.

Another important result obtained from this theoretical investigation is that, even though the arc attachments on both refractory and non-refractory cathodes appear substantially different, both types of cathode can be described by a unique model. It is only on the way the conditions necessary for a self-sustaining operation of the arc are achieved that both types of cathode differ strongly. Actually, the pressure of metallic vapors needed for a self-sustaining operation is shown to decrease according to an exponential decay law as the cathode material becomes more refractory. This is an extremely interesting finding in view of the complexity of such arc-cathode interaction systems.

Electron emission from the surface of non-refractory cathodes falls in the ion-enhanced thermo-field range where the surface temperature and electric field, the ion density and charge all play an important role. It was shown that the use of a simplified approach for the calculation of the electron emission current leads to an important underestimation of this parameter, and to an overestimation of important parameters such as the cathode surface temperature and metallic vapor pressure in the cathode region.

The present study allowed to define a framework for the calculation of the maximum erosion rates by vaporization, and by liquid volume formation and ejection as a function of the conditions prevailing in the cathode region of a non-refractory cathode. It was shown that a proper confinement of the cathode spots would lead to an enhancement of the vapor production to the detriment of the liquid droplet emission which is of interest in the AIP process for instance.

RECOMMENDATIONS FOR FUTURE STUDIES

This work aimed at a better theoretical understanding of the arc-cathode interactions in the special case where the cathode is made of a non-refractory material. It certainly helps to better understand the complex phenomena involved in the cathode region of high pressure arcs but, as it was suggested throughout the thesis, further developments are needed as much on the experimental as on the theoretical point-of-view. The following list contains some suggestions for future developments:

Experimental point-of-view:

1) The major problem encountered when developing a model of the cathode region is the lack of accurate data for validation. The principal parameter that should be measured with accuracy is the total current density per spot. The estimation of this current density from the measurement of the post-mortem crater radius is relatively simple but, it is questionable whether the craters left on the cathode surface during the arcing period really represent the current transfer areas or not. The possibility of optimizing the current density probe technique of Szente *et al* (1991) in order to allow a higher spatial and temporal resolution should be considered. The observation of the cathode spots with a high speed, high temporal and spatial resolution camera is also of interest to better understand their dynamics (e.g. Jüttner 1997).

2) The development of a new low- or free-erosion cathode material is certainly a challenging and exciting task for the future. Trying to develop a composite cathode material made of a base metallic element covered with a strong and adherent coating of diamond, diamond-like (DLC), or silicon-carbide (SiC) for instance could possibly lead to interesting developments. Such composite cathodes could show low erosion rates due to a different arc attachment mode. Diamond coatings on molybdenum tips are already being used as strong field effect emitters in electron microscopes (Schlesser *et*

al (1997)) and could possibly be used at elevated temperatures. SiC is of interest since this ceramic becomes semiconducting at high temperatures. The question is whether such coatings will sustain the high temperatures or not and if they will show better performances that the oxide-contaminated metallic cathodes.

3) The model suggests that a transition occurs in the arc attachment mode for tungsten as the chamber pressure changes from vacuum to atmospheric. Indeed, the constricted attachment of the cathode spots under vacuum changes to a diffuse, spotless attachment at atmospheric pressure. It would be interesting to determine at which pressure that phenomenon occurs. The same behavior is possibly true for non-refractory copper cathodes, but for pressures much higher than atmospheric.

Theoretical point-of-view:

1) The most important future theoretical development would be to extend the physical model of the cathode sheath region developed in Chapter 4 to include the ionization zone and the arc column. In doing so, the boundary conditions necessary for the model such as the chamber pressure and the arc temperature profile would become parameters that are more easily measurable than the parameters used in this study. Existing models of the ionization zone such as those of Scheuer and Emmert (1988) and Senda (1997) could be used as starting material. The pressure drop in the cathode region is to be considered in such future models.

2) The present model did not allow to calculate the self-sustaining operating conditions for W since for systems where the pressure of metallic vapors is below the ambient gas pressure, the cathode surface temperature cannot be related simply to the pressure of metallic vapors via a vapor pressure curve (i.e. $T_s=T_s(p)$). One would need to couple the cathode sheath model to a heat transfer model of the cathode in order to calculate the surface temperature, and also to extent the calculation of the plasma composition to mixtures of gases and metallic vapors (Ar+Cu for instance).

3) The development of a three-dimensional model for the heat transfer within the cathode is necessary for the calculation of liquid volumes formed under the arc attachment when several cathode spots exist at the same time and are closely grouped together. In such a case, material vaporization, condensation, and liquid volume displacement occur in between the cathode spots.

4) Develop a model for the current transfer through insulating and semiconducting layers covering metallic cathodes. This task will become essential for the understanding of arc-cathode interactions if one succeeds in making such stable and adherent coatings on metallic cathodes.

5) One should maintain a collaboration with research groups involved in the development of models describing the electron emission from the cathode (e.g. Spataru *et al* 1997, Gayet *et al* 1996, and Vasenin *et al* 1997). Indeed, as we have seen in Chapter 5, the presence of a high density of ions in the cathode region significantly enhances the electron emission. In this study, we did not consider the nature of the ion nor their possible neutralization before reaching the cathode surface. These effects should be taken into account as also mentioned recently by Josso (1997).

NOMENCLATURE

C_p	heat capacity of the cathode material (J kg^{-1} K^{-1})
C_s	local sound velocity (m s^{-1})
D	electron tunneling probability across the barrier at the metal surface (--)
e	unit charge (1.6022×10^{-19} C)
E	electric field strength (V m^{-1})
E_f	Fermi energy (J or eV)
E_r	erosion rate (μg C^{-1})
$E_{r,liq}$	erosion rate by liquid volume ejection (μg C^{-1})
$E_{r,vap}$	erosion rate by vaporization (μg C^{-1})
E_s	surface electric field strength (V m^{-1})
E_{ion}	ionization potential (eV)
F_m	location of the solid-liquid phase change moving boundary (m)
f	fraction of plasma ions sticking on the dielectric surface (--)
f_{bi}	fraction of the emitted electrons (beam electrons) left for ionization (--)
H	enthalpy of the cathode material (J m^{-3})
h	Planck's constant (6.626×10^{-34} J s)
I	arc current (A)
I_s	current per spot (A)
j_{bdc}	current density of back-diffusing plasma electrons (A m^{-2})
j_{ion}	total ion current density (A m^{-2})
j_i	current density of species i (A m^{-2})
j_{RD}	Richardson-Dushmann electron current density (A m^{-2})
j_{T-F}	current density of thermo-field electrons (A m^{-2})
j_{tot}	total current density (A m^{-2})
k_B	Boltzmann's constant (1.380658×10^{-23} J)
K_n	equilibrium constant for ionization/recombination based on species density (m^{-3})

K_e mean kinetic energy of the emitted electrons (J or eV)

L_m latent heat of melting of the cathode material (J kg^{-1})

L_v latent heat of vaporization of the cathode material (J kg^{-1})

m_c mass of a cathode material atom (kg)

m_e electron mass (9.1094×10^{-31} kg)

n_{bde} number density of back-diffusing plasma electrons (m^{-3})

n_e number density of electrons (m^{-3})

n_i number density of species i (m^{-3})

n_o number density of neutral atoms (m^{-3})

n_{sc} space charge density, $n_{sc}=n_{ion}-n_{T\text{-}F}-n_{bde}$ (m^{-3})

$n_{T\text{-}F}$ number density of thermo-field electrons (m^{-3})

NdW flux of Fermi-Dirac distributed electrons in the energy interval dW (m^{-2} s^{-1})

p metallic plasma pressure, vapor pressure at temperature T_s (Pa or atm)

p_{Cu} partial pressure of copper vapor (Pa or atm)

p_{tot} total pressure (Pa or atm)

p_M self-magnetic pinch pressure (Pa or atm)

p_{min} minimum metallic plasma pressure for self-sustaining operation (atm)

p_{max} maximum metallic plasma pressure for self-sustaining operation (atm)

q_{bde} heat input by back-diffusing plasma electrons bombardment (W m^{-2})

q_{ion} heat input by returning ions bombardment (W m^{-2})

q_{in} incoming heat flux, $q_{in}=q_{ion}+q_{bde}$ (W m^{-2})

q_{cond} heat loss by conduction (W m^{-2})

q_{not} heat loss by the Nottingham effect (W m^{-2})

q_{rad} heat loss by radiative heat exchange with the surrounding (W m^{-2})

q_{vap} heat loss by vaporization (W m^{-2})

Q_i electronic partition function of species i (--)

r_s cathode spot radius (m)

T temperature (K)

T_e electron temperature (K or eV)

T_h heavy species temperature (K)

T_{ini} initial temperature of the cathode (K)

T_m melting temperature of the cathode material (K)

T_s surface temperature of the cathode under the spot (K)

T_v vaporization temperature of the cathode material (K)

T_w reference temperature (K)

T_∞ surrounding temperature (K)

v_{arc} arc root velocity (m s^{-1})

v_{bde} thermal velocity of the back-diffusing plasma electrons (m s^{-1})

v_i velocity of species i (m s^{-1})

$v_{T\text{-}F}$ velocity of the thermo-field electrons (m s^{-1})

$v_{th,e}$ thermal velocity of the electrons (m s^{-1})

$v_{th,i}$ thermal velocity of the ions (m s^{-1})

V local potential in the cathode sheath (V)

V_{arc} arc voltage (V)

V_c cathode sheath voltage drop (V)

V_e electron potential energy (eV)

V_h Volt-equivalent of the ion energy at the cathode sheath edge (V)

W electron energy (J or eV)

W_a effective potential of the electron inside the metal surface (eV or J)

x distance from the cathode surface (m)

x_c cathode sheath thickness (m)

z_i number of charges carried by species i (--)

Z number of species in the plasma (--)

Greek Letters

β electron emission enhancement factor (--)

χ_{liq} fraction of liquid mass formed that stays on the cathode surface (--)

χ_{vap} fraction of vaporized mass formed that redeposite on the cathode surface (--)

Δ temperature interval for phase change (K)

ΔE_∞ lowering of ionization potential (eV)

Δp pressure correction (Pa)

Δr radial step (m)

Δt time step (s)

Δz axial step (m)

$\Delta\phi$ reduction of the material work function by the Schottky effect (eV)

ε emissivity (--)

ε_r dielectric constant (--)

ε_N Nottingham potential (eV)

ε_o vacuum permittivity (8.8542×10^{-12} F m^{-1})

ϕ work function (eV)

ϕ_{eff} effective work function, $\phi_{eff}=\phi-(eE_s/4\pi\varepsilon_o)^{1/2}$ (eV)

Γ_{vap} flux of vaporized atoms (m^{-2} s^{-1})

λ_D Debye length (m)

λ_{ab} mean free path between two collisions involving particles *a* and *b* (m)
b being the heaviest species.

λ thermal conductivity of the cathode material (W m^{-1} K^{-1})

μ_o vacuum permeability (1.2566×10^{-6} H m^{-1})

ν collision frequency (m^{-3} s^{-1})

θ Kirrchoff's transformation (K)

ρ density of the cathode material (kg m^{-3})

σ Stefan-Boltzmann constant (5.67×10^{-8} W m^{-2} K^{-4})

σ_{ab} cross section for collisions involving particles *a* and *b* (m^2)
b is the heaviest species.

σ_e electrical conductivity of the cathode material (A V^{-1} m^{-1})

τ characteristic time (s)

Superscripts and Subscripts

FEE	calculated using the field-enhanced thermionic equation
i	radial coordinate
j	axial coordinate
k	time coordinate
MG	calculated using the Murphy and Good formalism
MG–I	calculated using the Murphy and Good formalism and the ion-enhancement factor
se	at cathode sheath edge

APPENDICES

APPENDIX A: SOLUTION OF THE MURPHY AND GOOD EQUATIONS IN SI UNITS

The original resolution of the equations for T-F emission by Murphy and Good (1956) was performed using the CGS units. The aim of this appendix is to develop again the necessary equations, but now in the SI units system.

Taking the original expressions for $D(E_x,W)$ and $N(W,T_s,\phi)$ from Murphy and Good (1956), equation (2.2.5) rewrites:

$$j_{T-F}^{MG} = \frac{4\pi e m_e k_B T_s}{h^3}\int_{-W_a}^{W_i} \ln\left[1+\exp\left(-\frac{W+e\phi}{k_B T_s}\right)\right]\cdot\left(1+\exp\left(Bv(y)y^{-3/2}\right)\right)^{-1} dW + \ldots$$

$$\ldots + \frac{4\pi e m_e k_B T_s}{h^3}\int_{W_i}^{\infty} \ln\left[1+\exp\left(-\frac{W+e\phi}{k_B T_s}\right)\right] dW \qquad \text{(A.1)}$$

where

$$W_i = -\frac{1}{\sqrt{2}}\left(\frac{e^3 E_s}{4\pi\varepsilon_o}\right)^{1/2} \qquad \text{(A.2)}$$

is the energy above which the penetration probability for the electron is $D(E_x,W)=1$. The expressions for B, y and $v(y)$ are:

$$B = \frac{8\pi\sqrt{2}}{3}\frac{m_e^{1/2} e^{5/4}}{h E_s^{1/4}(4\pi\varepsilon_o)^{3/4}}, \qquad \text{(A.3)}$$

$$y = \left(\frac{e^3 E_s}{4\pi\varepsilon_o}\right)^{1/2} \frac{1}{|W|}, \tag{A.4}$$

$$v(y) = -(y/2)^{1/2}\left\{-2E\left[(y-1)^{1/2}/(2y)^{1/2}\right] + (y+1)K\left[(y-1)^{1/2}/(2y)^{1/2}\right]\right\} \text{ for } y>1 \tag{A.5a}$$

$$v(y) = (1+y)^{1/2}\left\{E\left[(1-y)^{1/2}/(1+y)^{1/2}\right] - yK\left[(1-y)^{1/2}/(1+y)^{1/2}\right]\right\} \text{ for } y<1 \tag{A.5b}$$

with
$$K[\xi] = \int_0^{\pi/2} (1-\xi^2 \sin^2\theta)^{-1/2} d\theta \tag{A.6}$$

and
$$E[\xi] = \int_0^{\pi/2} (1-\xi^2 \sin^2\theta)^{1/2} d\theta \tag{A.7}$$

The value of the integrand of equation A.1 being much smaller than unity for $W<-W_a$ ($-W_a \sim O(-10$ eV)), $-W_a$ can be replaced by $-\infty$. The integration of equation A.1 was performed with an electron energy interval $dW=1\times10^{-20}$ J (0.0625 eV) for all the calculations reported in this thesis.

APPENDIX B: DERIVATION OF THE FIELD-ENHANCED THERMIONIC EQUATION

Thermionic emission corresponds to the limiting case of T-F emission when the electric field strength goes to zero. Setting E_s=0 in the equation for T-F emission (equation A.1) allows to get:

$$j_{RD}(E_s, T_s, \phi) = \frac{4\pi e m_e k_B T_s}{h^3} \int_0^\infty \ln\left[1 + \exp\left(-\frac{W + e\phi}{k_B T_s}\right)\right] dW \qquad \text{(B.1)}$$

since the first integral in equation A.1 is negligibly small when $E_s \to 0$. Defining the new variable $u = \exp\left[-(W + e\phi)/k_B T_s\right]$ and noticing that $u << 1$ for the range of work functions and surface temperatures considered in this study (respectively $2<\phi<5$ eV and $1000<T_s<5000$ K), equation B.1 transforms to

$$j_{RD} = -\frac{4\pi e m_e (k_B T_s)^2}{h^3} \int_{\exp(-e\phi/k_B T_s)}^{0} \frac{\ln(1+u)}{u} du \cong -\frac{4\pi e m_e (k_B T_s)^2}{h^3} \int_{\exp(-e\phi/k_B T_s)}^{0} (1 - u/2) du \qquad \text{(B.2)}$$

which, knowing that $u^2 << u$, can easily be integrated to give the well-known Richardson-Dushman equation for thermionic emission (2.2.1):

$$j_{RD} = \frac{4\pi e m_e (k_B T_s)^2}{h^3} \exp\left(-\frac{e\phi}{k_B T_s}\right) \qquad \text{(B.3)}$$

Introducing the Schottky correction to the material work function induced by the presence of a macroscopic surface electric field ($\Delta\phi = (eE_s/4\pi\varepsilon_o)^{1/2}$), we obtain the Richardson-Dushman equation for thermo-field emission or simply the field-enhanced thermionic equation (2.2.4):

$$j_{T-F}^{FEE} = \frac{4\pi e m_e (k_B T_s)^2}{h^3} \exp\left(-\frac{e(\phi - \Delta\phi)}{k_B T_s}\right) \qquad \text{(B.4)}$$

APPENDIX C: THE NASA METHOD

The calculation of the plasma composition for given T_h, T_e and p using the NASA method (Boulos *et al* 1994) consists of solving iteratively a set of Z coupled non-linear equations relating the various particle number densities to the electron and heavy species temperatures starting from an initial guess of the plasma composition (Z corresponds to total number of species present in the plasma). These equations include the equation for electrical quasi-neutrality (equation 4.6.5), the Dalton's law (equation 4.6.6), and a set of Z-2 equations expressing the equilibrium constants for the chemical reactions taking place in the plasma (e.g. equation 4.6.4 for ionization/recombination reactions).

The iteration procedure consists of solving the linear system $-\Delta\vec{g} = F\Delta\vec{n}$ for each calculation step and recalculating the new values for n_i using $\Delta n_i = n_i - n_i^o$ (n_i is the new value for the species density while n_i^o is the actual species density). The vector $\Delta\vec{g}$ represents the deviations from the governing equations for each calculation step. In the case of a plasma containing the species e-, A, A+ and A++, the vector $\Delta\vec{g}$ has for components:

1) the deviation from the electrical neutrality law:

$$\Delta g_1 = n_e - \sum_i z_i n_i \qquad \text{(C.1)}$$

2) the deviation from the Dalton's law:

$$\Delta g_2 = n_e k_B T_e + \sum_i n_i k_B T_h - p + \Delta p \qquad \text{(C.2)}$$

3) the deviation from the equilibrium constant of species A:

$$\Delta g_3 = \ln(n_{A^+}) + \ln(n_e) - \ln(n_A) - \ln(K_n(A^-)) \qquad \text{(C.3)}$$

4) the deviation from the equilibrium constant of species A+:

$$\Delta g_4 = \ln(n_{A^{--}}) + \ln(n_e) - \ln(n_{A^+}) - \ln(K_n(A^{--})) \qquad \text{(C.4)}$$

At composition equilibrium, $\Delta \bar{g} = 0$ and $\Delta \bar{n} = 0$ for given p, T_h and T_e.

REFERENCES

Allen N K, Cox B M and Latham R V 1979 The source of high-β electron emission sites on broad-area high-voltage alloy electrodes *J. Phys. D: Appl. Phys.* **12** 969

Almeida R M and Benilov M S 1997 The near-cathode region in high-pressure arc discharge lamps *Proc. ISPC-13*, Beijing, China, 99

Anders S and Anders A 1991 On modes of arc cathode operation *IEEE Trans. Plasma Sci.* **19** 20

Anders A, Anders S, Förster A and Brown I G 1992 Pressure ionization: its role in metal vapor vacuum arc plasmas and ion sources *Plasma Sources Sci. Technol.* **1** 263

Baddorf A P and Zehner D M 1990 Chemisorption of nitrogen on Cu(110): coverage and site determination *Surface Sci.* **238** 255

Benilov 1993 Nonlinear heat structures and arc-discharge electrode spots *Phys. Rev. E* **48** 506

Benilov M S 1997 Theory of a collision-dominated space-charge sheath on an emitting cathode *J. Phys. D: Appl. Phys.* **30** 1115

Benilov M S and Marotta A 1995 A model of the cathode region of atmospheric pressure arcs *J. Phys. D: Appl. Phys.* **28** 1869

Bolotov A, Kozyrev A and Korolev Y 1995 A physical model of the low-current-density vacuum arc *IEEE Trans. Plasma Sci.* **23** 884

Boulos M I, Fauchais P and Pfender E 1994 *Thermal Plasmas. Fundamentals and Applications* (New York: Plenum Press)

Choueiri E Y 1992 Plasma propulsion *in McGraw-Hill Encyclopedia of Science and Technology* **14** 21

Christov S G 1966 General theory of electron emission from metals *Phys. Stat. Sol.* **17** 11

Christov S G and Vodenicharov C M 1968 On the experimental proof of the general theory of electron emission from metals *Solid-State Electronics* **11** 757

Cobine J D 1941 *Gaseous Conductors: Theory and Engineering Applications* (New York: McGraw-Hill)

Cobine J D and Burger E E 1955 Analysis of electrode phenomena in the high-current arc *J. Appl. Phys.* **26** 895

Crowell C R and Sze S M 1966 Current transport in metal-semiconductor barriers *Solid State Electron.* **9** 1035

Desaulniers-Soucy 1992 "Étude spectroscopique des vapeurs de cuivre d'un arc en rotation dans l'argon contaminé," M. Eng. Thesis, McGill University, Montréal, Canada.

Desaulniers-Soucy N and Meunier J -L 1995a Temperature and density profiles of magnetically rotating arcs burning in contaminated argon *Plasma Chem. Plasma Process.* **15** 629

Desaulniers-Soucy N and Meunier J -L 1995b A study of magnetically rotating arc stability using fluctuations in voltage, velocity and emission line intensity *J. Phys. D: Appl. Phys.* **28** 2505

Djakov B E and Holmes R 1974 Cathode spot structure and dynamics in low-current vacuum arcs *J. Phys. D: Appl. Phys.* **7** 569

Drawin H W and Felenbok P 1965 *Data for plasmas in local thermodynamic equilibrium* (Paris: Gauthier-Villars)

Drouet M G 1985 The physics of the retrograde motion of the electric arc *IEEE Trans. Plasma Sci.* **13** 235

Duke C B and Alferieff M E 1967 Field emission through atoms adsorbed on a metal surface *J. Chem. Phys.* **46** 923

Durpagal P 1993 Electrode phenomena in high-current, high-pressure arc heaters *J. Thermophys. Heat Transfer* **7** 412

Ecker 1973 Unified analysis of the metal vapour arc *Z. Naturforsch* **28a** 417

Ecker G 1980 Theoretical aspects of the vacumm arc *in Vacuum Arcs: Theory and Application*, Lafferty J M, Ed. (New York: Wiley) 228

Emtage P R 1975 Interaction of the cathode spot with low pressures of ambient gas *J. Appl. Phys.* **46** 3809

Farrall G A 1980 Electrical breakdown in vacuum *in Vacuum Arcs: Theory and Application* (Lafferty J M ed. New York: Wiley)

Fowler R H and Nordheim L W 1928 *Proc. Roy. Soc. (London)* **A119** 173

Freund R S, Wetzel R C, Shul R J and Hayes T R 1990 Cross-section measurements for electron-impact ionization of atoms *Phys. Rev. A* **41** 3575

Gayet R, Harel C, Josso T and Jouin H 1996 A simple model for cathodic electronic emission enhanced by low-energy ions in high pressure arcs *J. Phys. D: Appl. Phys.* **29** 3063

Gray E W and Pharney J R 1974 Electrode erosion by particle ejection in low-current arcs *J. Appl. Phys.* **45** 667

Griem H R 1964 *Plasma Spectroscopy* (New York: McGraw-Hill)

Guile A E 1971 Arc-electrode phenomena *Proc. IEE, IEE Reviews* **118** 1131

Guile A E and Hitchcock A H 1975 Oxide films on arc cathodes and their emission and erosion *J. Phys. D: Appl. Phys.* **8** 663

Halbritter J 1985 On contamination of electrode surfaces and electric field limitations *IEEE Trans. Electric. Insul.* **EI-20** 671

Hamilton D J and Guile A E 1968 Ionization in the cathode-fall region of moving arcs *Brit. J. Appl. Phys.* **2** 335

Hancox R 1960 Importance of insulating inclusions in arc initiation *Brit. J. Appl. Phys.* **10** 468

Haworth F E 1950 Experiments on the initiation of electric arcs *Phys. Rev.* **80** 223

He Z -J and Haug R 1997 Cathode spot initiation in different external conditions *J. Phys. D: Appl. Phys.* **30** 603

Honig R E and Kramer D E 1969 Vapor pressure data for the solid and liquid elements *RCA Review* **30** 285

Hsu K C and Pfender E 1983 Analysis of the cathode region of a free-burning high intensity argon arc *J. Appl. Phys.* **54** 3818

Hull A W 1962 Cathode spot *Phys. Rev.* **126** 1603

Hunter L W and Kuttler 1989 The enthalpy method for heat conduction problems with moving boundaries *J. Heat Transfer* **111** 239

Hurley R E and Dooley P J 1978 Vacuum breakdown from electroluminescent impurities on metallic cathode surfaces *Vacuum* **28** 147

Josso T 1997 "Étude théorique de l'émission électronique d'une cathode en présence d'ions lents," Docteur Thesis, Université de Bordeaux I, Bordeaux, France

Jüttner B 1985 On the plasma density of metal vapour arcs *J. Phys. D: Appl. Phys.* **18** 2221

Jüttner B 1987 Characterization of the cathode spot *IEEE Trans. Plasma Sci.* **PS-15** 474

Jüttner B 1997 The dynamics of arc cathode spots in vacuum: new measurements *J. Phys. D: Appl. Phys.* **30** 221

Kandah M 1997 "Particles emission control at graphite cathode in arc ion plating deposition," Ph.D. Thesis, McGill University, Montréal, Canada

Kesaev I G 1965 Laws governing the cathode drop and the threshold currents in an arc discharge on pure metals *Sov. Phys.-Tech. Phys.* **9** 1146

Kharin S N 1992 Mathematical model of arc erosion in electrical contacts *Proc. 16th Inter. Conf. Electrical Contacts*, Loughborough, 205

Kim G E, Meunier J -L and Ajersch F 1995 Experimental study of the effect of nitrogen on titanium-arc cathode erosion *IEEE Trans. Plasma Sci.* **23** 1001

Kimblin C W 1974 Cathode spot erosion and ionization phenomena in the transition from vacuum to atmospheric pressure arcs *J. Appl. Phys.* **45** 5235

Klein T, Paulini J and Simon G 1994 Time-resolved description of cathode spot development in vacuum arcs *J. Phys. D: Appl. Phys.* **27** 1914

Kwak J E 1994 "The behaviour of titanium, stainless steel and copper-nickel alloys as plasma torch cathodes," M. Eng. Thesis, McGill University, Montréal, Canada.

Kwak J E and Munz R J 1996 The behavior of titanium, stainless steel, and copper-nickel alloys as plasma torch cathodes *Plasma Chem. Plasma Process.* **16** 577

Latham R V 1983 Prebreakdown electron emission *IEEE Trans. Elec. Insul.* **18** 194

Lee T. H. 1959 T-F theory of electron emission in high-current arcs *J. Appl. Phys.* **30** 166

Lowke J J, Kovitya P and Schmidt H P 1992 Theory of free-burning arc columns including the influence of the cathode *J. Phys. D: Appl. Phys.* **25** 1600

Maecker H 1955 *Z. Phys.* **141** 198

Marotta A 1991 Air plasma torch with zirconium cathode *Proc. ISPC-10*, Bochum, Germany, paper 1.3-4

Marotta A and Sharakhovsky L I 1996 A theoretical and experimental investigation of copper electrode erosion in electric arc heaters: I. The thermophysical model *J. Phys. D: Appl. Phys.* **29** 2395

Mackeown S S 1929 The cathode drop in an electric arc *Phys. Rev.* **34** 611

Mentel J, Bayer R, Schein J and Schumann M 1994 Interaction of a dense plasma with cold electrodes *High Temp. Chem. Processes.* **3** 627

Mesyats G A 1995 Ecton mechanism of the vacuum arc cathode spot *IEEE Trans. Plasma Sci.* **23** 879

Meunier J -L and Drouet M G 1987 Experimental study of the effect of gas pressure on arc cathode erosion and redeposition in He, Ar, and SF_6 from vacuum to atmospheric pressure *IEEE Trans. Plasma Sci.* **PS-15** 515

Meunier J -L 1990 Pressure limits for the vacuum arc deposition technique *IEEE Trans. Plasma Sci.* **18** 904

Meunier J. -L. and Desaulniers-Soucy N. 1994 Erosion rate evaluation of plasma torch electrodes from measurements of the emitted metal vapour radiation *J. Phys. D: Appl. Phys.* **27** 2522

Miller S C and Good R H 1953 A WKB-type approximation to the Schrödinger equation *Phys. Rev.* **91** 174

Milos F S and Shepard C E 1994 Thermal analysis of an arc-heater electrode with a rotating arc foot *J. Thermophys. Heat Transfer* **8** 723

Morrow R and Lowke J J 1993 A one-dimensional theory for the electrode sheaths of electric arcs *J. Phys. D: Appl. Phys.* **26** 634

Munz R J and Habelrih M 1992 Cathode erosion on copper electrodes in steam, hydrogen, and oxygen plasmas *Plasma Chem. Plasma Process.* **12** 203

Munz R J, Szente R N and Drouet M G 1992 Arc behaviour and plasma chemistry in electrode erosion *Pure & Appl. Chem.* **64** 657

Murphy E L and Good R H 1956 Thermionic, field emission, and the transition region *Phys. Rev.* **102** 1464

Nachtigall K P and Mentel J 1991 Optical investigation of arc spot formation on cold cathodes in air *IEEE Trans. Plasma Sci.* **19** 947

Nottingham W B 1941 *Phys. Rev.* **59** 907

Nürnberg A W, Fang D Y, Bauder U H, Behrisch R and Brossa F 1981 Temperature dependence of the erosion of Al and TiC by vacuum arcs in a magnetic field *J. Nucl. Materials* **103&104** 305

Padovani F A and Stratton R 1966 Field and thermionic-field emission in Schottky barriers *Solid State Electron.* **9** 695

Paulini J, Klein T and Simon G 1993 Thermo-field emission and the Nottingham effect *J. Phys. D: Appl. Phys.* **26** 1310

Prewett P D and Allen J E 1976 The double sheath associated with a hot cathode *Proc. R. Soc. Lond.* A **348** 435

Raja L L, Varghese P L and Wilson D E 1997 Modeling of the electrongun metal vapor plasma discharge *J. Thermophys. Heat Transfer* **11** 353

Rakhovskii V I 1976 Experimental study of the dynamics of cathode spots development *IEEE Trans. Plasma Sci.* **4** 81

Rethfeld B, Wendelstorf J, Klein T and Simon G 1996 A self-consistent model for the cathode fall region of an electric arc *J. Phys. D: Appl. Phys.* **29** 121

Richardson O W 1901 *Proc. Camb. Phil. Soc. Math. Phys. Sci.* **11** 281

Richley E and Tuma D T 1982 On the determination of particle concentrations in multitemperature plasmas *J. Appl. Phys.* **53** 8537

Riemann K -U 1991 The Bohm criterion and sheath formation *J. Phys. D: Appl. Phys.* **24** 493

Roth J R 1981 Impurity generation *J. Nucl. Materials* **103&104** 291

Roth J R 1995 *Industrial Plasma Engineering* (United Kingdom: IOP Publishing Ltd)

Satheesh K A, Okumura Y and Okazaki 1992 Arc transition and growth of big-arcs in magnetohydrodynamics generator channels *J. Thermophysics and Heat Transfer* **6** 452

Schlesser R, McClure M T, Choi W B, Hren J J and Sitar Z 1997 Energy distribution of field emitted electrons from diamond coated molybdenum tips *Appl. Phys. Lett.* **70** 1596

Schmidt H -P and Speckhofer G 1996 Experimental and theoretical investigation of high-pressure arcs - Part I: the cylindrical arc column (two-dimensional modeling) *IEEE Trans. Plasma Sci.* **24** 1229

Schmoll R and Hartmann W 1997 Interaction of cathode microtips and dense plasmas *Proc. ICPIG-23*, Toulouse, France, paper IV-164

Scheuer J T and Emmert G A 1988 A collisional model of the plasma presheath *Phys. Fluids* **31** 1748

Schwirzke F, Hallal M P and Maruyama X K 1993 Onset of breakdown and formation of cathode spots *IEEE Trans. Plasma Sci.* **21** 410

Senda I 1997 A model of ions interacting with neutrals in high electric field and the application to presheath formations *Phys. Plasmas* **4** 1308

Siemroth P, Schülke T and Witke T 1995 Microscopic high speed investigations of vacuum arc cathode spots *IEEE Trans. Plasma Sci.* **23** 919

Spataru C, Teillet-Billy D, Gauyacq J P, Testé P and Chabrerie J P 1997 Ion-assisted electron emission from a cathode in an electric arc *J. Phys. D: Appl. Phys.* **30** 1135

Sun M, Wang Q and Lindmayer M 1994 The model of interaction between arc and AgMeO contact materials *IEEE Trans. Comp., Packag., Manufact. Technol., Part A* **17** 490

Swanson L W, Crouser L C and Charbonnier F M 1966 Energy exchanges attending field electron emission *Phys. Rev.* **151** 327

Szente R N 1989 "Erosion of plasma torch electrodes," Ph. D. Thesis, McGill University, Montréal, Canada.

Szente R N, Drouet M G and Munz R J 1991 Current distribution of an electric arc at the surface of plasma torch electrodes *J. Appl. Phys.* **69** 1263

Szente R N, Munz R J and Drouet M G 1992 Electrode erosion in plasma torches *Plasma Chem. Plasma Process.* **12** 327

Szente R N, Munz R J and Drouet M G 1994 Copper-niobium and copper-tungsten composites as plasma torch cathodes *J. Phys. D: Appl. Phys.* **27** 1443

Tamaki S and Kuroda T 1987 The electronic partition function of atoms and ions between 7000 and 12000 K *Spect. Act.* **42B** 1105

Testé Ph, Leblanc T and Chabrerie J -P 1995 Study of the arc root displacement and three-dimensional modelling of the thermal phenomena occurring in a hollow cathode submitted to an electric moving arc *J. Phys. D: Appl. Phys.* **28** 888

Testé Ph and Chabrerie J -P 1996 Some improvements concerning the modelling of the cathodic zone of an electric arc (ion incidence on electron emission and the 'cooling effect') *J. Phys. D: Appl. Phys.* **29** 697

Tioursi M and Haug R 1997 Relation between crater dimensions and voltage fluctuations in low current cold cathode electric arcs *Proc. ICPIG-23*, Toulouse, France, paper IV-166

Trajmar S, Williams W and Srivastava S K 1977 Electron-impact cross sections for Cu atoms *J. Phys. B: Atom. Molec. Phys.* **10** 3323

Ushio M, Fan D and Tanaka M 1994 A method of estimating the space-charge voltage drop for thermionic arc cathodes *J. Phys. D: Appl. Phys.* **27** 561

Vasenin Y L, Gvozdetsky V S, Krivtsun I V, Zel'nichenko A T, Vladimirov V V, Jüttner B and Pursch H 1997 Therory of the cathode region of electric arcs in vacuum, private communication

Zemansky M W and Dittman R H 1981 *Heat and Thermodynamics, Sixth Edition* (McGraw-Hill Book Compagny)

Zhou X and Heberlein J 1994 Analysis of the arc-cathode interaction of free-burning arcs *Plasma Sources Sci. Technol.* **3** 564

Zhou and Heberlein 1996 Characterization of the arc cathode attachment by emission spectroscopy and comparison to theoretical predictions *Plasma Chem. Plasma Process.* **16** 229S

Zhou X, Ding B and Heberlein J V R 1996 Temperature measurement and metallurgical study of cathodes in DC arcs *IEEE Trans. Comp., Packag., Manufact. Technol. A* **19** 320

Zhu P, Lowke J J and Morrow R 1992 A unified theory of free burning arcs, cathode sheaths and cathodes *J. Phys. D: Appl. Phys.* **25** 1221